Title

Development of Single-Walled Carbon Nanotube Protein Optical Nanosensors

Author

Chio, Linda

Publication Date

2020

Peer reviewed|Thesis/dissertation

Development of Single-Walled Carbon Nanotube Protein Optical Nanosensors

By

Linda Chio

A thesis submitted in partial satisfaction of the

requirements for the degree of

Doctor of Philosophy

in

Chemical Engineering

in the

Graduate Division

of the

University of California, Berkeley

Committee in charge:

Professor Markita P. Landry, Chair

Professor Roya Maboudian

Professor Wenjun Zhang

Professor Matthew B. Francis

Spring 2020

Abstract

Developing Single-Walled Carbon Nanotube Protein Optical Nanosensors

by

Linda Chio

Doctor of Philosophy in Chemical Engineering

University of California, Berkeley

Professor Markita P. Landry, Chair

Many diseases, such as neurodegenerative disorders, cancer, and autoimmune diseases are caused by or exhibit symptoms of abnormal regulation of signaling proteins. In order to obtain a molecular understanding of diseases, we require tools capable of probing the intricate signaling pathways that govern biological function. Understanding the role these proteins play as they circulate between cells will allow us to examine disease progression from an intercellular point of view. Currently, it is difficult to study these proteins in their natural environment, *in vivo*, because they are created and function on very broad time and length scales. Existing protein detection methods have several limitations as they are optimized for intracellular imaging, performed *in vitro*, require lengthy sample handling, function over short time scales, or have molecular recognition elements that are unstable in biological media.

This dissertation presents a modular platform to create optical nanosensors that are able to address current limitations in signaling protein detection. Nanosensor elements require optimization of both signal transduction and molecular recognition elements. Single-walled carbon nanotubes (SWCNTs) are nanoparticles that are ideal signal transducers for biological imaging. SWCNTs have optical properties well-suited for biological sensing such as infinite fluorescence lifetime, no blinking, small size, and fluorescence in the near-infrared region of the electromagnetic spectrum that is least attenuated by biological systems. Several SWCNT nanosensors have already been developed for signaling small molecule targets and peptides, but, to date, none have been created for signaling proteins.

In order to create a robust imaging platform based on SWCNTs for sensing signaling proteins, it is possible to couple molecular recognition elements to SWCNT signal transducers using dual noncovalent and covalent functionalization strategies. The development of noncovalent molecular recognition elements is explored using peptide mimetic polymers called peptoids. The discovery of a synthetic peptoid binding loop for wheat germ agglutinin protein as a proof-of-principle case study shows the ability to utilize diverse chemical materials to create a fully synthetic binding element for desired protein targets. Additionally, the development of covalently functionalized SWCNTs is explored for the creation of multifunctional optical SWCNT nanosensors. Here covalently functional groups provide functional handles that work synergistically with noncovalent passivation to enable the development of a diverse nanosensor toolbox.

The findings presented in this dissertation lay the foundation of valuable techniques and materials to optimize the binding to and study of signaling proteins. Future work to streamline the development of novel nanosensors is discussed, and the framework for the creation of other biological nanomaterial tools through these noncovalent and covalent techniques is also explored.

This thesis is dedicated to my mother, I Kam Chio, and my father, Tong Tak Chio, for their unwavering commitment in helping their children succeed.

Table of Contents

List of Figures

List of Tables

List of Abbreviations

AFM	atomic force microscopy
APTES	(3-aminopropyl)triethoxysilane
Con A	concanavalin A
CoPhMoRe	corona phase molecular recognition
CRISPR	clustered regularly interspaced short palindromic repeats
DMEM	Dulbecco's modified eagle medium
DNA	deoxynucleic acid
ELISA	enzyme linked immunosorbent assay
FRET	Förster resonance energy transfer
GlcNAc	N-acetylglucosamine
GOx	glucose oxidase
HRP	horseradish peroxidase
I	intensity
I_0	initial intensity
ICG	indocyanine green
IgG	immunoglobulin G
IL-6	interleukin 6
InGaAs	indium gallium arsenide
IR	infrared
Neu5Ac	N-acetylneuraminic acid
NIR	near-infrared
PA	Anthrax protective antigen
PBS	phosphate buffered saline
PEG	polyethylene glycol
PNA	peanut agglutinin
RCF	relative centrifugal force
SD	standard deviation
SEM	standard error to the mean
SELEX	systematic evolution of ligands by exponential enrichment
SWCNT	single-walled carbon nanotube
UV	ultraviolet
Vis	visible
WGA	wheat germ agglutinin

Acknowledgements

Getting a PhD was never something I had dreamed of doing, for it had seemed like frivolous training for dull academics. Even up to the beginning of the summer after my junior year in college I resisted the idea of having to go to school for another four to six (!) years. Part of this was cockiness, part of this was familial pressure to pursue the "American Dream" and make money immediately out of college, and part of this was the eagerness to just get out there and do something cool. After getting a taste of biotech research in real life, I realized that I had a lot to learn about asking interesting scientific questions, and that getting a PhD would be a useful next step to accomplish. So, I began my next adventure at UC Berkeley.

Having gone through the process of getting a PhD, I am happy I made this decision. This has been an incredibly fun and rewarding journey that has prepared me for the next phase of my life. There were definitely highs and lows to graduate school, but I have learned to view the PhD as a marathon and not a sprint. The past 5 years seemed to go so slowly until this last month, and this entire process would have been impossible without the help and support of many people.

First, I would like to thank my advisor Professor Markita Landry, for her tremendous guidance during this journey. I think that I am a perpetual planner, and when I started at UC Berkeley, I had already formulated my plan of the type of research I would do, the kind of advisor that I would work with, and the sort of accomplishments I would achieve along the way. Markita came in as a new assistant professor with no physical lab space set up, and upended all of my previous plans to set me on a path of exploration I had not expected. I feel honored for this amazing experience and all of the opportunities that she has enabled for me. She helped us build a scientific playground where I intellectually explored a burgeoning field of single-walled carbon nanotube optical nanosensors. At times, I was frustrated that she would never tell me no or which research path to take, but I am happy that I had the opportunity to take charge of my own work from day one, and it didn't hurt that she helped build a network of world-class researchers on whom I can turn to for advice along the way. She also pushed me to strive for the best professionally and personally, and is one of my greatest supporters whether it is for the job that I want to pursue, the conference that I find interesting, or the honors that I was worried that I would not win. Being one of the first students in the Landry Lab was truly a privilege, and I am incredibly happy that I was in the right place and the right time to meet Markita. It is hard to emphasize just how much my advisor and my lab have made this journey great.

I am incredibly grateful for the three other brave souls, Abraham Beyene, Gözde Demirer, and Darwin Yang, who joined me at the beginning of this journey. I was not sure what starting a new lab would be like, and it definitely helped to have friends along the way. I remember that little office in Stanley where we crammed for our prelims before our lab was officially open. I remember unpacking each of the new (or second-hand) equipment, and having to figure out how it worked. I remember when we first bought the bath sonicator we didn't have any floats for our samples and had to use our engineering degrees to figure out that we could tape Styrofoam to our tubes to make them float. I remember having to ask a lot of people in Stanley Hall for little favors, but always having one of the other members by my side. How daunting this whole process would have been if I were all alone! Thanks also for being awesome friends! Gözde and Darwin, thanks for all the fun memories in Mexico. Of course, when speaking of the first members of the lab, I also have to

thank Dr. Jackson Travis Del Bonis-O'Donnell, who put together the optical set up I would spend some many hours toiling over and who was a wise and positive influence on all of our developments from the beginning.

That was then, and now to the present I need to thank the almost innumerable number of people who have joined our lab: Rebecca Pinals, Gabriel Dorliac, Dr. Sanghwa Jeong, Dr. Younghun Sung, Dr. Ian McFarlane, Frankie Cunningham, Natalie Goh, Sarah Yang, Dr. Huan Zhang, Dr. Eduardo Gonzalez Grandio, Alison Lui, Nick Ouassil, Jeff Wang, Chris Jackson, Nicole Navarro, Madeline Klinger, Josh Hubbard, and Francis Ledesma. Thank you for all the awesome memories: Halloween parties, group retreats, boba runs, game nights, and countless celebrations after each person's accomplishment! I hope I had contributed a bit to the growth of each of you whether it is from formal training on an instrument, conversations about science, or just casual conversations about life over a glass of wine (or at times, a glass of scotch). You all have certainly taught me about how to be part of a team, how to manage large organizational changes, and a lot of science! Specific shoutouts to Becca and Nat for sitting next to me for years and making it a fun desk corner, and for also liking cats and boba! Shoutout to Ian, Travis, and Maroof Adil for being Gloomhaven buddies! Also, for the opportunity to learn as a mentor, I want to thank the undergraduate students of whom I've had the pleasure of training: Nicole Sugiono, Aishy Murali, and Alisa Pershina.

Research is not done as an island, and I have to thank the number of collaborators I have worked with to make scientific discovery possible. I am so happy I met Dr. Ron Zuckermann and his team at the Molecular Foundry of Lawrence Berkeley National Lab: Dr. Mark Kline, Dr. Jae Hong Kim, Dr. Michael Connolly, Dr. Behzad Rad, Dr. Andy Nguyen, and Dr. Blake Tresca. Thanks for all the help from the facilities and labs on UC Berkeley campus who have helped me with my research. I would also like to thank the members of my dissertation committee for their guidance and feedback during graduate school: Professor Roya Maboudian, Professor Wenjun Zhang, and Professor Matt Francis.

Of course, I also need to thank all the people who took care of the boring parts that made the PhD happen. Thank you for the administrative support from our Graduate Student Administrator Carlet Altamirano, our Faculty Support Administrator Sigrid Allen, QB3 staff at Stanley Hall, and all other UC Berkeley staff. I also appreciate all the funding sources that allow me to pursue my own independent work: Lam Research and the National Defense Science and Engineering Graduate Fellowship.

Grad school would have been hard without the support of friends, and I thank all the friends who have been there to hang out and talk about not lab things (although, sometimes also lab things). To Jacqueline Avery Maslyn and Sidney Douglas Buchbinder, thanks for dealing with me the last nine years and keeping me sane with friendship. It is crazy watching the Lord of the Rings with the two of you and hearing both of you quote the movie lines. Thanks for all the fun travel buddies I've had over the years: Becky Chao, Lorraine Kwok, and Heidi Tan. Thanks to Jamie Gaskin for being a converted foodie and celebrating my accomplishments with Michelin starred restaurants or adventurous home-cooked meals. I'd also like to thank the wonderful student organizations I was able to participate in, especially the resources provided to me through the Graduate Women of Engineering group and the Berkeley Art Studio.

Finally, I would like to thank my loving family. Mom, Dad, Tiffany, and Melanie thanks for supporting me in all of your unique ways, even when you have no idea what I do or why I do the things I do. I'm not sure from where I get my eccentricity, but you have dealt with it with grace and love. This dissertation is also written in loving memory of my grandmother, Peng Peng Chio, who raised my sisters and I when my parents worked. Right now, the world has been thrown into chaos and confusion, and I appreciate the unwavering love and resilience of all those around me.

Chapter 1: Introduction

1.1 The Importance of Extracellular Protein Sensing

Many of the diseases that we seek to understand, such as neurodegenerative disorders, cancer, and autoimmune diseases are mechanistic breakdowns of cellular signaling pathways or present symptoms of aberrant cellular communication. The biological processes of the body are communicated through the release, uptake, and response to extracellular signaling molecules. Signaling molecules are secreted from one cell and are taken up by neighboring cells through channels and receptors to trigger biological processes (Fig. 1.1 a). In order to obtain a molecular understanding of diseases, scientists require tools that are capable of probing the intricate signaling pathways that govern biological function.

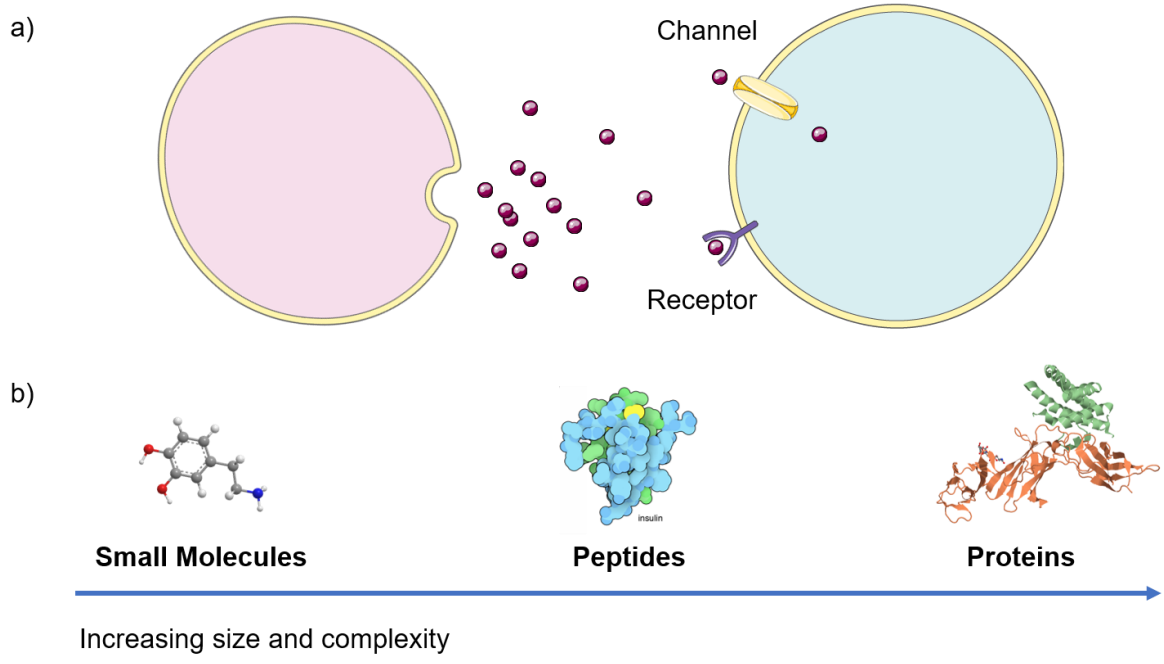

Figure 1.1: Cellular Communication Via Extracellular Signaling Molecules.

a) Cells communicate through the release and uptake of signaling molecules. These signaling molecules are taken up through channels or receptors and trigger downstream biological processes. Images of cells, receptors, and channels were obtained from Servier Medical Art by Servier licensed under a Creative Commons Attribution 3.0 Unported License. b) Cellular signaling molecules appear in a range of sizes and complexities and include small molecules, peptides, and proteins. Protein images are from the RCSB PDB (rcsb.org) of PDB ID 4INS and 1F45.[1,2]

Signaling molecules come in many forms such as small molecule chemicals, peptides, and proteins, and have major impact on diverse diseases (Fig. 1.1b). For example, the small chemical neurotransmitter dopamine is implicated in a wide range of neurological and psychiatric disorders, including the second most prevalent neurodegenerative disease in America: Parkinson's disease.[3] The modulation of dopamine is known to act on both the synaptic cleft, the space between the

terminals of two neurons, and can also diffuse to act on extrasynaptically-expressed receptors.[4,5] This long-range spatial distribution of signaling molecules can be seen in systemic diseases with the signaling peptide insulin, where abnormal secretion and uptake of or insensitivity to insulin during the metabolism of nutrients is the hallmark of diabetes.[6,7] Similarly, signaling proteins, such as cytokines and chemokines, have been shown to play an important role in chronic inflammation implicated in tumor development.[8] Among cytokines, interleukin-6 (IL-6) has been shown to be critical with roles in regulating the tumor microenvironment and activating important oncogenic pathways.[9–11] Although these signaling molecules control the fate of different processes, they are similar in that they are secreted factors and are trafficked extracellularly.

These signaling molecules are implicated in many prevalent diseases, but they are difficult to study in their extracellular environments because their modes of action occur on disparate time and length scales. In terms of temporal information, each release event lasts for the order of seconds, but the manifestation of disease occurs following a sustained history of aberrant signaling. Spatially, release and uptake events can happen locally between two neighboring cells or travel through the bloodstream to affect distant cells. Additionally, it is necessary to understand simultaneous temporal and spatial patterns to uncover disease mechanisms. In order to study these cellular signaling phenomena, a robust method is necessary to capture spatial and temporal information locally, and optical imaging using nano-scale sensors (nanosensors) is a promising technique. Optical imaging has the capability to simultaneously measure both temporal and spatial information through the collection of two-dimensional arrays: videos. When designing optical nanosensors, there are two parts to optimize: the signal transduction element, which provides the readout of the system, and the molecular recognition element, the region that interacts and binds with the analyte of interest. For optical signal transduction, several properties are necessary: spatial mobility, minimal signal diminution by the system, and temporal stability to measure transient events. For molecular recognition, it is important for the element to be sensitive to the range of analyte concentrations that are biologically relevant, selective towards the analyte of interest, and stable for use in the body.

Protein signaling molecules are particularly difficult to study due to their complexity and large size, and conventional protein sensing methods exist almost exclusively *in vitro* or intracellularly. Standard protocols for signaling protein detection involve immunological analytical methods such as, enzyme-linked immunosorbent assays (ELISA), western blotting, or mass spectrometry.[12] Recent advances have explored electrochemical detection of proteins with antibodies and aptamers, with great success for temporal quantification of protein from purified samples, several with nanomolar detection capabilities.[13,14,15] However, these methods are not amenable to *in vivo* sensing due to their extensive sample handling prior to detection. Proteins could be fluorescently labeled using *in situ* probes, like SpyCatcher that target specific chemical handles, or genetic labels like green fluorescent protein fusion tags, but these methods require extensive protein engineering.[16–18] Additionally, most fluorescent detection tools are only suitable for intracellular imaging, where fluorophores are confined within the cell, due to the rapid loss of fluorescence because of the photobleaching nature of current tools for protein imaging. An ideal protein nanosensor will be able to address these limitations of extensive and difficult sample handling to provide a robust system for obtaining both spatial and temporal information.

1.2 The Optical Properties of Single-Walled Carbon Nanotubes

Single-walled carbon nanotubes, referred to as SWCNTs for the rest of this dissertation, are a cylindrical allotrope of a single-atomic layer of carbon first discovered by Iijima in 1993 (Fig. 1.2a).[19] Their structures can be envisioned as graphene sheets rolled up along a unique vector resulting in SWCNT structures with a particular handedness, or chirality (Fig. 1.2b).[20] The chirality of SWCNTs are denoted as (n,m), where n and m are assigned based on their roll-up vector. SWCNTs have a very high-aspect ratio with an average diameter of 1 nm and an average length of 500 nm, and this gives rise to the one-dimensional confinement of electronic states resulting in van Hove singularities in the nanotube density of states.[21] Based on their chirality, SWCNTs are capable of states with different energy levels leading to the formation of metallic, conducting, and semiconducting materials.[22] SWCNTs are hydrophobic and will self-associate, but can be individualized with different amphiphilic coatings. Individualized semiconducting SWCNTs are fluorescent in the near-infrared (NIR) region (900 - 1500 nm) of the electromagnetic spectrum with distinct fluorescent excitation and emission wavelengths that correspond to each chirality of SWCNTs (Fig. 1.2c). For spectral data, such as excitation wavelength, emission wavelength, and bandgap energy, of individual chiralities, refer to appendix 1.

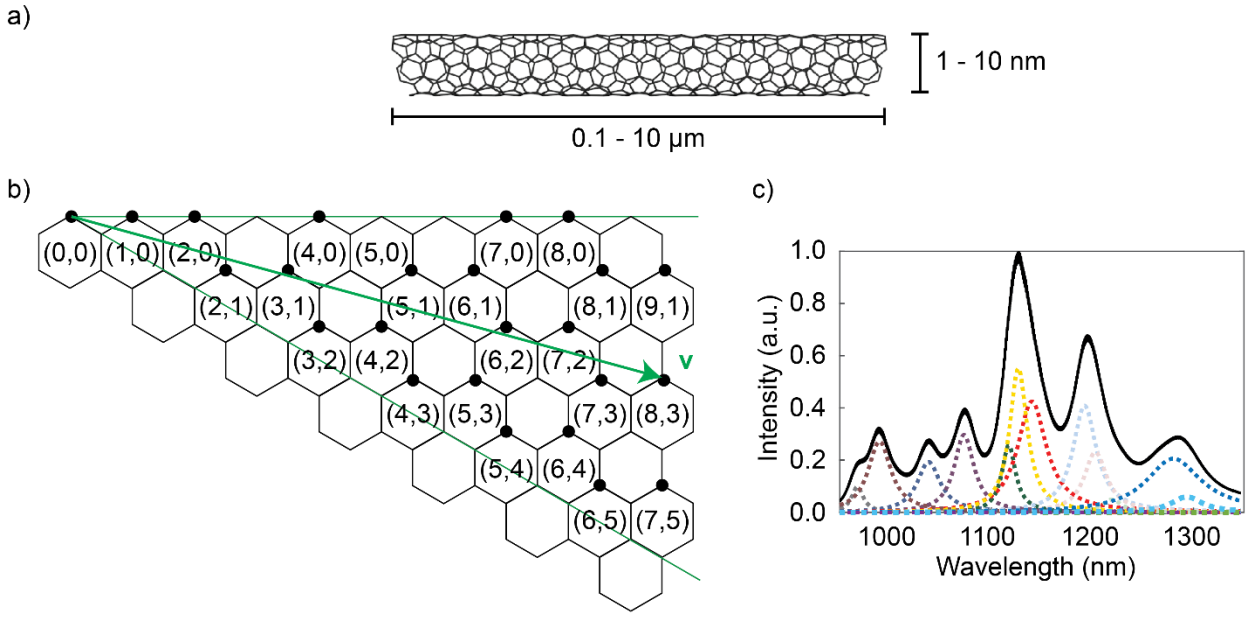

Figure 1.2: Single-Walled Carbon Nanotube Structure.

a) SWCNTs are a cylindrical allotrope of carbon with very high aspect ratio with diameters ranging from 1 – 10 nm and lengths ranging from 0.1 – 10 µm. b) SWCNTs are chiral molecules whose diameter and electronic properties are determined from their roll-up vector that connects (0,0) to another top point of a hexagon. Semiconducting SWCNTs are labeled on this diagram based on their roll-up vector **v**. c) Semiconducting SWCNTs have a characteristic NIR spectrum. The solid black spectrum is a convolution of single chirality fluorescence spectra denoted in the dotted colored plots.

Fluorescent SWCNTs are uniquely suited for the use of *in vivo* extracellular sensing because of their superior physical and optical characteristics. SWCNTs' small dimensions make them spatially mobile and able to access extracellular environments. For example, a synapse between

two neurons is 20 - 40 nm and blood vessels are microns in diameter.[23,24] Their NIR fluorescence is optimally located between the scattering of blood and the absorbance of water, which constitutes two major components of the body, and thus are minimally attenuated optical probes for *in vivo* imaging (Fig. 1.3a).[25,26] Finally, SWCNTs are temporally stable optical probes and are shown not to photobleach upon constant laser irradiation as compared to conventional fluorophores, such as the FDA-approved indocyanine green (ICG) dye used in clinic to visualize tumors in the far red of the visible spectrum (Fig. 1.3b).[27] Additionally, SWCNTs have high photostability and do not blink like other optical nanoparticles, such as quantum dots, which require extensive particle design to suppress non-radiative Augur recombination events.[28] Outside of these characteristics, SWCNTs have an added benefit of being cost-effective optical nanomaterial probes that are synthesized typically through vapor deposition of carbonaceous gases on metal catalyst particles, as compared to other optical nanomaterials that are created with precious or rare earth metals.[29,30] When chemically functionalized and stably encapsulated, although SWCNTs show high bioaccumulation, they are found to have low toxicity.[31] Taking these characteristics together, SWCNTs are excellent biological signal transducers for optical imaging, especially since they are spatially mobile, minimally attenuated, and optically stable.

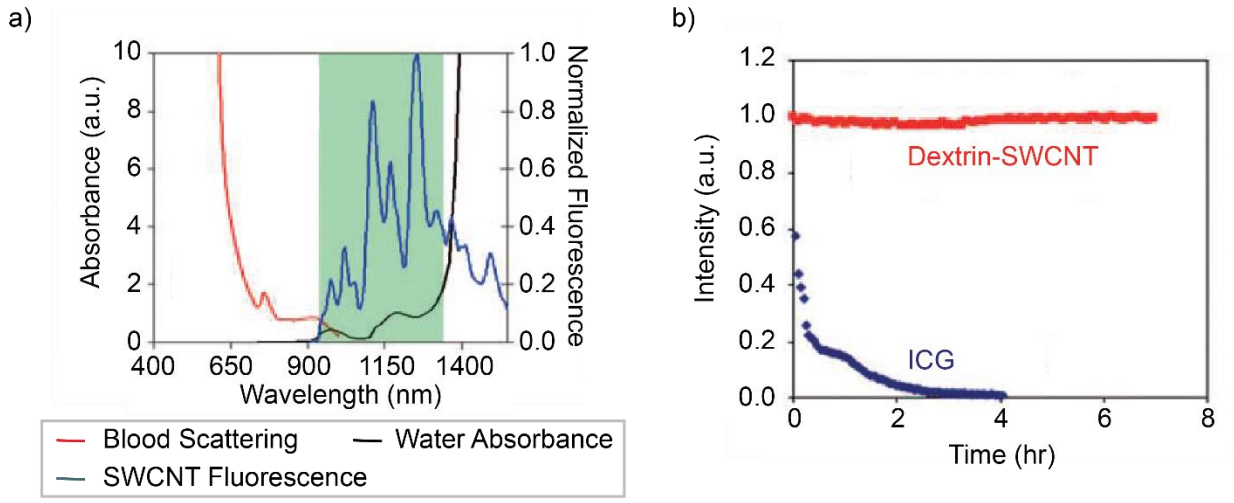

Figure 1.3: Optical Properties of SWCNTs.

a) SWCNTs have intrinsic near-infrared fluorescence that is found in a tissue-transparent region of the electromagnetic spectrum between blood scattering and water absorbance. b) SWCNTs have been shown to be remarkably photostable as compared to conventional fluorophores such as ICG. Figures were reproduced with permission from Boghossian , A.A., et. al. (2011), Near-Infrared Fluorescent Sensors based on Single-Walled Carbon Nanotubes for Life Sciences Applications. ChemSusChem, 4: 848-863. doi:10.1002/cssc.201100070.

SWCNTs have been successfully utilized as the signal transduction element of biological nanosensors since they exhibit fluorescence modulation upon analyte binding. SWCNT fluorescence modulation could be caused by electronic structure perturbations, charge transfer, or dielectric screening effects, resulting in reduction of the excitonic optical transition energies and exciton lifetimes.[32] In particular, SWCNT nanosensors have been created for extracellular signaling molecules with the most success for small molecule chemicals found both systemically or localized to specific organs. Nanosensors exist for vitamins and metabolites that are often found

in systemic circulation such as riboflavin, sugars, nitric oxide, and reactive oxygen species.[33,34] Additionally, SWCNT nanosensors are capable of detecting neurotransmitters in the brain such as dopamine, epinephrine, and serotonin.[35] Similarly, for larger signaling molecules such as peptides, SWCNT nanosensors have been created for the detection of insulin.[36] Signaling protein SWCNT nanosensors will be discussed at length in section 1.3.

SWCNT have been successfully implemented as optical probes for *in vivo* biological imaging. Phospholipid-coated SWCNT were intraveneously administered to mice and could be imaged *in vivo* to determine their biodistribution before and after the incorporation of a tumor-targeting probe.[37] The unattenuated fluorescence emission of SWCNTs enables imaging of traditionally difficult to access biological environments, such as the brain where imaging must occur through optically dense skull bone and tissue components.[38] The first *in vivo* experiments utilizing SWCNTs for imaging in neural tissue were conducted in drosophila larvae by Leeuw et al., SWCNTs were incorporated into feed stock and found to distribute throughout different tissues, including the brain, with no observed short-term toxicity.[39] Additional studies have shown unprecedented resolution of neural vasculature after intravenous administration in mice using NIR SWCNT imaging through skull.[40] These findings support the use of SWCNTs as *in vivo* probes for extracellular signaling molecules.

The optical characteristics of SWCNTs also lend themselves well for coupling with high-resolution imaging techniques, such as two-photon microscopy, hyperspectral imaging, and Raman imaging. Two-photon microscopy of SWCNTs utilizes the simultaneous excitation by two-photons from a 1560 nm laser diode to bypass the absorption of water in the visible range. This technique with SWCNTs reduces the scattering as seen in one-photon excitation from 42% scattering to 4% scattering.[41] Hyperspectral imaging involves the collection both intensity and wavelength data, which can lead to simultaneous multi-channeled imaging of different SWCNT chiralities to track complex biological processes or multiple analytes at the same time. For example, hyperspectral imaging was used to determine nuclear entry of a SWCNT nanosensor via a noncanonical pathway.[42] Raman spectroscopy can also be used for multiplexed imaging and relies on the measurement of specific vibrational fingerprints of each chemical of interest. Raman spectroscopy can also be used to reveal temporal information of SWCNT localized *in vivo* in live mice.[43] This abundance of imaging tools available to SWCNTs will allow for the detailed tracking of biomolecules after the development of SWCNT nanosensors for analytes of interest.

1.3 Single-Walled Carbon Nanotubes as Protein Nanosensors

A survey of contemporary SWCNT literature reveals a distinct lack of protein SWCNT optical nanosensors, since proteins are larger and more complex macromolecules that require more sophisticated molecular recognition elements. SWCNT protein nanosensors rely on the use of antibodies, aptamers, and phospholipid coatings through both targeted and untargeted recognition elements. Although SWCNTs have favorable optical and physical properties for biological detection and imaging, there needs to be ways to create a larger number of molecular recognition elements for protein analytes.

Antibodies are natural molecular recognition elements with high sensitivity and selectivity for specific proteins due to their diverse variable regions, and they have been coupled with SWCNTs

to form protein nanosensors. Examples of antibody-SWCNT constructs as optical nanosensors remain sparse. To date, antibody-SWCNT nanosensors have been constructed for ovarian and prostate cancer surface biomarkers: cancer antigen 125, human epididymis protein 4, and urokinase plasminogen activator.[44,45] For these nanosensors, fluorescence response to analyte results in a wavelength shift of 1 - 4 nm, which may be difficult to detect using conventional imaging set-ups. These nanosensors can be used to test samples *in vitro* or, when immobilized on a chip, can be implanted locally to a region of interest, such as an affected organ. However, it remains to be shown that these antibody-SWCNT nanosensors are stable to degradases in the blood and are capable of circulation in the body for the detection of signaling proteins.

Few other examples exist for protein optical SWCNT nanosensors that do not use naturally occurring molecular recognition elements. Antibody-mimetic molecular recognition elements called aptamers, which are nucleotide sequences with a secondary structure capable of selective binding to an analyte, have been successfully incorporated into SWCNT optical nanosensors. Aptamer sequences successfully incorporated to SWCNTs for the detection of proteins include the blood clotting protein thrombin, protein fragments of RAP1 and HIV integrase 1, and platelet-derived growth factor.[46,47] Another example is the use of a phospholipid coating that is capable of selectively binding to the serum protein fibrinogen.[48] Other examples of molecular recognition for optical protein SWCNT nanosensors need to be developed for biological imaging.

Although there exist examples of previously successful SWCNT protein optical nanosensors, the challenge remains that the discovery of novel nanosensors for protein analytes is dependent on low-throughput screening. This dissertation seeks to bridge the technological gap in nanosensor development by implementing strategies to create a variety of molecular recognition elements using highly modular chemical techniques. To promote the discovery and implementation of SWCNT protein nanosensors, I sought to create a modular toolbox that is chemically diverse in both materials and methods.

1.4 Structure of The Dissertation

This dissertation will describe methods in creating SWCNT protein optical nanosensors, especially with a focus on the creation of novel molecular recognition elements that interact with SWCNT surfaces. Chapter 2 will discuss general strategies and techniques to create molecular recognition elements, how to validate SWCNT nanosensors, common failure modes for molecular recognition elements, and troubleshooting techniques for these common issues. Chapters 3 and 4 will discuss specific examples of nanosensor development techniques that I have created and validated during my PhD. Chapter 3 will detail the use of peptoid polymers for the creation of noncovalently functionalized SWCNT protein nanosensors. Chapter 4 will discuss the application of novel covalent chemistries towards the creation of multifunctional SWCNT optical nanosensors. Finally, chapter 5 will round out the discussion with a look at recent developments and remaining challenges on utilizing the techniques from chapters 3 and 4 for protein nanosensor development, as well as for other applications that these techniques enable.

Chapter 2: Strategies to Create Nanosensor Molecular Recognition*

2.1 Introduction

Although SWCNTs have remarkable optical properties, they do not possess intrinsic molecular recognition to signaling proteins that are of interest to understanding diseases. Several noncovalent and covalent functionalization strategies exist for creating SWCNT nanosensors (Fig. 2.1). For noncovalent strategies, the surface of the SWCNT is passivated with a surface-adsorbed coating to create a recognition domain. For covalent strategies, the surface of the SWCNT undergoes a chemical reaction to create functional groups that can be utilized for further chemical conjugation with existing molecular recognition elements. This chapter will discuss strategies and challenges in utilizing noncovalent and covalent methods for the creation of SWCNT nanosensors. Furthermore, techniques for validating and troubleshooting nanosensors are also discussed.

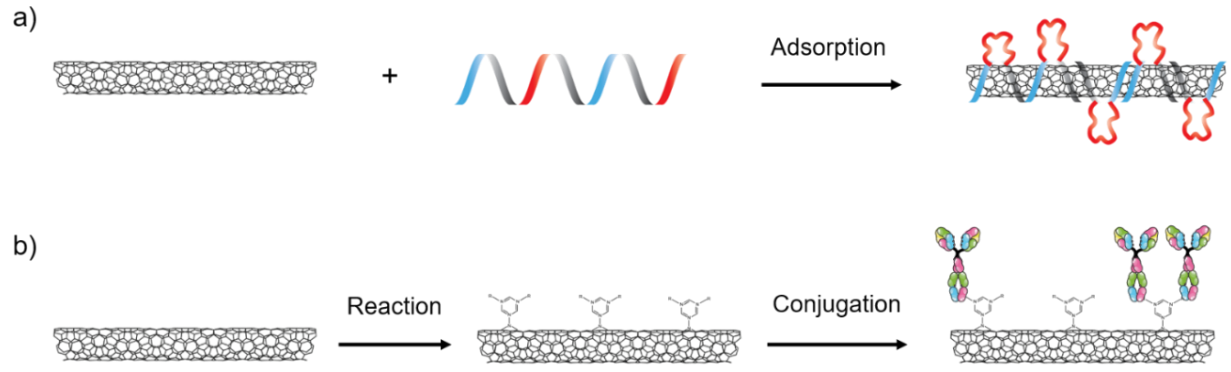

Figure 2.1: Molecular Recognition Development Strategies.

The creation of molecular recognition on SWCNTs through a) a noncovalent functionalization method in which SWCNTs are passivated with a surface adsorbed coating to create recognition sites or b) a covalent functionalization method in which the SWCNT surface is decorated with functional groups that are capable of utilizing known recognition elements, such as antibodies that are depicted in this example. Images of antibodies were obtained from Servier Medical Art by Servier licensed under a Creative Commons Attribution 3.0 Unported License.

2.2 Noncovalent Strategies for Nanosensor Molecular Recognition Development

The noncovalent attachment of molecular recognition elements to SWCNTs is driven by several intermolecular forces. The surface lattice of SWCNTs is composed of sp2-hybridized carbons, which results in a highly hydrophobic and aromatic surface that is prone to self-association and aggregation in aqueous solutions, such as those that commonly comprise biological environments.

* Portions of this chapter are adapted from Chio, L., Yang, D., and Landry, M. P., Surface Engineering of Nanoparticles to Create Synthetic Antibodies, Thomas Tiller (ed.), *Synthetic Antibodies: Methods and Protocols*, Methods in Molecular Biology, vol. 1575. Written permission was obtained from the co-authors: Darwin Yang and Markita Landry.

Noncovalent attachment is used to create molecular recognition elements, but has the additional advantage of making SWCNTs suitable for biological applications through the addition of hydrophilic groups that stabilize SWCNTs in aqueous solution. In order to obtain a hydrophilic surface, noncovalent strategies utilize amphiphilic coatings such as polymers, phospholipids, and surfactants.

SWCNT nanosensors are assembled from SWCNTs and an amphiphilic coating through several methods capable of disrupting the strong self-associations of SWCNTs. One common method is ultrasonication where high-energy sound waves are used to unbundle SWCNTs and subsequently allow amphiphilic coatings to passivate the individualized SWCNTs. Ultrasonication is a fast method of SWCNT nanosensor assembly that requires only a few minutes of treatment, and gives high yields of SWCNT nanosensors. However, ultrasonication could damage some amphiphilic coatings, such as fragile polymers or proteins, through chemical degradation and mechanical shearing.[49] Other methods first require dispersion using ultrasonication in a surfactant that colloidally stabilizes the SWCNTs, followed by exchange with the desired final amphiphilic coating. One way to drive this exchange is through dialysis, a method in which surfactant-coated SWCNTs and the desired amphiphilic coating are placed in a size exclusion membrane. The pore size of the membrane is chosen so that surfactant is capable of passing through, but SWCNTs and the amphiphilic coating are trapped within the membrane and has time to associate. Another method for surfactant-to-coating exchange is driven by solvent exchange. The critical micelle concentration of surfactants, the concentration at which the surfactant can form micelles, changes in different solvents based on polarity and other intermolecular forces. The addition of a polar solvent, such as ethanol or methanol, will dilute and destabilize the surfactant on the SWCNT surface allowing for passivation by the amphiphilic coating. Exchange methods are more gentle compared to ultrasonication, and have shown success in the addition of proteins and DNA to SWCNT surfaces.[34,50–52] However, exchange methods give lower nanosensor yields as compared to ultrasonication, and these protocols are more time-consuming and take several days. These exchange protocols have the potential for optimization, and in one case, Streit et al. was able to show high yields and a quick protocol time of several minutes through the use of methanol driven exchange between sodium cholate-coated SWCNTs with DNA polymers.[53] In all assembly methods, the resultant SWCNT suspension can be purified of any nonfluorescent SWCNT bundles through centrifugation, since the heavier unfunctionalized bundles can be precipitated out of solution. The appropriate method of nanosensor assembly can be chosen based on the robustness of the amphiphilic coating utilized.

Typically, noncovalently functionalized SWCNT nanosensors are created and validated using two approaches: (1) library screening and (2) rational design of molecular recognition elements (Fig. 2.2). Both approaches have advantages and disadvantages that are highlighted below.

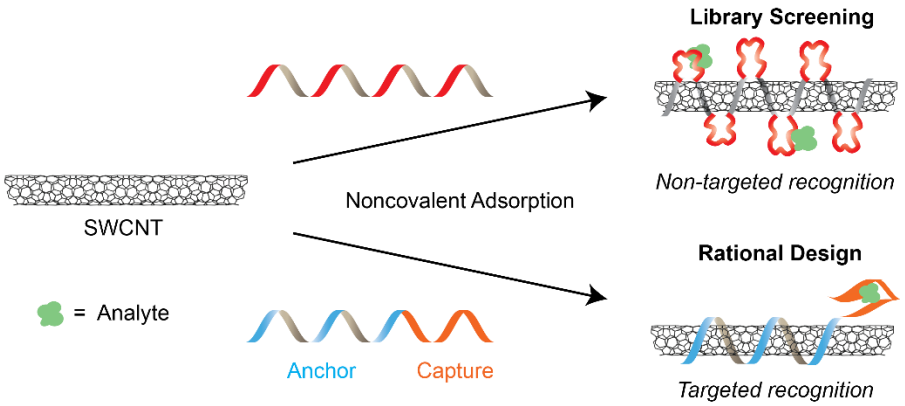

Figure 2.2: Noncovalent Strategies for Molecular Recognition Development.

There are two main methods for the creation of noncovalent molecular recognition on the surface of SWCNTs: (1) library screening and (2) rational design of polymers to include an anchor and capture region.

Library screening for protein nanosensors provides a robust technique capable of uncovering novel molecular recognition elements. This method requires the development of a candidate nanosensor library, followed by screening of candidate nanosensors against a library of analytes (screening validation is addressed in section 2.4). A candidate nanosensor library can comprise of SWCNT surface-engineered with different polymers such as polynucleic acids, synthetic peptides and peptoids, amphiphilic heteropolymers, surfactants, and functionalized phospholipids. In order to validate a selective and responsive nanosensor, a broad range of SWCNT constructs needs to be screened. This method has yielded successful nanosensors for neurotransmitters,[35] vitamins and metabolites,[33] drugs,[54] peptides,[36] and proteins.[48] The selectivity of these varied SWCNT nanosensors is created through a phenomenon termed corona phase molecular recognition (CoPhMoRe). CoPhMoRe nanosensors have molecular recognition elements created by the unique constrained surface conformation of the coating on the SWCNT lattice, and so nanosensors could be generated with no prior knowledge of the intermolecular interactions between the SWCNT nanosensor and the target analyte. This method could allow for the creation of nanosensors for analyte that do not have any known molecular recognition elements. However, library screening is often hampered by inefficient workflow in creating novel SWCNT nanosensors as the synthesis and screening of amphiphilic coatings is time-consuming and requires many costly materials.

Recently, SWCNT nanosensor library screening is being expedited and diversified using inspiration from previously implemented library screens. High-throughput methods are often utilized for the discovery of novel chemical reactivity in enzymes by directed evolution and the development of protein recognition elements using nucleotide sequences, called aptamers, through systematic evolution of ligands by exponential enrichment (SELEX).[55,56] Here large libraries are screened and enriched for a desired trait, which allows for the narrowing of the library in subsequent rounds towards the best hit. Several expedited library screens for SWCNT nanosensors involve the use of DNA polymers, as DNA is one of the most characterized systems for noncovalent SWCNT nanosensors and has a wide-array of techniques and instrumentation available for replication and analysis. The advent of new technologies like next-generation sequencing, in which millions of DNA sequences can be amplified, read, and identified through barcoding, has enabled the discovery of a DNA-SWCNT nanosensor for the neurotransmitter serotonin using a high-throughput library screening process termed SELEC.[57] Similarly, the optoelectronic properties of SWCNTs can also be optimized using a directed evolution screening

approach and DNA-coated SWCNTs were enriched for greater fluorescence intensity.[58] The generation of large polymer libraries for nanosensor development also leads to better understanding of design rules for nanosensor creation. These large datasets are being used to inform the novel design of nanosensors, and machine learning has been utilized to predict SWCNT recognition DNA sequences.[59]

Design-based engineering of nanosensors involves the tethering of known molecular recognition elements to SWCNT surfaces. This is accomplished noncovalently through the attachment of a coating, typically a polymer, with separate anchor and capture domains. Anchor domains must be capable of adsorbing to the surface of the SWCNT often through hydrophobic or π-stacking interactions. The strength of the interaction between the anchor and the SWCNT surface can be examined through several fluorescence assays that can track the perturbation of the anchor.[60,61] Capture domains are typically chosen for predetermined molecular recognition properties to a desired analyte. Some examples of design-based SWCNT nanosensors include aptamer-anchor sequences for RAP1 GTPase protein and HIV integrase proteins, as well as mRNA complementarity probes for diseases like HIV.[46,62,63] An anchor-capture strategy has also been utilized for the conjugation of recognition elements such as antibodies to anchor-coated DNA-SWCNT nanosensors.[44,45] Design-based strategies can also be used in series through a layer-by-layer method that allows for the creation of SWCNT nanosensors through the layering of His-tagged proteins and ligand-receptor affinity pairs, such as protein A and IgG antibodies.[64–67] This method is advantageous over a screening approach in that it leverages specific coatings with predetermined affinities for protein analytes, and as such requires a smaller polymer and analyte library at the onset.

Noncovalent strategies can be robustly applied to any analyte of interest since it has the capability to generate novel binding domains or take advantage of known molecule recognition elements.
The main disadvantage with utilizing noncovalent strategies for the creation of molecular recognition elements is stability. Noncovalent coatings are susceptible to desorption from the SWCNT surface when placed in complex biological environments that is driven by a variety of environmental factors including ionic strength, buffer composition, and pH.[68,69] Desorption can also be driven by proteins in blood plasma, leading to the inactivation of constructs that are validated *in vitro* to be ineffective *in vivo*.[61]

2.3 Covalent Strategies for Nanosensor Molecular Recognition Development

Covalent strategies provide a stable covalent bond between the SWCNT surface and molecular recognition elements. In this method, SWCNT nanosensors are stable against surface desorption of the recognition elements. Additionally, this method can utilize known molecular recognition elements, such as aptamers, ligands, and antibodies, and enable the modular creation of SWCNT protein nanosensors.

The covalent functionalization of SWCNTs is well studied, but only recently has it become a viable strategy for the development of molecular recognition elements for optical sensing. A survey of SWCNT literature reveals different surface functionalization of SWCNTs with a variety of functional groups by nucleophilic addition, oxidation, ozonation, alkylation, hydrogenation, cycloaddition, carbene addition, and radical addition.[70] However, due to the stable structure of

SWCNTs (it is known for having stronger tensile strength than steel!),[71] reactions to add functional groups to the SWCNT lattice requires lengthy protocols, dangerous chemicals, and the creation of many defects along the sidewall.[72] Breaking the pristine SWCNT lattice through the addition of covalent bonds typically leads to the formation of new routes for nonradiative decay of excitons and the subsequent loss of intrinsic SWCNT fluorescence.[73]

Several covalent methods have been shown to preserve SWCNT fluorescence. The endcaps of carbon nanotubes are more sterically strained and thus, are more reactive. Upon mechanical stress through probe-tip ultrasonication, SWCNT endcaps can open up and react with reactive oxygen species generated by the concentrated heating from the probe-tip on the local aqueous solution to create carboxyl functional groups.[74] These functional groups can be further reacted to create junctions between nanotubes or with other moieties, such as quantum dots to create molecular nanosensors.[75,76] However, these covalent handles are localized only to the ends of SWCNTs and provide low density of labeling. Other methods are capable of adding substituents along the entire SWCNT sidewall at higher functional group densities. One method involves the controlled addition of sp3 defects that reside at an energy level lower than the predicted energy level of dark exciton states that quench fluorescence (Fig. 2.3a).[77] The tunable addition of aryl and alkyl defects leads to the creation of defect fluorescence often redshifted from the original fluorescence profile.[78] Another method is through the use of diazonium salts to perform a 1,2-cycloaddition capable of subsequent ring-closing and rearomatization that maintains the pristine SWCNT surface lattice (Fig. 2.3b).[79] This closing of the sidewall defect results in a covalently functionalized SWCNT that maintains its intrinsic NIR fluorescence.

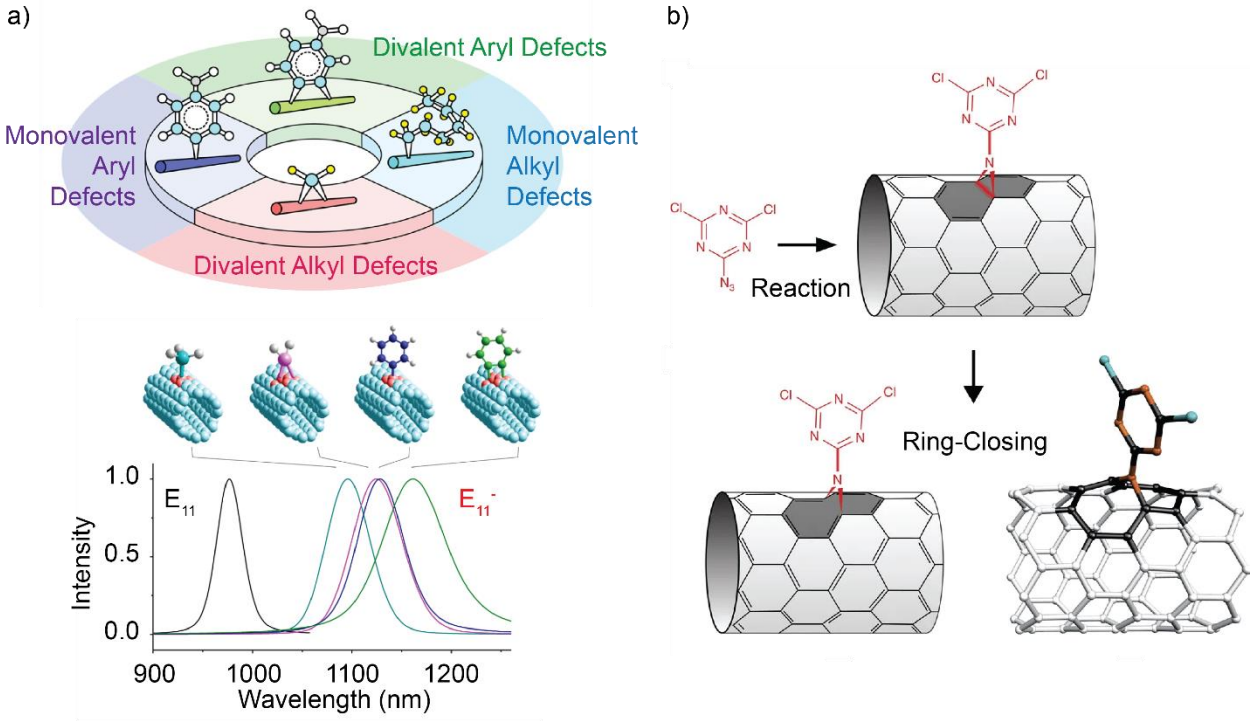

Figure 2.3: Covalent Strategies for Molecular Recognition Development.

a) The introduction of sp3 alkyl and aryl defects at a lower energy level than dark exciton levels result in red-shifted defect emission. Intrinsic fluorescence is denoted E_{11} and the defect fluorescence is denoted E_{11}^{-}. Figure

was adapted with permission from J. *Am. Chem. Soc*. 2016, 138, 21, 6878-6885 (https://pubs.acs.org/doi/10.1021/jacs.6b03618); further permissions related to the material excerpted should be directed to the American Chemical Society. b) Through the addition of a diazonium cyanuric chloride salt, functional handles can be added to the SWCNT surface that rearomatizes to preserve native SWCNT lattice and intrinsic fluorescence. Figure was adapted with permission from Setaro, A., *et al.* Preserving π-conjugation in covalently functionalized carbon nanotubes for optoelectronic applications. *Nat Commun* **8,** 14281 (2017). https://doi.org/10.1038/ncomms14281

At the moment, these covalent methods require further validation for the addition of molecular recognition elements through chemical conjugation. Many existing molecular recognition elements are antibodies, enzymes, and ligands that are amenable to mild bioconjugation reactions.[80] Most of the alkyl and aryl substituents verified for use in defect engineering are long hydrocarbon chains that are not compatible with bioconjugation techniques. The 1,2-cycloaddition is capable of the addition of several functional groups widely utilized in bioconjugation including thiols, primary amines, and carboxylic acid groups. As explored in this dissertation, there is an opportunity to utilize a variety of existing molecular recognition elements for the creation of optical protein nanosensors.

Covalent strategies are robust techniques that can allow the anchoring of molecular recognition elements directly to the SWCNT surface. This can lead to a modular toolbox in which multiple ligands and coatings can be pinned to the SWCNT lattice simultaneously. However, covalent strategies currently are incapable of dispersing SWCNTs in solution independently without the use of a noncovalent coating. This is presumably due to the lack of control of the density of functional groups along the SWCNT sidewall that future investigation might enable.

2.4 Validation of Nanosensor Activity

Candidate nanosensors created through noncovalent and covalent strategies require validation against analytes of interest. As mentioned previously, SWCNTs are sensitive to changes to their surface electronic properties and exhibit a change in fluorescence upon binding of an analyte. The optical sensing of particular analytes can be validated and visualized using NIR spectroscopy and microscopy and requires equipment capable of detecting NIR fluorescence. The NIR region of the electromagnetic spectrum includes wavelengths from ~900 - 1500 nm. Typical silicon detectors found in conventional charge coupled devices are only capable of detecting wavelengths from ~200 - 1100 nm.[81] For NIR spectroscopy and imaging, indium gallium arsenide (InGaAs) detectors that are cryogenically cooled are suitable for fluorescent detection in this range. A schematic of the optical set-up used in our experiments capable of dual microscopy and spectroscopy is depicted below (Fig. 2.4).

If there is successful binding of the SWCNT nanosensor to the analyte of interest, there will be a measurable fluorescence modulation. This modulation could be observed as an increase or decrease of the magnitude of fluorescence intensity or a solvatochromic wavelength shift. Although the cause of this fluorescence modulation is still under investigation and not easily predicted, there are several proposed mechanisms: (i) Fermi level shifting via redox-active analyte adsorption to the nanotube surface, (ii) quenching induced by exciton disruption in response to analyte binding (iii) solvatochromic shifting due to perturbation of a SWCNT-bound coating, (iv) selectivity of analyte binding mediated by the coating, (v) analyte-activated coating switching

resulting in intensity and/or wavelength modulation.[82] These fluorescence modulations should be reproducibly measured and have a signal greater than the noise of the detector.

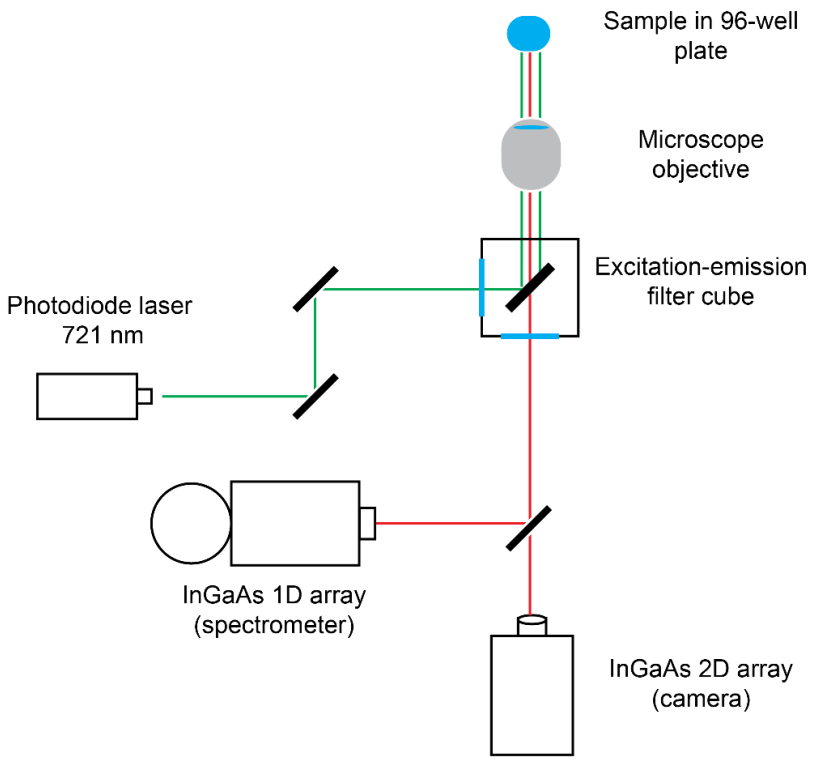

Figure 2.4: Schematic for NIR Spectroscopy and Microscopy.

NIR spectroscopy and microscopy are utilized to validate nanosensor response. In this set up, samples are excited with a 721 nm photodiode laser. NIR light emitted from the sample is passed through a long-pass filter and collected using an InGaAs spectrometer or camera to reconstruct fluorescence spectra or images, respectively.

A successful SWCNT nanosensor is one that is sensitive and selective towards the desired analyte, as well as stable in the applicable biological environment. For sensitivity, the physiological concentration range of the analyte must be tested. Often times, this concentration range is difficult to ascertain as the physiological concentration of analytes in the body are often reported as the average concentration in blood serum. It is believed that the local concentration of protein analyte will be more concentrated than this reported number, especially when looking at cellular protein efflux events confined between cells. Using NIR microscopy, it has been possible to track single-molecule release events of excreted proteins and neurotransmitters between cells immobilized on a nanosensor-passivated glass slide.[46,83] For selectivity, the nanosensors must be tested against a panel of small molecules, peptides, and proteins that might also be in the presence of the desired analyte. For example, a SWCNT nanosensor for dopamine needs to be validated for selectivity against other neurotransmitters and metabolites in the region such as serotonin, norepinephrine, and glutamate.[35] Similarly, the nanosensor must be tested against structural analogues of the desired analyte to show selectivity. Finally, the nanosensor must be tested in relevant biological environments, such as cell growth medium, whole human plasma, or *in vivo*, to determine nanosensor stability. Studies have shown that the behavior of a nanoparticle tested *in vitro* could

vastly differ from its behavior *in vivo* due to the adsorption of plasma proteins or the destabilization of the nanoparticle surface.[84]

2.5 Troubleshooting Nanosensor Molecular Recognition Design

Successful implementation of noncovalent and covalent strategies for SWCNT nanosensor creation requires careful choice of development method and validation, but there are common issues that could arise during nanosensor development and implementation that this section seeks to troubleshoot. The activity of molecular recognition elements used for noncovalent rational design or covalent attachment could strongly depend on their structural conformation, and attachment to SWCNT surfaces could disrupt this property. Additionally, sensitive nanosensors might suffer from a lack of selectivity or be difficult to image due to shifting background noise. This section discusses some strategies to combat these issues through structural preservation strategies for molecular recognition elements and ratiometric sensing.

Preservation of Molecular Recognition Element Structural Conformation

The sensitivity and selectivity of SWCNT nanosensors could strongly depend on the structural conformation of molecular recognition elements. For example, an aptamer is dependent on its secondary structure to exploit various binding mechanisms such as hydrophobicity, molecular shape complementarity, or the intercalation of small molecules to double-stranded nucleotide regions.[85] Similarly, the function of proteins, such as enzymes and antibodies used for molecular recognition, are directly dependent on their tertiary structures. The active site of enzymes and the variable regions of antibodies are particularly important for the substrates and epitopes that they interact with, respectively.[86] To take advantage of these existing molecular recognition elements, it is important to preserve their structural conformation.

Proximity to the hydrophobic SWCNT surface could lead to the destabilization and unfolding of these molecular recognition elements, as well as impact the orientation of these structures. The hydrophobic cores of enzyme active sites, such as that found in horseradish peroxidase, are found to preferentially interact with SWCNT surfaces and reduce enzyme activity.[52] Raman spectroscopy was able to detect the denaturation of lysozyme on SWCNT as well.[87] Site directed modifications can be employed to preserve nucleotide aptamer and protein-based molecular recognition elements (Fig. 2.5a). In this method, the attachment of the molecular recognition element can be directed to a region far from the binding domain.

There are several strategies unique to the preservation of aptamer molecular recognition elements. The application of heat to misfolded aptamer on SWCNT surfaces could provide enough energy to drive the proper folding of the aptamer.[88] Nucleotide-based nanosensors are also able to take advantage of nucleotide hybridization. Nanosensors can be developed through the initial attachment of an anchor sequence to the SWCNT surface followed by hybridization with a complementary stem attached to an aptamer molecular recognition element. Atomic force microscopy has been used to show that hybridized nucleotides are peeled back from the SWCNT surface and add distance from the SWCNT lattice.[63] This extra distance could allow for the proper folding and subsequent activity of the aptamer. Similarly, a spacer domain can be added to the nucleotide sequence between the anchor and the capture domains to improve activity as in the case of a thrombin-aptamer-anchor SWCNT nanosensor.[46] Interestingly, it is shown that there is an

optimal distance between the aptamer and the SWCNT surface, for when too many spacers were added and the aptamer is too far from the surface the nanosensor response was attenuated.

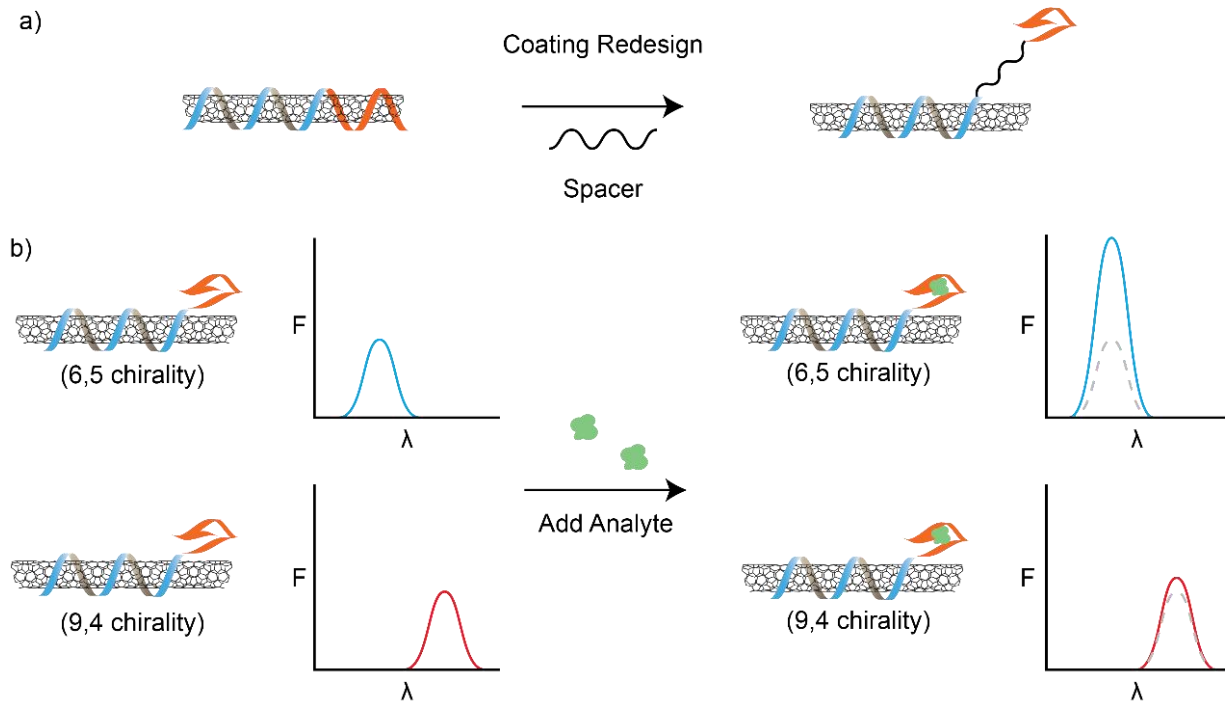

Figure 2.5: Troubleshooting SWCNT Nanosensors.

a) The loss of proper conformation for molecular recognition elements can impact nanosensor interaction with analyte. Several strategies can be implemented to solve this issue, such as site-specific engineering of the recognition element through the addition of a molecular spacer between the recognition element and the SWCNT surface. b) To safeguard against false responses and to provide a reliable background signal, ratiometric sensing deploys two chiralities of SWCNT with differential response to an analyte. In this case the (6,5) chirality of SWCNT shows an increase in fluorescence upon binding analyte that is absent for the (9,4) chirality of SWCNT. The ratio of these change in fluorescence will determine the presence of an analyte. Although the figure depicts noncovalently functionalized SWCNT, these methods are general to all nanosensors.

Site-specific modifications can ensure the correct conformation of protein and peptide molecular recognition elements on SWCNT surfaces as well. A spacer can be conjugated to the N-terminus of peptide sequences or to specific amino acids to prevent denaturation on the SWCNT surface. For larger proteins, site-directed mutagenesis can be utilized to promote modification at specific regions that will not impact function, such as on the Fc stem region of an antibody far from the variable binding region or on the surface of an enzyme away from the active site.[89]

Ratiometric Sensing to Improve Signal-to-Noise of Measurements

If the design strategies above produce a nanosensor that is highly sensitive but not selective to a desired analyte, a ratiometric detection strategy can be developed. This approach has been successfully implemented in the *in vivo* detection of nitric oxide and hydrogen peroxide.[34] A SWCNT nanosensor can be created using a ratio of two distinct fluorescence peaks from SWCNT chiralities with different emission wavelengths. Chiralities of SWCNT should be chosen so that there is no overlap in emission wavelengths (refer to Appendix I to choose proper chiralities). For example, the (6,5)-SWCNT chirality emits at ~970 nm and the (9,4)-SWCNT chirality emits at

~1110 nm. A ratiometric relationship between the signal of different chiralities can provide additional information about the system by monitoring one signal as invariant to the analyte and the second signal as responsive to the analyte. Ratiometric monitoring can also eliminate baseline noise of biologically complex sensing environments. While some chirality-purified SWCNTs are available commercially, they can also be prepared in the laboratory from a mix-chirality SWCNT sample through methods including density centrifugation, column chromatography, and aqueous two-phase separation.[90–93]

Chapter 3: Electrostatic-Assemblies of Single-Walled Carbon Nanotubes and Sequence-Tunable Peptoid Polymers Detect a Lectin Protein and its Target Sugars[†]

3.1 Abstract

A primary limitation to real-time imaging of metabolites and proteins has been the selective detection of biomolecules that have no naturally-occurring or stable molecular recognition counterparts. We present developments in the design of synthetic near-infrared fluorescent nanosensors based on the fluorescence modulation of single-walled carbon nanotubes (SWCNT) with select sequences of surface-adsorbed *N*-substituted glycine peptoid polymers. We assess the stability of the peptoid-SWCNT nanosensor candidates under variable ionic strengths, protease exposure, and cell culture media conditions, and find that the stability of peptoid-SWCNTs depends on the composition and length of the peptoid polymer. From our library, we identify a peptoid-SWCNT assembly that can detect lectin protein wheat germ agglutinin (WGA) with a sensitivity comparable to the concentration of serum proteins. To demonstrate the retention of nanosensor-bound protein activity, we show that WGA on the nanosensor produces an additional fluorescent signal modulation upon exposure to the lectin's target sugars, suggesting the lectin protein remains active and selectively binds its target sugars through ternary molecular recognition interactions relayed to the nanosensor. Our results inform design considerations for developing synthetic molecular recognition elements by assembling peptoid polymers on SWCNTs, and also demonstrate these assemblies can serve as optical nanosensors for lectin proteins and their target sugars. Together, these data suggest certain peptoid sequences can be assembled with SWCNTs to serve as versatile optical probes to detect proteins and their molecular substrates.

3.2 Introduction

This chapter discusses the use of a noncovalent strategy through the development of peptoid polymer coatings for the creation of SWCNT protein nanosensors with chemically diverse molecular recognition elements. In order to reorient the reader, we start with a brief introduction on the use of SWCNT as nanosensors, previous examples of polymer-coated nanosensors, and peptoid polymers.

Single-walled carbon nanotubes (SWCNTs) have emerged as promising signal transduction elements for molecular imaging owing to their relatively tissue-transparent optical properties, photostability, low toxicity when functionalized, and nanometer size.[27,31,94] SWCNTs exist in many distinct chiralities described by the chiral vector of the carbon lattice which dictates the SWCNT fluorescence excitation and emission wavelength, making SWCNTs suitable for ratiometric detection.[22,92] SWCNTs notably fluoresce through exciton recombination in the near-

[†] Reprinted (adapted) with permission from *Nano Lett.* 2019, 19, 11, 7563-7572. Copyright 2019 American Chemical Society. Permission was obtained from supporting authors: Jackson Travis Del Bonis-O'Donnell, Mark A. Kline, Ian R. McFarlane, Ronald N. Zuckermann, and Markita P. Landry.

infrared (NIR), a region of the electromagnetic spectrum following visible wavelength photon scattering by biological tissues, but prior to absorption of photons by water.[26,95] This NIR window exhibits minimal photon attenuation, suitable for deep tissue bio-imaging applications.[96] Pristine SWCNTs exhibit a hydrophobic π-conjugated surface lattice and require polymer or surfactant encapsulation for both colloidal stability and for exciton radiative recombination-based NIR fluorescence. This NIR fluorescence is sensitive to the SWCNT local dielectric environment and charge transfer.[21,94] Several mechanisms have been proposed for the fluorescence modulation of SWCNT including Fermi level shifting through redox-active analyte adsorption, exciton disruption in response to analyte binding, solvatochromic shifting due to perturbation of the polymer wrapping, and analyte-activated polymer-switching.[82]

The encapsulation of SWCNTs with biomolecules and biopolymers can therefore serve a dual purpose of conferring biocompatibility, but can also enable molecular recognition for biological analytes of interest. In particular, SWCNTs can be functionalized to be selective and sensitive optical nanosensors via surface adsorption by polymers with a method known as corona phase molecular recognition (CoPhMoRe).[97] In this technique, polymers are electrostatically pinned to the surface of the SWCNT and adopt a specific conformation that can bind and optically recognize a small molecule via selective modulation of the SWCNT exciton recombination rate (intensity change), or band-gap (wavelength shift).[98] To date, polymer-SWCNT nanosensors have been created with DNA oligomers, peptides, and fluorescein-, rhodamine-, or carbodiimide-derived polymers as the nanosensor corona phase.[33,35,46,63,99,100] These polymer-SWCNT nanosensors have been successful in the detection of DNA hybridization, neurotransmitters, vitamins, cellular metabolites, and proteins. However, detection of proteins remains a challenging task, owing to the complexity of these larger analytes. Several methods exist in which recognition is conferred through a His-tagged capture protein grafted to a chitosan-wrapped SWCNT microarray or through an antibody tethered to polymer-SWCNT through bioconjugation.[44,45,101] These methods rely on the naturally-occurring molecular recognition of capture proteins and antibodies involved in protein detection. Conversely, SWCNT CoPhMoRe is an attractive synthetic platform that does not rely on biologically-derived molecular recognition elements for optical detection of protein analytes, with Rap1, HIV-1, fibrinogen, and insulin protein SWCNT-based CoPhMoRe nanosensors developed recently.[36,46,48]

Of the polymers leveraged for SWCNT nanosensor design, biopolymers such as polynucleotides and peptides are often preferred owing to sequence tunability with which they can be synthesized or produced by bio-organisms. However, polynucleotides and peptides are susceptible to enzymatic degradation by nucleases or proteases, respectively, and as such their conditional stability limits long-term use in complex biological systems. Conversely, synthetic polymers may require lengthy synthesis and are difficult to control in terms of sequence, length dispersity, and structural tunability. Furthermore, both biopolymers and synthetic polymers are limited by a lack of monomer sets for creating chemical diversity. Therefore, future advancements in the area of synthetic protein nanosensors will require generation of biomimetic polymers amenable to facile synthesis, with a large monomer space, which are also resistant to enzymatic degradation. To this end, herein we synthesize a library of peptoids, *N*-substituted glycine polymers, to serve as protein molecular recognition elements when adsorbed on SWCNT surfaces. Peptoids are sequence-defined synthetic polymers that draw inspiration from peptides, the building blocks of proteins, with synthesis that is amenable to robotic automation and a large monomer space of primary

amines.[102] Peptoids are created through stepwise solid phase submonomer synthesis with high sequence specificity and can include a wide variety of non-proteinogenic chemical functionalities such as alkynes, glycosylation, and fluorophores.[103–105] Peptoids are resistant to proteases and can remain stable in the body for day-long timescales.[106] Recently, peptoids have been shown to self-assemble into supramolecular nanosheets that are capable of specific multivalent interactions with enzymes and proteins such as kinases, lectins, and Shiga toxin.[107,108] Because peptoids are designable and tunable proteomimetic materials, they are well suited to address the current need of chemical diversity of SWCNT polymer coronas.[109]

We present the development of peptoid polymer-SWCNT (peptoid-SWCNT) assemblies and their characterization for implementation as protein nanosensors. We first investigate the primary interactions of the peptoid polymer with SWCNT, and present our findings on the stability of these peptoid-SWCNT assemblies upon exposure to long-term laser illumination, variable solution ionic strength conditions, complex biological media, and proteases. We next show that certain peptoid-SWCNT assemblies can serve as nanosensors through secondary interactions to enable moderately selective and sensitive WGA lectin protein detection. We further show that these peptoid-SWCNT nanosensors have the capacity for ternary analyte interaction and detection, where the WGA protein tethered to the nanosensor can in turn detect WGA's target sugars. Our work informs key design parameters for the noncovalent adsorption of peptoids with SWCNT and their development as molecular recognition elements for protein detection and ternary analyte interactions.

3.3 Experimental

Materials Reagents were purchased from Sigma-Aldrich, unless otherwise noted. Wheat germ agglutinin (lectin from *Triticum vulgaris* (wheat)), peanut agglutinin (lectin from *Arachis hypogaea* (peanut)), and concanavalin A (from *Canavalia ensiformis* (Jack bean), Type VI) were purchased from Sigma Aldrich as lyophilized powder from plant sources as indicated in parenthesis. Peptoid oligomers were synthesized on a Symphony X Synthesizer using the solid-phase submonomer method and purified by preparative reverse-phase HPLC, as previously described.[102] Beta-alanine tert-butylester hydrochloride was purchased from Chem-Impex International. 2-(2-(2-methoxyethoxy)ethoxy)-ethylamine was purchased from Peptide Solutions, Inc. All reagents were used without further purification. Raw HiPco single-walled carbon nanotubes were purchased from NanoIntegris. Neutravidin protein, Gibco Dulbecco's Modified Eagle Medium, and Gibco Fetal Bovine Serum was purchased from Thermo Fisher Scientific. Trypsin gold was purchased from Promega. Proteinase K was purchased from New England Biosciences.

FRET Binding Assay for Detecting WGA-Peptoid Interactions
The interactions between WGA and the ProLoop WGA-binding peptoid was validated using a FRET assay as previously described.[108] Briefly, nanosheet-forming peptoids with L016 loops were placed solution with 5 μM BODIPY-FL C16 and self- assembled by a rocking machine (rocking number was ∼250 and the waiting time per rock was 10 s). Subsequently, the BODIPY-FL C16 incorporated peptoid nanosheets were mixed with the Alexa647-conjugated protein solutions at the following final concentrations: 10 mM nanosheets, 2.5 mM BODIPY-FL C16, and 250 nM Alexa-conjugated proteins in 25 mM phosphate buffer, 150 mM NaCl, pH 7.4.

Analytical High Performance Liquid Chromatography of Peptoid
Purified peptoids were analyzed using analytical HPLC to determine the relative polarity of the peptoid sequences. An eluent gradient of A (0.1% TFA, v/v in water) and B (0.1% TFA, v/v in acetonitrile) was utilized. The sample was run at 1 mL/min with a gradient of 5-95% B in 20 min and UV detection at 214 nm.

Peptoid-SWCNT Adsorption
Adsorption of SWCNT with peptoid was achieved using a protocol previously described.[110] Briefly, 1 mg of SWCNT was added to 500 μL of buffer (50 mM borate buffer pH 9.2, 1X buffered saline pH 7.4, or 100 mM acetate buffer, as specified in the main text) and 100 nmol of peptoid. The solution was bath sonicated for 10 minutes, and then probe-tip sonicated using a Cole Parmer ultrasonic processor with pulses of 3-7 watts every 3 seconds for 5 minutes. The solution was subsequently allowed to equilibrate at the bench for 1 hour before centrifugation at 16.1 x 10^3 Relative Centrifugal Force (RCF) for 30 minutes to remove any unsuspended nanotube aggregates. Assemblies were dark gray in color and concentration was characterized by UV-Vis-IR absorbance using a Shimadzu UV-3600 Plus. SWCNT concentration is calculated from absorbance at 632 nm using Beer-Lambert law with extinction coefficient, ε_{632} = 0.036 L mg^{-1} cm^{-1}.[95]

NIR Spectroscopy of Peptoid-SWCNT Assemblies
All peptoid-SWCNT nanosensor solutions were diluted to a final SWCNT concentration of 5 mg L^{-1} in PBS. Spectroscopic analysis was performed by measuring the resulting SWCNT photoluminescence with a home-built near infrared fluorescence microscope. Briefly, a Zeiss AxioVision inverted microscope was coupled to a Princeton Instruments IsoPlane 320 containing a liquid nitrogen-cooled Princeton Instruments PyLoN-IR 1D InGaAs array. The spectra of peptoid-SWCNT samples were acquired, each in a separate well of a glass-bottom 384-well plate (Corning). Peptoid-SWCNT assemblies were illuminated by a 500 mW, 721 nm laser with an exposure time of 10 s, reaching a sample equilibrium temperature of 37 ºC and a final power of 77 mW at the sample plane. All fluorescence spectral analysis was conducted using the (7,6) chirality emission peak, which is in high abundance in our SWCNT samples.

Temperature Equilibration Experiments
NIR fluorescence measurements of 5 mg L^{-1} peptoid-SWCNTS were performed with illumination by a 721 nm, 500 mW laser. We measured the temperature of a 30 μL sample well in a 384-well Corning glass bottom plate with continuous laser illumination over 60 minutes, representing the standard time-course of our peptoid-SWCNT fluorescence assays, using a FLIR thermal camera. Temperature measurements were taken every 10 minutes, with additional timepoints taken at 30 seconds and 1 minute.

Atomic Force Microscopy of Peptoid-SWCNT Nanosensors
Monodispersed peptoid-SWCNT nanosensors were analyzed with atomic force microscopy using an Asylum Research MFP-3D AFM and TAP150AL-G-10 Silicon AFM probes (Ted Pella, tip radius < 10 nm). 20 μL of peptoid-SWCNT assemblies (20 mg L^{-1}) in PBS were deposited on freshly cleaved mica, and incubated for 1 hour at room temperature. Unbound nanosensors and salts were washed from the mica 3 times using MilliQ water. For AFM of protein on nanosensors, ProLoop-SWCNT nanosensors (20 mg L^{-1}) were incubated with 10 μM WGA for 1 hour and the samples were next deposited on freshly cleaved mica and incubated for an additional hour.

Unbound nanosensors, salts, and proteins were washed 3x with MilliQ water prior to AFM imaging. AFM was performed at a scan rate of 1 Hz using a sample rate of 256 lines.

Proteolysis Tests with Peptoid-SWCNT

Peptoid-SWCNT assemblies were diluted to a final concentration of 5 mg L^{-1}. Trypsin or proteinase K was added to the peptoid-SWCNT assembly solutions to a final concentration of 1 mg mL^{-1} and 2 mg mL^{-1}, respectively. The solutions were incubated at room temperature and NIR spectra were collected 3 hours and 24 hours following the addition of protease. The fluorescence spectra were compared with a control where buffer only was added to the peptoid-SWCNT sample.

Protein Screening Experiments with Peptoid-SWCNT Nanosensors

Peptoid-SWCNT nanosensors were diluted to a final working concentration of 5 mg L^{-1}. 27 μL of nanosensors were pipetted into each well of a 384-well glass-bottom plate and initial fluorescence spectra were recorded using NIR spectroscopy as detailed above. 3 μL of protein was added by pipetting to final protein concentrations as denoted in the manuscript, and fluorescence spectra were taken every 10 minutes following the addition of protein.

NIR Microscopy of Peptoid-SWCNT Nanosensors

Peptoid-SWCNT nanosensors are immobilized on a Mattek microwell dish with a 1.5 coverslip. The 1.5 coverslip surface was treated with 3-aminopropyltriethoxysilane (APTES) diluted to 10% (m/v) APTES in ethanol to create a positively charged surface onto which the nanosensors could immobilize. 100 μL of APTES solution was incubated on the coverslip for 2 minutes and followed by 3 washes with 1x PBS. 100 μL of peptoid-SWCNT (20 mg L^{-1}) was incubated on the surface for 5 minutes, and followed by 3 washes with 1x PBS to rid the surface of unbound nanosensors. Single peptoid-SWCNT nanosensors were excited with a 500 mW, 721 nm laser with a final power of 77 mW at the objective, and imaged using a ZEISS α Plan-APOCHROMAT 100x oil immersion objective (numerical aperture (NA) = 1.46) on a Zeiss AxioVision inverted microscope coupled to a Princeton Instruments NIRVana 640 InGaAs camera. Regions of interest were identified around areas where initial fluorescence was over 5-fold the fluorescence of the background.

Detection of Wheat Germ Agglutinin Protein in Cell Media

Peptoid-SWCNT nanosensors were diluted in Gibco Dulbecco's Modified Eagle Medium or Gibco Fetal Bovine Serum to a SWCNT concentration of 5 mg L^{-1}. The nanosensors were allowed to equilibrate for 2 hours before spectroscopy using the NIR spectrometer as described above. WGA was added to the well to a final concentration of 10 μM.

Detection of Sugars Using Peptoid-SWCNT Nanosensors

Peptoid-SWCNT nanosensors were diluted to a SWCNT concentration of 5 mg L^{-1} in PBS. Wheat germ agglutinin protein was added to the nanosensors to a final concentration of 10 μM, and the nanosensors were allowed to equilibrate for 1.5 hours before spectroscopy using the NIR spectrometer described above. 1 mM final concentration of sugar was added to each well and spectra were acquired every 10 minutes for 1 hour.

Surfactant-Induced Solvatochromic Shift of Peptoid-SWCNTs

Peptoid-SWCNT nanosensors were diluted to a SWCNT concentration of 5 mg L^{-1} in PBS and imaged with NIR fluorescence spectroscopy as detailed above. NIR fluorescence spectra of 27 μL

peptoid-SWCNTs were acquired every 10 minutes for 30 minutes before and after the addition of 3 μL 5% (w/v) sodium cholate for a final 0.5% (w/v) concentration of sodium cholate.

Spectral Deconvolution

Fluorescence spectra were deconvoluted using a MATLAB script previously discussed in reference 16 in the main text. Briefly, the photoluminescence of each chirality peak is estimated as a Lorentzian and the sum of the chiralities' Lorentzians was compared to the full fluorescence spectrum and optimized using least squares.

3.4 Results and Discussion

Peptoid Polymer Design for Surface Adsorption to SWCNT

Peptoid polymers are created with an automated submonomer approach that provides ease of synthesis and control over polymer length and sequence (Scheme 3.1).[111] The chemical sequence of the peptoid is dictated by the selective order in which variable side chain groups are added to the growing peptoid chain via primary amines.

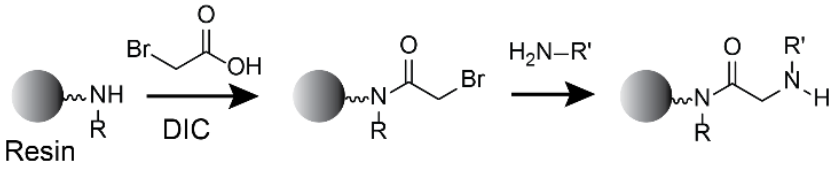

Scheme 3.1: Peptoid Synthesis Using a Solid-Phase Two-Step Submonomer Method.

Peptoids are synthesized through acylation using bromoacetic acid and *N,N'*-diisopropylcarbodiimide (DIC) followed by displacement with a primary amine.

To gauge the possibility of creating peptoid-SWCNT assemblies for use as protein nanosensors, we first elucidated the peptoid design parameters necessary for rendering colloidally stable peptoid-SWCNT assemblies. We synthesized a small library of 11 amphiphilic peptoid sequences, outlined in Table 3.1, of variable sequences, charges, polarities, and lengths to probe peptoid-SWCNT assembly efficacy using monomers that are nonpolar: *N*-(2-phenylethyl)glycine (Npe), *N*-isoamylglycine (Nia), and *N*-phenylglycine (Nph); polar and uncharged: *N*-(2-methoxyethyl)glycine (Nme) and *N*-2-(2-(2-methoxyethoxy)ethoxy)ethylglycine (Nte); positively charged: *N*-(2-aminoethyl)glycine (Nae); and negatively charged: *N*-(2-carboxyethyl)glycine (Nce) (Scheme 3.2). We included several diblock peptoids similar to previous antibody-mimetic nanosheet forming peptoids such as Block36 $(Nae\text{-}Npe)_9$-$(Nce\text{-}Npe)_9$, DB1 $(Nae\text{-}Nia)_7$-$(Nce\text{-}Nia)_7$, and DB2 $(Nae\text{-}Nph)_4$-$(Nce\text{-}Nph)_4$.[112] We synthesized several polar but uncharged peptoid polymers such as Pep1 $(Nte\text{-}Npe)_{14}$, Pep3 $(Nme\text{-}Npe)_{14}$, as well as a hybrid charged and uncharged polar polymer Pep2 $(Nte\text{-}Npe\text{-}Nce\text{-}Npe)_7$. We included a positively charged polymer, PA28 $(Nae\text{-}Npe)_{14}$, and negatively charged polymers of alternating Npe and Nce (PC) monomers with final polymer lengths of 18, 28, and 36 (PC18, PC28, and PC36, respectively), and an anchor-loop peptoid consisting of a $(Nce\text{-}Npe)_9$ 'anchor' peptoid sequence that can adsorb to the carbon nanotube flanking a synthetic 6-monomer loop consisting of 3 *N*-butylglycine (Nbu) and 3 *N*-*(N'*-pyrrolidinonylpropyl)glycine (Npp) monomers ($(Nce\text{-}Npe)_9$-Nbu-Nbu-Npp-Npp-Nbu-Npp-$(Nce\text{-}Npe)_9$, and further abbreviated as ProLoop).

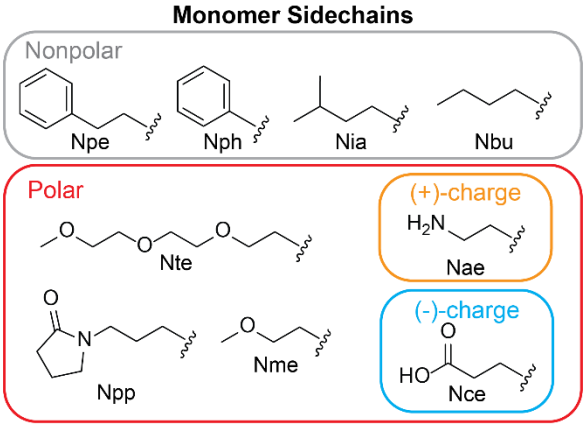

Scheme 3.2: Monomers Used to Synthesize the Peptoid Polymers in this Study.

Peptoid polymers can be created using a combination of monomers with different polarities and charge.

Table 3.1: Library of Peptoid Structures Tested for Adsorption to SWCNT.

Peptoids denoted with an asterisk (*) successfully adsorb on SWCNT to form peptoid-SWCNT assemblies; while other peptoids do not suspend SWCNT at pH 7.

Peptoid	Sequence
Block36	(Nae-Npe)$_9$-(Nce-Npe)$_9$
DB1	(Nae-Nia)$_7$-(Nce-Nia)$_7$
DB2	(Nae-Nph)$_4$-(Nce-Nph)$_4$
Pep1	(Nte-Npe)$_{14}$
Pep2*	(Nte-Npe-Nce-Npe)$_7$
Pep3	(Nme-Npe)$_{14}$
PA28	(Nae-Npe)$_{14}$
PC18	(Nce-Npe)$_9$
PC28*	(Nce-Npe)$_{14}$
PC36*	(Nce-Npe)$_{18}$
ProLoop*	PC18-(Nbu-Nbu-Npp-Npp-Nbu-Npp)-PC18

The loop segment within the ProLoop peptoid interacts semi-selectively with wheat germ agglutinin (WGA), a 36 kDa lectin, a sugar-binding protein, as assessed with a Förster resonance energy transfer (FRET) binding assay on a peptoid system independent of SWCNTs (Fig. 3.1). In this assay, a peptoid nanosheet displaying ProLoop was labeled with a donor fluorophore BODIPY-FL C16, while WGA was labeled with an acceptor fluorophore Alexa647. When the ProLoop binds WGA, there is a transfer of energy from the donor fluorophore to the acceptor fluorophore leading to a quenching of the donor fluorescence and an increase in the acceptor fluorescence. FRET is a proximity assay in which energy transfer can only occur if the two fluorophores are within several nanometers apart, the exact working distance depends on the fluorophores used in the system. The FRET assay further shows that WGA does not interact with the peptoid nanosheet in the absence of the peptoid loop. WGA was chosen as a target protein analyte since it is a commercially procurable lectin protein that does not require special handling, making it ideal for proof-of-principle experiments. Lectins have an important biological function in the body by binding to cell-surface glycans that act as molecular beacons for viral and bacterial infection of cells in several diseases and as biomarkers on cancer cells.[113–115] Furthermore, WGA was previously shown to bind to glycosylated loops on peptoid nanosheet self-assemblies, and therefore serves as a good system for experimental validation of peptoid-SWCNT based recognition of protein targets.[108]

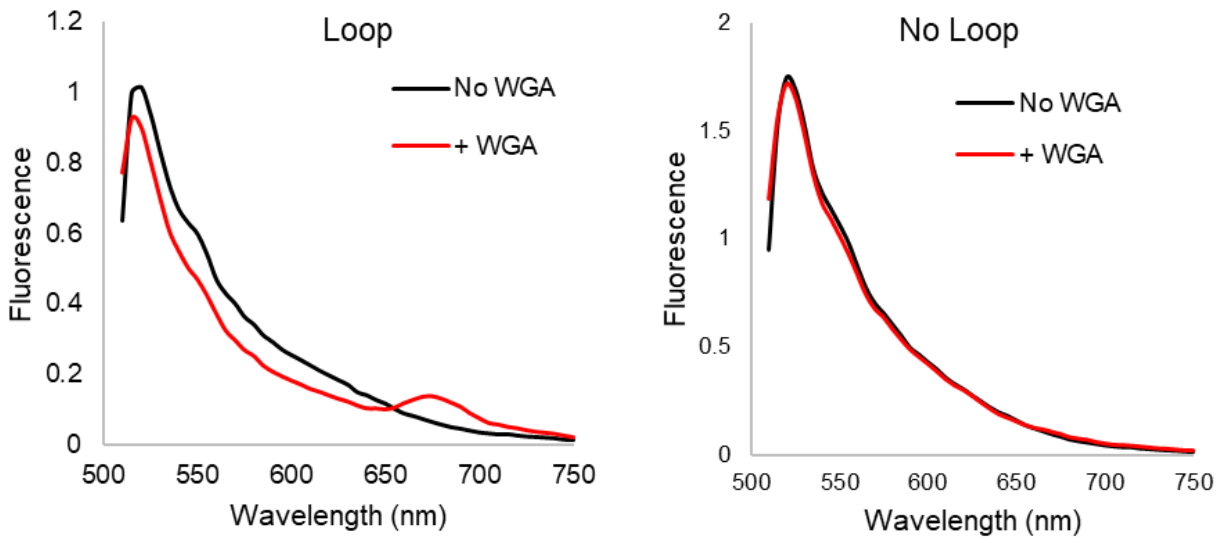

Figure 3.1: FRET Assay to Assess Peptoid Loop Interaction with WGA.

FRET assay shows interaction between the 6-monomer peptoid loop and WGA protein. Peptoid nanosheets with and without peptoid loops were assembled with BODIPY-FL C16 fluorophore (donor) with a peak emission wavelength at 528 nm. The addition of Alexa647-labeled WGA (acceptor) to peptoid-containing loops exhibited in a decrease in donor fluorescence and an increase in acceptor fluorescence indicating an increase in FRET. The FRET ratio (calculated as the ratio of increase in acceptor fluorescence to decrease in donor fluorescence) for peptoid with the peptoid loop was 0.678, while the FRET ratio for peptoid without loops was -0.172.

The peptoid library was evaluated for each peptoid's ability to adsorb to SWCNTs. Peptoid-SWCNT adsorption was attempted with solution-phase probe-tip sonication of peptoids and SWCNT (see Section 3.3) and adsorption efficacy was confirmed with UV-Vis-NIR absorbance spectroscopy (Fig. 3.2). UV-Vis-NIR absorbance was used to measure the sample optical density, from which yield of colloidally stable peptoid-SWCNT assemblies can be calculated (see Section 3.3). Absorbance spectroscopy can also reveal qualitative information of the relative stability of each peptoid-SWCNT assembly. NIR fluorescence spectroscopy further confirms peptoid adsorption as only stable and indidivually suspended peptoid-SWCNT assemblies can exhibit NIR fluorescence (Fig. 3.3). Probe-tip sonication was performed in 50 mM borate buffer (pH 9.2) and peptoid-SWCNT assemblies were diluted in phosphate buffered saline (PBS, pH 7.4) prior to spectroscopy and fluorescence measurements, to represent physiological conditions in preparation for downstream biological applications in protein detection.

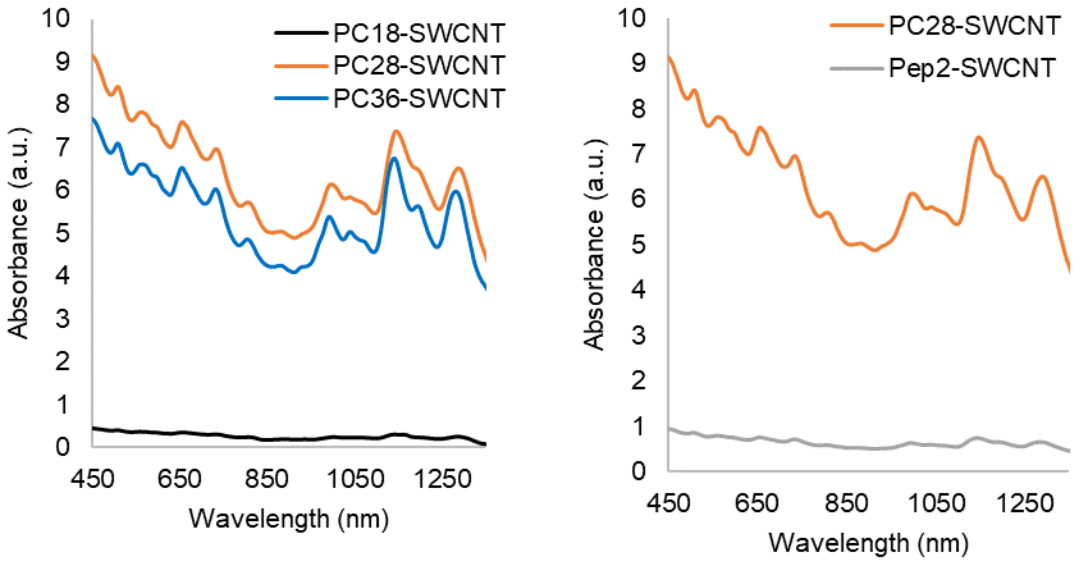

Figure 3.2: Absorbance Spectra of Peptoid-SWCNTs.

Peptoid suspension efficiency on SWCNTs and relative stability of peptoid-SWCNT assemblies were measured by optical absorption of the sample at 632 nm, from a broad-spectrum absorption scan by a UV-Vis-IR spectrophotometer. SWCNT concentration is calculated from absorbance at 632 nm using the Beer-Lambert law with extinction coefficient, ε_{632} = 0.036 L mg^{-1} cm^{-1}.[95]

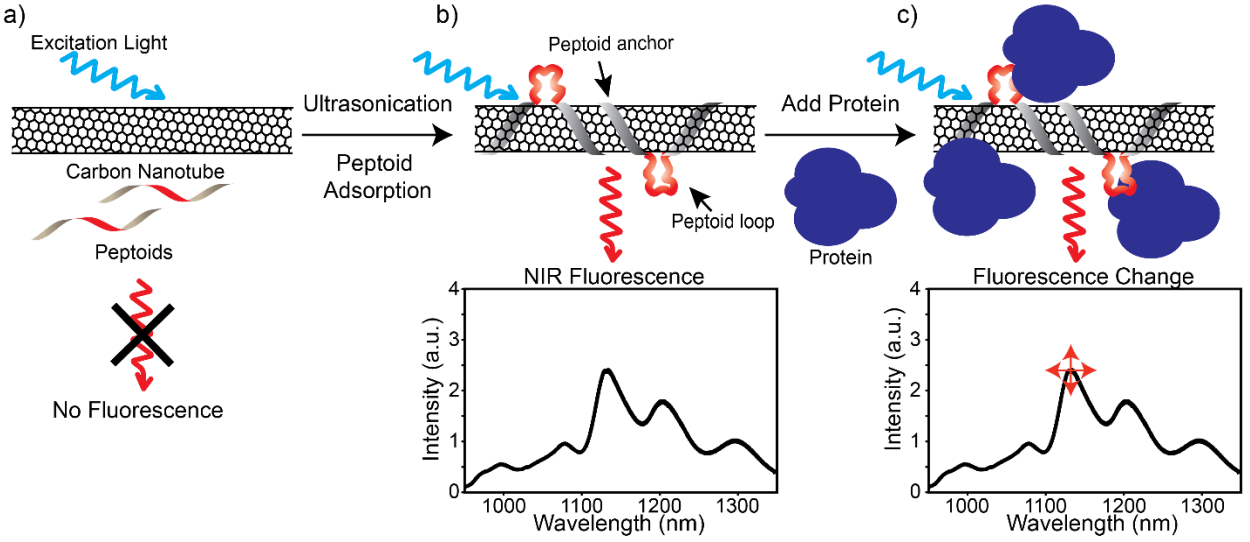

Figure 3.3: Platform for Peptoid-SWCNT Assembly.

a) No NIR fluorescence is observed prior to adsorption of peptoids to SWCNT surfaces. b) Ultrasonication promotes the formation of peptoid-SWCNT assemblies with a distinct NIR fluorescence spectrum that is c) modulated by the addition of a target protein (blue) that binds to the protein-recognition loop (red). (Schematics not to scale.)

Four of the eleven peptoids stably adsorb onto SWCNTs and remained stable at physiological pH, with successful peptoid-SWCNT assemblies labeled with an asterisk (*) in Table 1. Adsorption efficiency was compared by measuring the UV-Vis-IR absorbance spectrum of the assembly,

where a higher absorbance is indicative of higher peptoid-SWCNT yield (Fig. 3.2). We found that peptoid polymer length affects the effectiveness of peptoid-SWCNT adsorption. To assess the effect of peptoid length on peptoid-SWCNT stability, we compared peptoids comprised of the same carboxyethyl-phenethyl repeat with lengths of 18, 28, and 36 monomers. We found the peptoid-SWCNT adsorption efficiency is roughly proportional to peptoid length: PC36 (yield = 165.1 mg L^{-1}) ≈ PC28 (194.9 mg L^{-1}) > PC18 (9.2 mg L^{-1}). We posit that longer peptoid polymers adsorb more strongly to SWCNTs owing to the increased number of contacts made between a longer peptoid polymer and the surface of the SWCNT. We also found that peptoid hydrophilicity is an important contributor to peptoid-SWCNT adsorption efficiency. Pep1, Pep2, Pep3, and PC28 peptoids are of the same 28 monomer length, with alternating monomers of aromatic phenethyl and hydrophilic monomers of either triethyloxy, monoethoxy, or carboxyethyl. We show that the efficiency of peptoid adsorption to SWCNT follows the trend of PC28 > Pep2 > Pep1 ≈ Pep3, with Pep1 and Pep3 unable to suspend SWCNT, and follows the trend of peptoid hydrophilicity as observed by HPLC. Lastly, we note that peptoid charge also facilitates peptoid-SWCNT colloidal stabilization: both the peptoid backbone and the SWCNT are nonpolar and hydrophobic, and require hydrophilicity by charge or polarity to create stable peptoid-SWCNT assemblies in aqueous buffer. Of the charged 28-mer peptoids, the highly negatively charged PC28 best adsorbed to SWCNT with a yield of 194.9 mg L^{-1}, whereas the less charged Pep2 adsorbed least with a yield of 19.8 mg $L^{-1}$and the neutrally charged Pep1 and Pep3 failed to adsorb onto SWCNT. PA28, with positively charged monomers, showed low adsorption to SWCNT putatively due to the difficulty of protonation of the polymer's primary amines.[116] We tested this hypothesis by attempting to suspend SWCNT with PA28 at low pH conditions, and found we could only maintain stable peptoid-SWCNT assemblies at very acidic conditions (100 mM acetate buffer pH < 5), a regime not suitable for biological applications. Therefore, we find that certain charged monomers can confer colloidal stabilization of SWCNT.

Several peptoids did not adsorb to SWCNT. Peptoids lacking aromatic hydrophobic residues, such as DB1, did not suspend SWCNT presumably due to a lack of π-π interactions. Conversely, peptoids with aromatic groups such as Block36 have previously been shown to self-assemble into supramolecular nanosheets driven by zwitterionic stabilizing interactions of the charged groups, hydrophobic interactions, and π-π stabilization between the aromatic rings of the peptoid.[112] Thus, when Block36 is adsorbed to SWCNTs, we propose that peptoid zwitterionic and hydrophobically-driven self-interactions dominate over peptoid-SWCNT interactions, resulting in unstable SWCNT assemblies in favor of spontaneous formation of peptoid nanosheets as confirmed by AFM (Fig. 3.4). These aggregates are not observed in AFM of successful peptoid-SWCNT assemblies. DB2 also did not adsorb to SWCNT, presumably due to the larger steric hinderance of phenyl monomers compared to the 2-phenylethyl monomers.

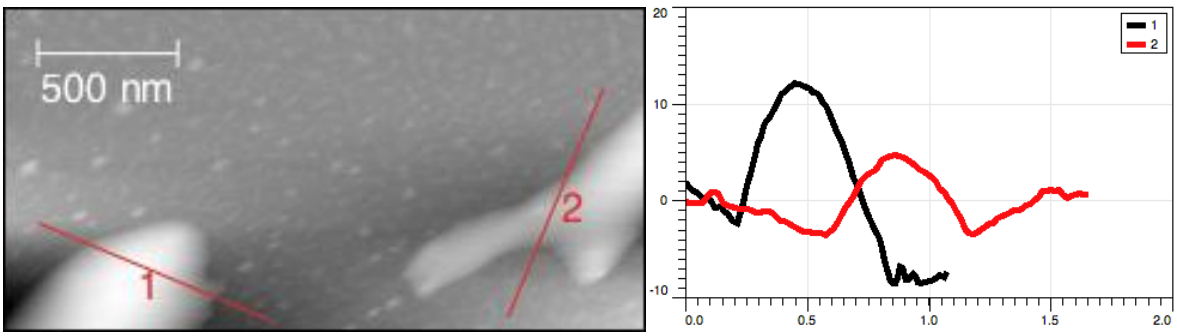

Figure 3.4: Block36 Favors Nanosheet Formation Over SWCNT Adsorption.

Atomic force microscopy of Block36 reveals large peptoid aggregates absent from other stable peptoid-SWCNT assemblies. These results suggest that Block36 peptoid nanosheet formation is thermodynamically favorable over B36-SWNT assembly formation. For traces 1 and 2, x axis is length in μm, and y axis is height in nm.

From our initial screen, we identified repeats of (Nce-Npe) as highly stable peptoid sequences for SWCNT stabilization at physiological pH, and utilized this Nce-Npe repeat as an 'anchor' for peptoid adsorption to SWCNT. Next, from FRET binding assays between WGA and libraries of peptoid sequences, we identified a 6-monomer peptoid segment that demonstrated high binding affinity for lectin protein WGA (Fig. 3.1). We inserted this WGA-binding segment between Nce-Npe anchor repeats to form the ProLoop peptoid (Table 1). We also identified ProLoop as a stable peptoid for SWCNT adsorption with a moderate yield of 103.1 mg L^{-1}. Thus, the ProLoop-SWCNT assembly, and the PC36-SWCNT assembly with equal numbers of (Nce-Npe) monomers as ProLoop, were selected for downstream stability characterization and for use as fluorescent WGA protein nanosensors.

Peptoid-SWCNT Nanosensor Fluorescence Stability

To validate peptoid-SWCNT assemblies as fluorescent protein nanosensors, we next demonstrated the stability of peptoid-SWCNT assemblies in a range of conditions suitable for bioimaging applications. We first examined the effect of salt and buffer conditions, as such parameters have been shown to affect the stability of SWCNT assemblies.[68,69,117] We also examined the stability of the SWCNT assemblies to continuous laser exposure and protease activity.

To test solution stability, peptoid-SWCNT assemblies were incubated overnight in sodium chloride (NaCl) solutions ranging in concentration from 1 mM to 500 mM, and peptoid-SWCNT fluorescence was subsequently measured. PC28 and PC36 peptoid-SWCNT assemblies remained colloidally stable and exhibited NIR fluorescence under a 1 mM to 500 mM NaCl range of ionic strengths (Fig. 3.5a, b). NaCl concentrations higher than 500 mM destabilized the peptoid-SWCNT assemblies and induced SWCNT aggregation leading to a loss of SWCNT fluorescence. Pep2-SWCNT assemblies were unstable in NaCl solutions with concentrations higher than 10 mM and formed visible aggregates at higher ionic strength (Fig. 3.5c). Recent work demonstrates that DNA-SWCNT fluorescence is proportional to ionic strength,[68] thus we compared fluorescence of peptoid-SWCNT assemblies under above-mentioned salt concentrations. In concurrence with prior results, peptoid-SWCNT assemblies show high NIR fluorescence at higher ionic strengths, presumably due to a tighter association between the peptoid and the SWCNT. Conversely, at lower ionic strengths, peptoids are putatively more loosely associated to the surface of the SWCNT, resulting in lower SWCNT fluorescence (Fig. 3.5d).[68] Additionally, we tested the effect of salt composition on the fluorescence of peptoid-SWCNT assemblies. Recently, divalent salts have been shown to induce a wavelength shift in the fluorescence spectra of DNA-SWCNT assemblies. In these studies, it is hypothesized that solvatochromic shifts are due to induced conformational changes in the DNA backbone along the SWCNT, and correlated with the stiffness of the polymer backbone.[69] We observed significant wavelength shifts in the fluorescence spectra of PC28 and PC36 peptoid-SWCNT assemblies upon addition of $CaCl_2$ salt, and minor shifts in the fluorescence spectra of ProLoop and Pep2 peptoid-SWCNT assemblies (Fig. 3.6), suggesting that

multiple factors, of which salts may be but one, affect peptoid flexibility and thus binding stability on SWCNT.

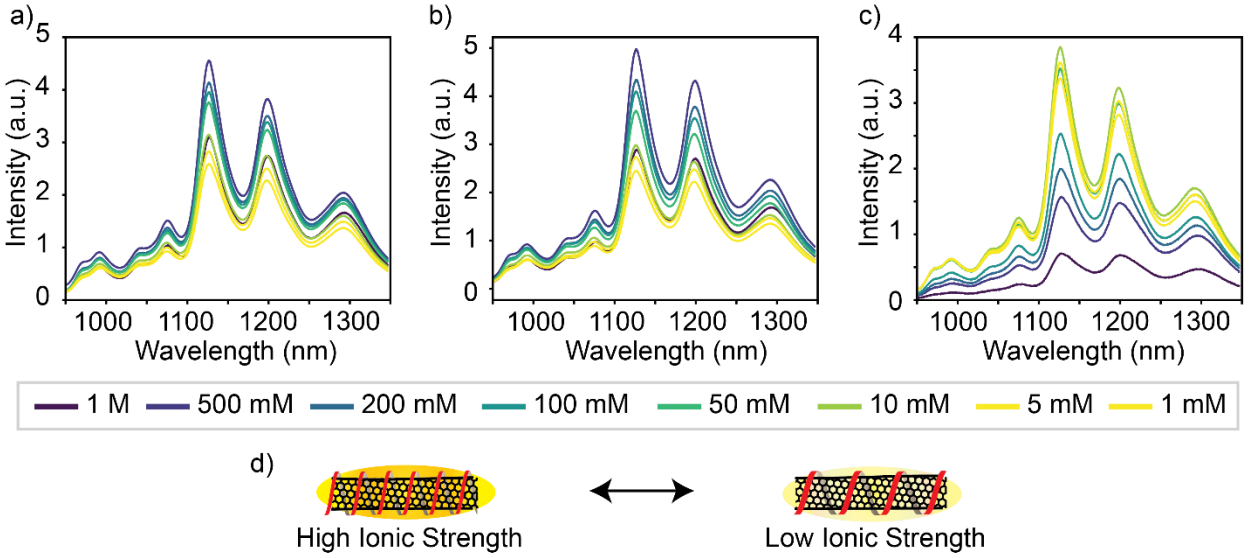

Figure 3.5: Peptoid-SWCNT Fluorescence Under Variable Ionic Strength Conditions.

Solution ionic strength affects the fluorescence of peptoid-SWCNT assemblies: a) PC36-SWCNT, b) PC28-SWCNT, and c) Pep2-SWCNT, whereby higher ionic strengths yield higher peptoid-SWCNT fluorescence. At ionic strengths greater than 500 mM aggregation of the assemblies occurs because of electrostatic screening between polymer and SWCNT, and the loss of NIR fluorescence. d) The change in fluorescence as a result of variable ionic strength suggest peptoid surface coverage of SWCNT increases with ionic strength.

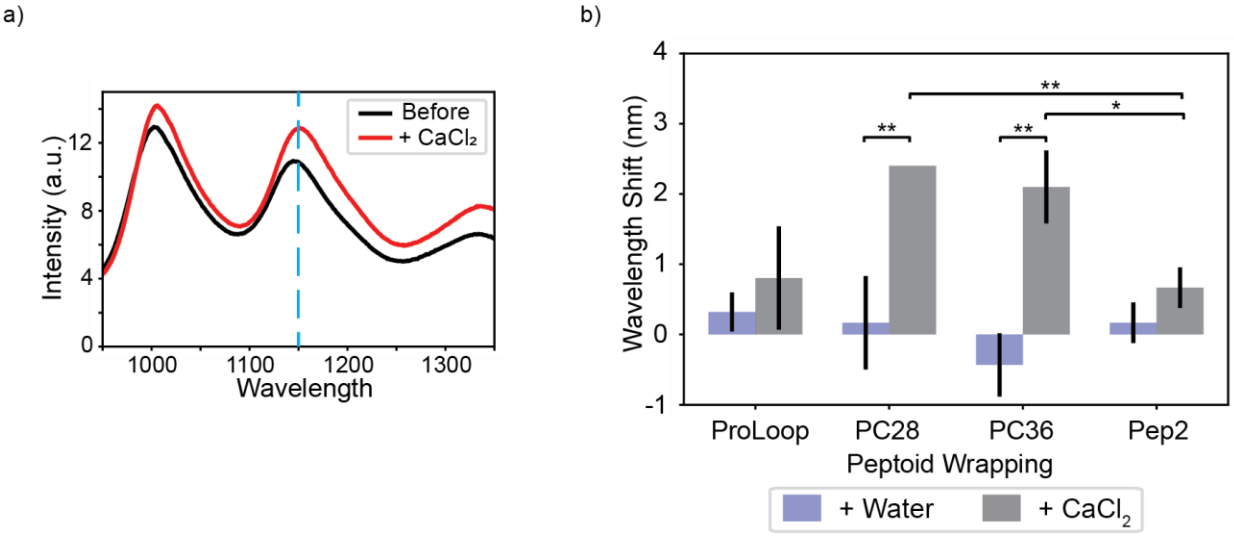

Figure 3.6: Peptoid-SWCNT Solvatochromic Shifting in Divalent Salt Conditions.

a) Peptoid-SWCNT assemblies, such as PC36-SWCNT, exhibit a solvatochromic shift upon addition of divalent cations from $CaCl_2$. b) Addition of $CaCl_2$ to PC28-SWCNT and PC36-SWCNT induces a significant solvatochromic shift at 1195 nm compared to water addition, although all peptoid-SWCNT showed a red-shift in fluorescence wavelength upon addition of 500 mM $CaCl_2$. Notably, PC28-SWCNT and PC36-SWCNT, which have the same monomeric composition, show a significantly different response to divalent salts compared to Pep2-SWCNT (* denotes $p < 0.05$, ** denotes $p < 0.005$).

We next subjected each peptoid-SWCNT assembly to an hour-long imaging experiment to probe peptoid-SWCNT stability to continuous laser exposure. Excitation of peptoid-SWCNT samples by a 77 mW 721 nm laser for SWCNT spectroscopy stabilizes to a temperature of 37˚C in the sample well within 1 minute of laser irradiation (Fig. 3.7). Peptoid-SWCNT assemblies did not show wavelength shifts during the hour-long spectral measurement with largely chirality-independent changes in fluorescence (Fig. 3.8a). Our results showed that the ProLoop-SWCNT construct exhibits the most stable fluorescence with a negligible 2.1 ± 6.6 % (mean ± standard deviation (SD)) increase in fluorescence after 1 hour of laser illumination (Fig. 3.8b). In contrast, PC28 and PC36 both showed moderate fluorescence perturbations of -12.2 ± 8.9 % (mean ± SD) and -36.8 ± 17.8 % (mean ± SD) decrease in fluorescence, respectively, while Pep2-SWCNT showed the largest fluorescence perturbation with a -69.7 ± 27.1% (mean ± SD) decrease in fluorescence. We note that peptoid-SWCNT stability trends observed herein follow trends in peptoid-SWCNT adsorption efficiency, although the ProLoop-SWCNT exhibited moderate adsorption efficiency and highest stability. The superior fluorescence stability and the incorporation of a WGA molecular recognition loop sequence led us to choose the ProLoop-SWCNT assembly as an exploratory candidate for use as an optical nanosensor to detect WGA protein.

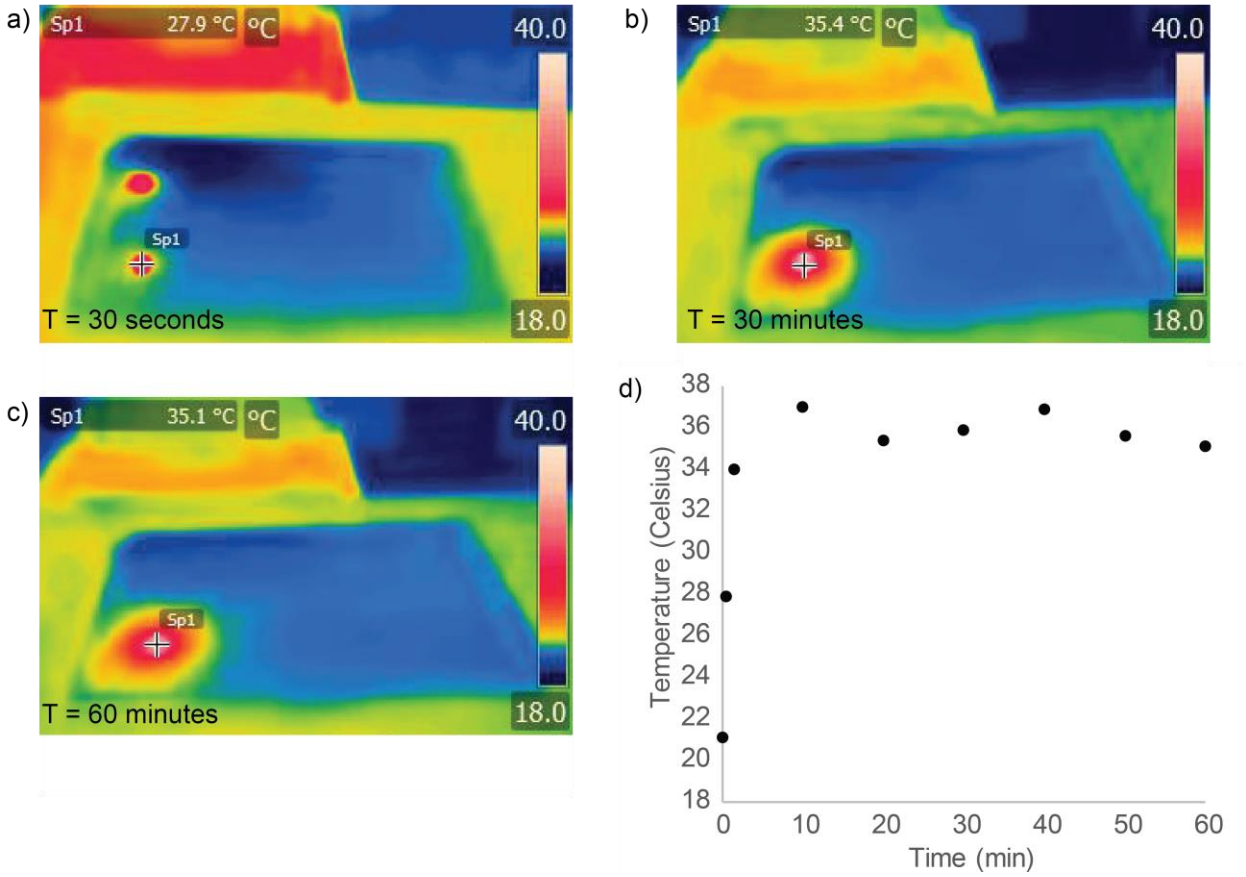

Figure 3.7: Temperature Equilibration of Peptoid-SWCNT NIR Fluorescence Spectroscopy.

FLIR thermal camera images of the sample well (Sp1) at a) 30 seconds, b) 30 minutes, and c) 60 minutes. d) Time-dependent temperature changes show rapid temperature equilibration in the well with a maximum temperature stabilizing at ~37 ºC.

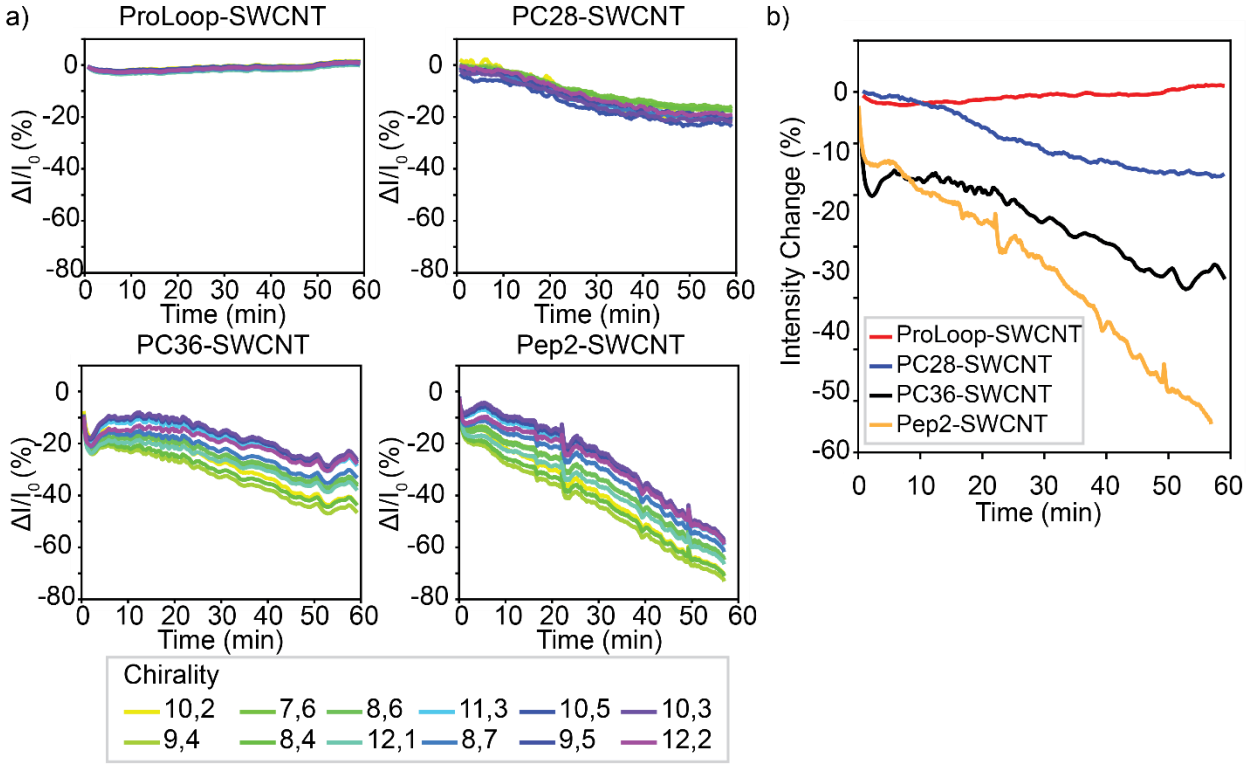

Figure 3.8: Peptoid-SWCNT Thermostability.

a) Upon continuous laser illumination, there are largely chirality-independent changes in fluorescence. b) Fluorescence of peptoid-SWNT assemblies under continuous laser heating shows that ProLoop-SWNT is the most stable assembly in this study.

An advantage of using peptide-mimetic peptoid polymers is their stability against degradases, so we tested the stability of the ProLoop-SWCNT nanosensor against two proteases: trypsin and proteinase K. These proteases were chosen for their ability to digest a wide range of peptide sequences, specifically positively charged, aromatic, and aliphatic amino acids, which mimics the function of the major proteases in the human body. We measured peptoid-SWCNT optical properties after 24-hour incubation in proteases as a proxy for the stability of the construct. The NIR fluorescence intensities of the peptoid-SWCNT assemblies were invariant indicating stability, as degradation of the surface coating would lead to the aggregation and loss of fluorescence for the system (Fig. 3.9).[118] Similarly, the absorbance of the assemblies were assessed using a protein turbidity assay, and showed largely invariant absorbance spectra for ProLoop-SWCNT (Fig. 3.10).[119] A change in absorbance would indicate the destabilization of the peptoid coating on the SWCNT, as an increase in absorbance is caused by the increased scattering by loose aggregates in solution and a decrease in absorbance indicates the bundling and loss of SWCNT assemblies from solution. Additionally, this assay shows that ProLoop-SWCNT is not aggregating upon the addition of WGA protein.

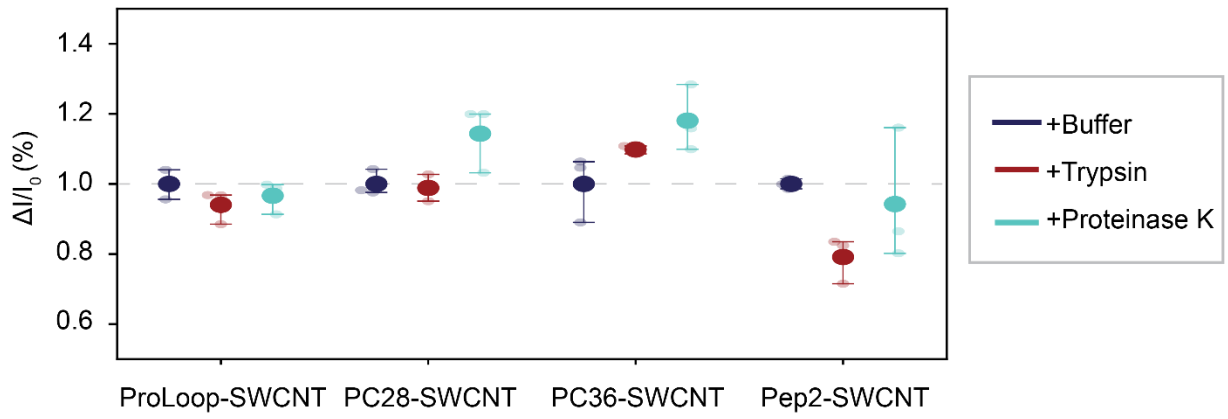

Figure 3.9: Peptoid-SWCNT Resistance to Proteases.

Peptoid-SWCNT assemblies were incubated in proteases for 24 hours before their NIR fluorescence was measured and normalized against the fluorescence change observed in the absence of protease. ProLoop-SWCNT is shown have the most invariant NIR fluorescence and therefore the most stable to the addition of proteases. Large filled circles denote the mean fluorescence, smaller transparent circles denote individual trials, and error bars denote standard deviation for n = 3.

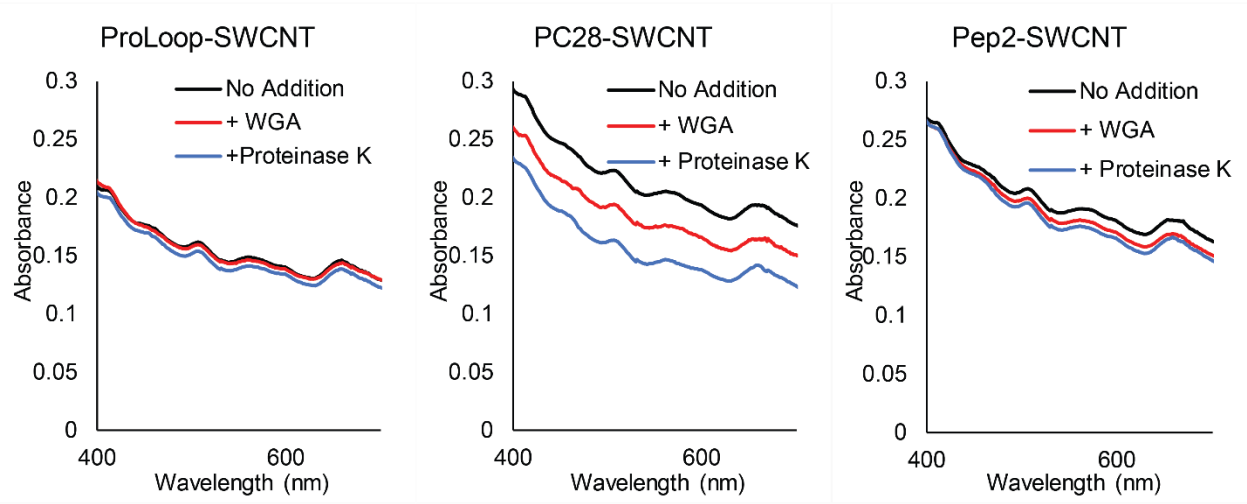

Figure 3.10: Assessing Peptoid-SWCNT Aggregation.

Peptoid-SWCNT conjugates were incubated with either protease for 24 hours prior to acquiring the sample UV-Vis-IR absorbance spectra. ProLoop-SWCNT shows no loss of absorbance following incubation with WGA and minimal loss of absorbance following incubation with Proteinase K suggesting ProLoop-SWCNT stability.

ProLoop-SWCNT Nanosensors Exhibit Fluorescence Modulation in Response to Wheat Germ Agglutinin Protein

The ProLoop-SWCNT assembly was assessed for use as a fluorescent nanosensor for WGA protein, via binding of WGA to the ProLoop peptoid sequence.[120] ProLoop-SWCNT nanosensors were diluted to a concentration of 5 mg L^{-1} and the baseline fluorescence (I_0) was measured. WGA was added to the nanosensor and subsequent fluorescence (I) was measured at consecutive timepoints. We found that the ProLoop-SWCNT nanosensor exhibited a decrease in fluorescence upon the introduction of WGA. The fluorescent response was time-dependent and reached

equilibrium within 60 minutes following addition of 10 μM WGA (Fig. 3.11a). We next characterized the ProLoop-SWCNT nanosensor sensitivity to WGA through a concentration screen of 0.1 μM to 14.9 μM WGA. We measured the ProLoop-SWCNT nanosensor fluorescence change 60 minutes after WGA addition. Several models for SWCNT nanosensor responses have been developed that take into account exciton diffusion or molecular interactions.[121] Given that our data (AFM, FRET, absorption) are largely based on molecular binding affinity between WGA and the ProLoop-SWCNT construct, we modeled our data using an equilibrium binding curve with Langmuirian adsorption. Assuming a single protein binding to each peptoid binding site, we modeled the equilibrium binding of ProLoop-SWCNT with an enzyme-substrate binding model, as denoted by the red curve on the concentration plot (Fig. 3.11b).

$$\frac{I-I_0}{I_0} = a\frac{(K[WGA])^n}{(K[WGA])^n+1} + b \qquad (1)$$

In equation 1, I denotes the ProLoop-SWCNT nanosensor intensity after 60 minutes, I_0 denotes the initial nanosensor intensity at 0 minutes, *[WGA]* the concentration of WGA in the system, K the equilibrium binding constant, and *a* and *b* denote scaling factors. For more information on the development of a model for SWCNT nanosensor fluorescence modulation upon analyte binding, refer to the discussion in appendix 2. Since WGA is composed of two symmetric monomeric units, we assumed the Hill coefficient (n), which denotes the cooperativity of the analyte bound, to be 2 for the fit to converge (determination of goodness of fit of the model is discussed in appendix 2).[122] Using nonlinear least-squares fitting, the model parameters were found to be a = -14.47, K = 0.192 μM^{-1}, and b = 0.009, and R^2 = 0.83. With this equilibrium model of WGA binding to ProLoop-SWCNT, we calculated the limit of detection for WGA binding to ProLoop-SWCNT as 3.4 μM, a concentration comparable to the average serum concentration of common blood proteins such as albumin (600 μM), IgG (100 μM), and fibrinogen (7.5 μM).[123] Furthermore, ProLoop-SWCNT binding to WGA was confirmed through atomic force microscopy (Fig. 3.12). Since WGA is procured from a commercial source, we tested the possibility that ProLoop-SWCNT nanosensor fluorescence response results from optical interference of byproduct contaminants from the protein purification process. WGA was reconstituted in 200 μL of water at a concentration of 100 μM, and was filtered through an Amicon Ultra-0.5 mL centrifugal filter with a 3 kDa molecular weight cutoff. This molecular weight cutoff will allow the passage of any contaminants and ions less than 3 kDa, but not WGA protein, which is 36 kDa. The ProLoop-SWCNT nanosensor response was confirmed to be in response to WGA protein, rather than protein contaminants (Fig. 3.13).

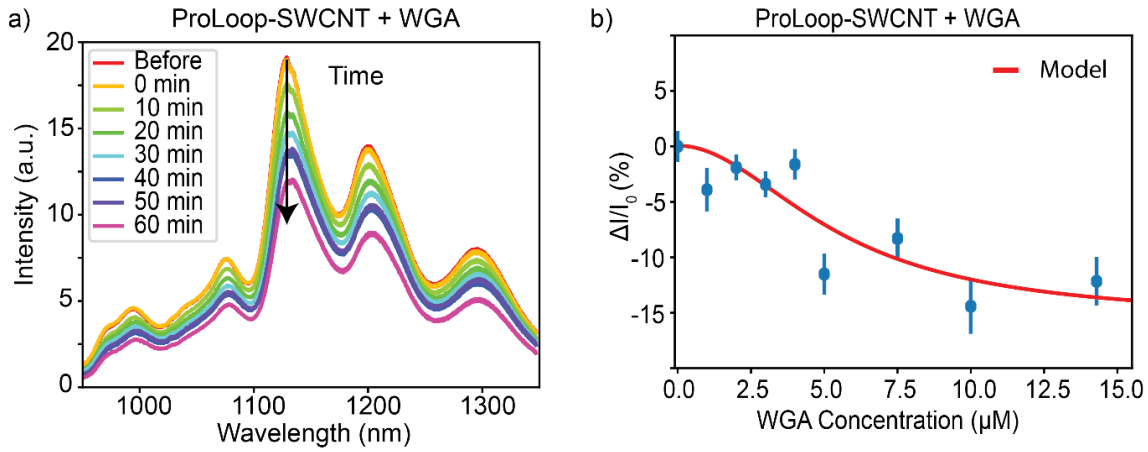

Figure 3.11: ProLoop-SWCNT Nanosensor Sensitivity Characterization.

a) ProLoop-SWCNT exhibited a decrease in fluorescence upon addition of WGA protein. b) The equilibrium decreases in fluorescence of ProLoop-SWCNT as a function of WGA concentration yields a 3.4 μM limit of WGA detection. Fluorescence change was baselined to 0% at 0 μM WGA to account for nanosensor dilution, and error bars denote standard error (n = 6 to 15).

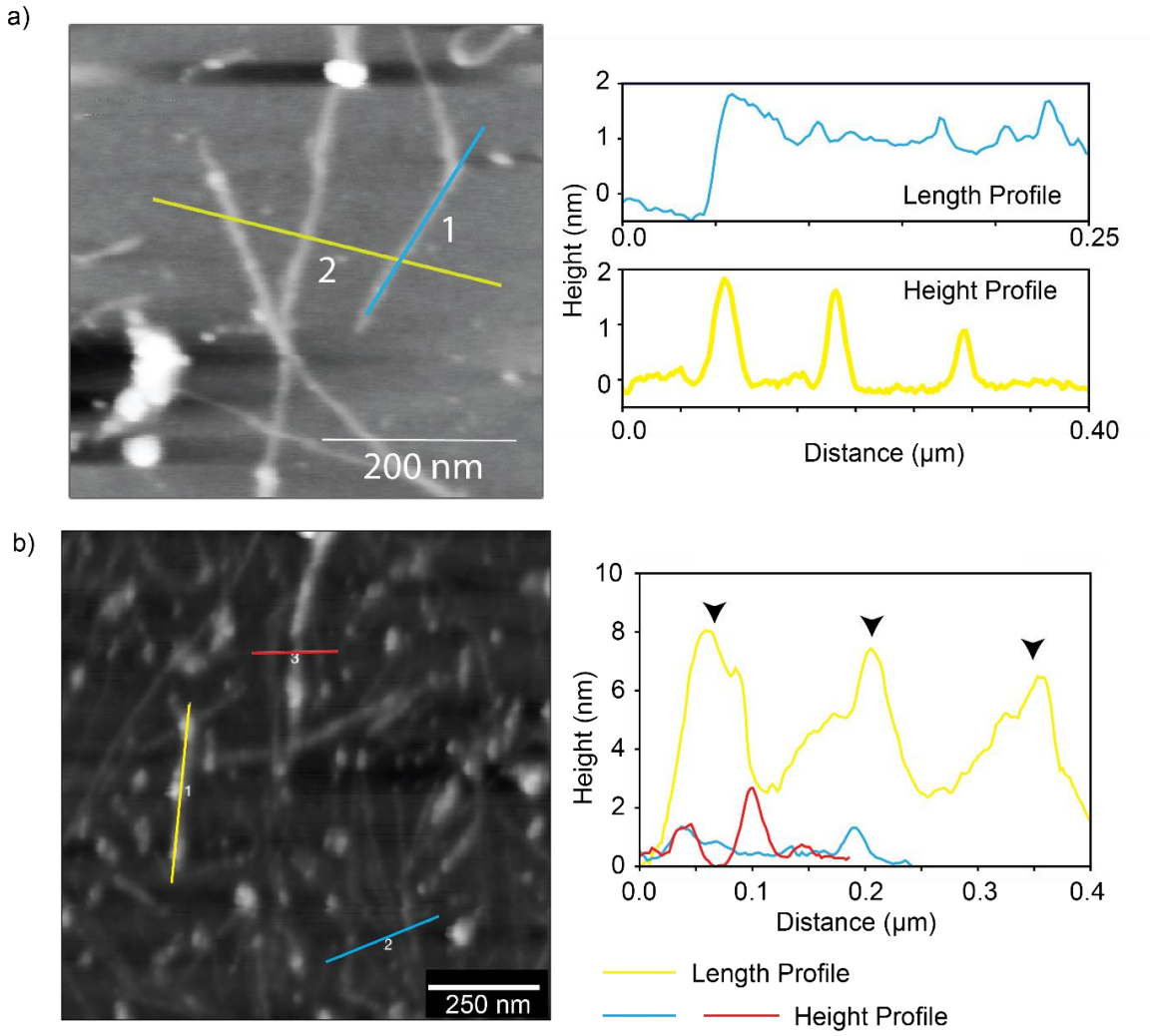

Figure 3.12: AFM of Peptoid-SWCNT and Peptoid-SWCNT with Bound WGA Protein.

a) AFM imaging of ProLoop-SWCNT nanosensors shows heights of 1 nm to 2 nm. b) Upon addition of WGA, ProLoop-SWCNT bound to WGA exhibit an increase in heights of 6 nm to 8 nm, expected from adsorption of a 36 kDa, or ~2 nm globular protein such as WGA. Several globular features 6-8 nm in size were observed along the length of the ProLoop-SWCNT following incubation with WGA.

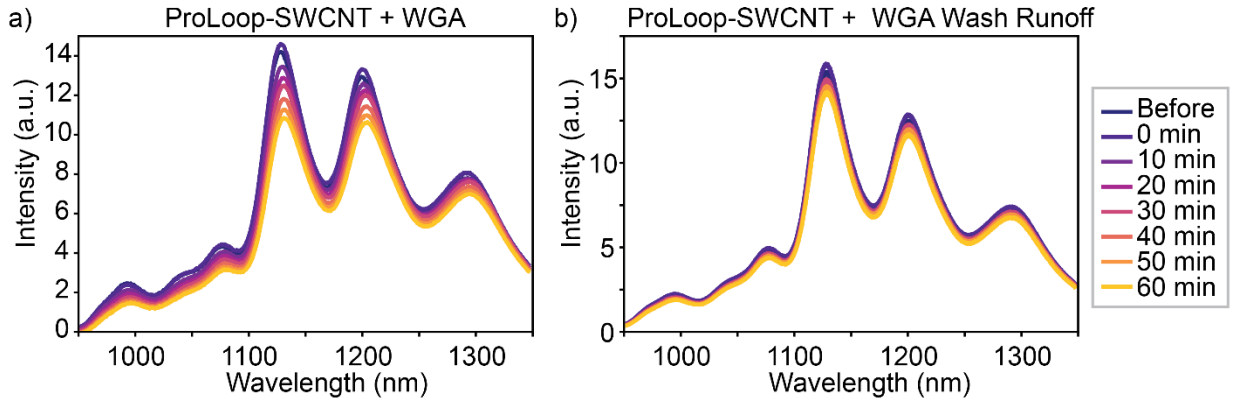

Figure 3.13: ProLoop-SWCNT Response is Not Due to Processing Contaminants.

ProLoop-SWCNT response to WGA is due to interactions with a) the protein, and not b) the addition of filtrate containing any byproducts of WGA production, which showed negligible fluorescence modulation with NIR spectroscopy.

We next assessed the selectivity of the ProLoop-SWCNT nanosensor by measuring the fluorescence response of ProLoop-SWCNT upon exposure to a small library of other protein targets of various sizes and isoelectric points (Table 3.2), including two other lectins: protein A, peanut agglutinin, concanavalin A, bovine serum albumin (BSA), neutravidin, and lysozyme (Fig. 3.14). Peanut agglutinin (PNA) is a lectin that binds selectively to galactose, and concanavalin A (ConA) is a lectin that binds selectively to mannose. Both BSA and neutravidin are proteins known to bind nonspecifically to the surface of SWCNT. In order to test the contribution of electrostatics to binding, protein A is a negatively charged protein at physiological pH, and lysozyme is a positively charged protein at physiological pH.[46,124] This modest protein library afforded a screen for ProLoop-SWCNT selectivity towards WGA. We found that ProLoop-SWCNT nanosensors show the highest magnitude in fluorescence decrease of -34.5 ± 13.9% (mean ± SD) upon addition of 10 µM WGA, with minor fluorescence modulation upon addition of 5 mg mL^{-1} protein A, 10 mg mL^{-1} BSA, 5 mg mL^{-1} neutravidin, or 5 mg mL^{-1} lysozyme (2.0 ± 8.2%, -10.3 ± 12.5, -13.2 ± 5.2, and -17.3 ± 6.4% (mean ± SD), respectively). Conversely, ProLoop-SWCNT showed an increase in fluorescence upon the addition of 10 mg mL^{-1} PNA (22.3 ± 3.9, mean ± SD) and 10 mg mL^{-1} ConA (33.9 ± 1.1, mean ± SD). Interestingly, fluorescence changes upon addition of PNA and ConA were both near-immediate and also largest in magnitude for the least stable peptoid-SWCNT assembly, Pep2-SWCNT. These results suggest ProLoop-SWCNT interactions with these two lectins is through a different and possibly non-specific mechanism than the one described for WGA. PC28-SWCNT and Pep2-SWCNT assemblies also showed a decrease in fluorescence response upon addition of 10 µM WGA (-27.9 ± 18.1% and -36.3 ± 10.0% (mean ± SD), respectively). However, addition of proteins, buffer, or nothing to PC28-SWCNT and Pep2-SWCNT also induced monotonic decreases in fluorescence, indicating that fluorescence modulation of PC28 and Pep2 constructs derives primarily from their low colloidal stability. Furthermore, the magnitude of response of PC28-SWCNT correlates with the protein isoelectric point, suggesting the negative monomers of the PC28 anchor interact more strongly with proteins that have higher isoelectric points (neutravidin, WGA, and lysozyme). Therefore, ProLoop-SWCNT with its 6-monomer loop exhibited the highest selectivity towards WGA protein, concurrent with our FRET peptoid-WGA binding data (Fig. 3.1).

Table 3.2: Proteins Assayed for this Study.

Proteins were chosen based on their functional similarity to WGA, nonspecific binding to SWCNTs, or isoelectric point.

Protein	Size (kDa)	Isoelectric Point
BSA	69	4.7
NeutrAvidin	67-68	6.3
Protein A	42	5.1
Wheat Germ Agglutinin (WGA)	36	8.7
Lysozyme	14.1	11.35
Peanut Agglutinin (PNA)	100.8	5.0-7.0
Concanavalin A (Con A)	106	4.5-5.5

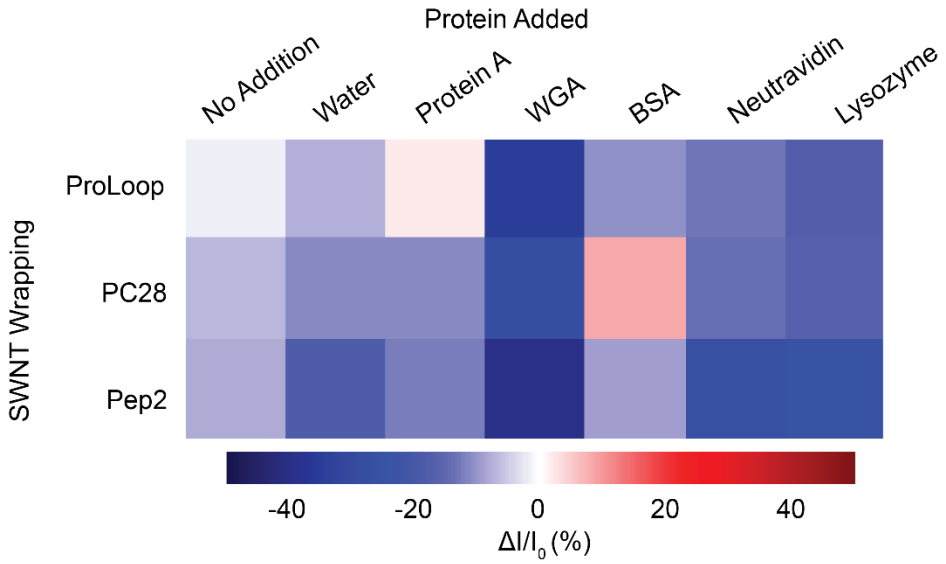

Figure 3.14: ProLoop-SWCNT Selectivity to WGA.

Decrease in fluorescence of ProLoop-SWCNT was most selective for WGA against other proteins (n = 6 to 21). For all values of mean and standard deviation refer to Table 3.3.

Table 3.3: Selectivity Screen Data.

Values reported for the heatmap in figure 3.14

	Protein Added – Mean Percent Fluorescence Change (SD)								
Nano-sensor	No Addition	Water	Protein A	WGA	PNA	ConA	BSA	Neutravidin	Lysozyme
ProLoop-SWCNT	-10.3 (12.5)	-7.7 (5.5)	2.0 (8.2)	-34.5 (13.9)	22.3 (3.9)	33.9 (1.1)	-10.3 (12.5)	-13.2 (5.2)	-17.3 (6.4)
PC28-SWCNT	-7.0 (5.3)	-10.9 (22.8)	-11.0 (8.8)	-27.9 (18.1)	27.1 (4.5)	48.5 (14.4)	8.6 (1.3)	-14.0 (4.4)	-16.4 (4.7)
Pep2-SWCNT	-7.8 (1.7)	-18.0 (12.5)	-12.1 (0.2)	-36.3 (10.0)	70.3 (16.2)	65.8 (14.8)	-9.0 (2.8)	-26.8 (1.4)	-25.1 (1.0)

Probing the Interaction Between Peptoid-SWCNTs and WGA

To further understand the interactions of WGA with peptoid-SWCNT assemblies, we studied the fluorescence change of the assemblies upon surface perturbation by surfactant. Previous studies have shown that surfactants including sodium dodecyl sulfate, sodium cholate (SC), and sodium dodecylbenzenesulfonate, can bind to the exposed SWCNT surface of polymer-SWCNTs and exclude water from the SWCNT surface.[63] This water exclusion causes a change in the dielectric environment of the nanosensors and induces a solvatochromic shift that could be implemented to study the accessibility of the SWCNT surface in a polymer-SWCNT construct.

Addition of 0.5% (w/v) SC to ProLoop-SWCNT nanosensors induced a solvatochromic blue shift in fluorescence for most nanotube chiralities, with the peaks at shorter fluorescence emission wavelengths showing the largest peak wavelength perturbation with peak wavelength shifts ranging from 0.97 nm to 11.76 nm (Fig. 3.15a, b). Interestingly, addition of WGA to the ProLoop-SWCNT assemblies prior to the addition of 0.5% SC eliminates the solvatochromic shift, suggesting WGA stabilizes the ProLoop-SWCNT assemblies against surfactant perturbation (Fig. 3.15c). Prior work has confirmed that this stabilization effect represents a strong and selective binding interaction between the molecular analyte and the polymer-SWCNT assembly.[125] This wavelength shift was also exhibited by the other peptoid-SWCNT. Notably, Pep2-SWCNT was only minimally perturbed by SC addition, showing on average less than 1 nm shift after the addition of SC (Fig. 3.15d). This is likely due to the triethylether monomer sidechains in Pep2 that resemble polyethylene glycol (PEG), which may limit accessibility of SC to the SWCNT surface. PEG is often used as an antifouling and biocompatibility coating on biological device and nanoparticle surfaces, and antifouling peptoids have previously been synthesized to recreate this property of PEG or other antifouling polymers.[126] Perhaps similarly, the triethylether monomers of the peptoid polymer may create an antifouling polymer brush along the surface of the Pep2-SWCNT assembly. Thus, in future implementations of peptoid-SWCNT nanosensors, antifouling properties may be engineered into the construct with the addition of PEG-like monomers to the peptoid. We also find that chiralities with diameters around 0.9 nm to 1.0 nm are the least perturbed by the addition of surfactant and presumably have the highest packing density of peptoid (Fig. 3.15e, f). Several nanotube chiralities that seemingly appear as outliers, for example (10, 3) and (10, 5), have low populations in HiPco SWCNTs, and are difficulty to account for properly using our deconvolution code. Taken together, these results suggest that the sensitivity to protein analyte can be tuned in the future using nanotube chiralities with lower packing densities, as they might be more perturbed upon addition of analyte.

To confirm that additional stability to SC is provided to ProLoop-SWCNT assemblies after the selective binding of WGA, we showed that WGA by itself does not associate strongly to SWCNT. The attempted assembly of WGA with SWCNT produced a highly unstable complex upon probe-tip sonication that was destabilized from solution following centrifugation (Fig. 3.16a). Furthermore, the WGA-SWCNT constructs do not appear to respond to further sensing applications that will be revisited later in this dissertation (Fig. 3.16 b-d). These results suggest that the peptoid-coating of the SWCNT assembly is necessary to stably bind WGA, and the binding of the target analyte further promotes surface stability of the nanosensor-protein complex.

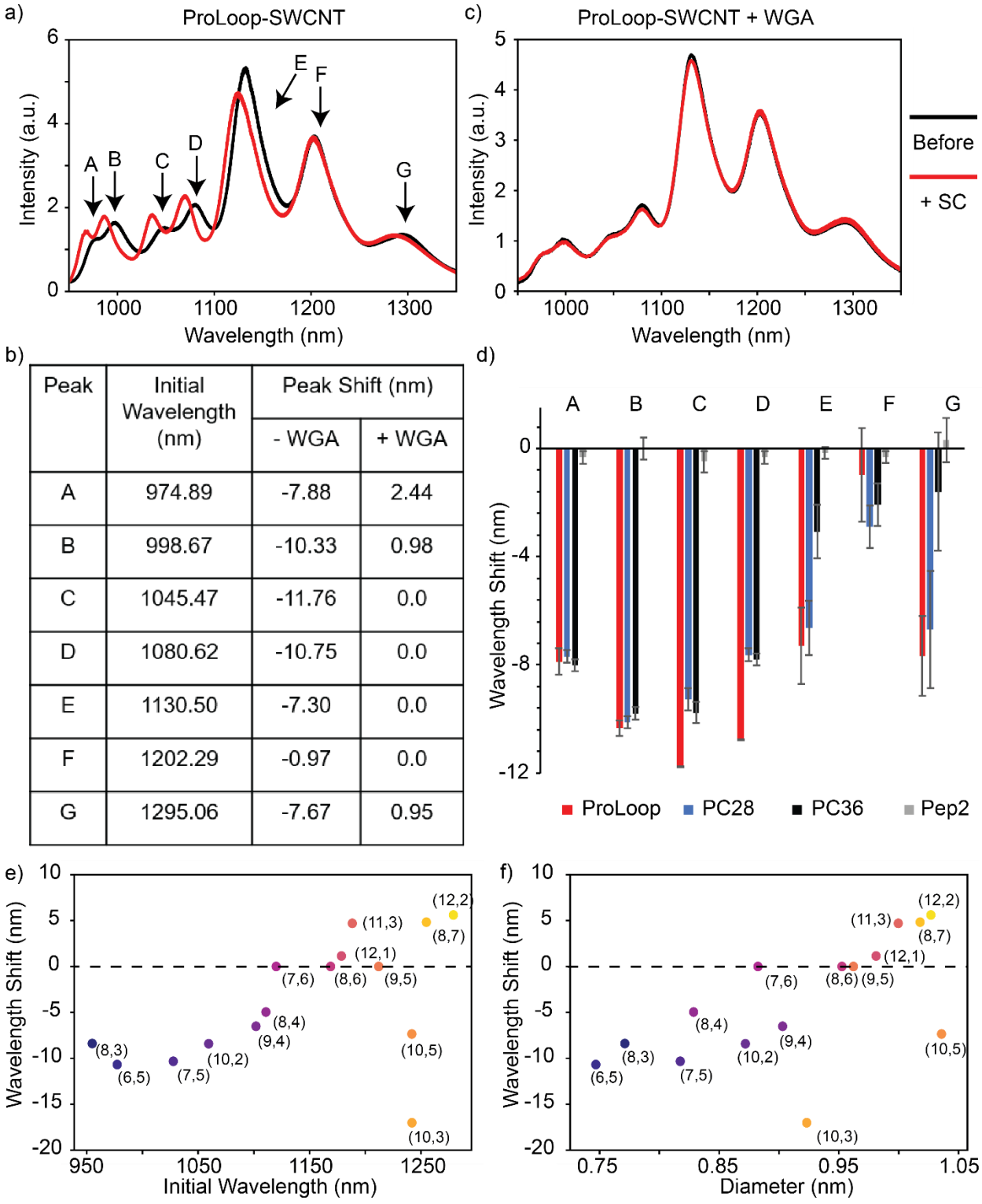

Peak	Initial Wavelength (nm)	Peak Shift (nm)	
		- WGA	+ WGA
A	974.89	-7.88	2.44
B	998.67	-10.33	0.98
C	1045.47	-11.76	0.0
D	1080.62	-10.75	0.0
E	1130.50	-7.30	0.0
F	1202.29	-0.97	0.0
G	1295.06	-7.67	0.95

Figure 3.15: ProLoop-SWCNT Nanosensor Sodium Cholate Stability.

a) Introduction of 0.5% (w/v) sodium cholate to the ProLoop-SWCNT nanosensor induced solvatochromic shifts. b) Peak wavelength shifts for multiple chiralities of ProLoop-SWCNT. c) Pre-incubation of ProLoop-SWCNT nanosensors with WGA prior to introduction of 0.5% sodium cholate eliminated the solvatochromic

shift, indicating WGA binds to and stabilizes the ProLoop-SWCNT assembly. d) Peak wavelength shifts observed for ProLoop, PC28, PC36, and Pep2 peptoid-SWCNT assemblies. Notably, Pep2-SWCNT is invariant to the addition of SC. Error denotes standard deviation for n = 6. e) Surfactant-mediated wavelength shift correlates with the initial wavelength of SWCNT chiralities. f) Surfactant-mediated wavelength shifts correlate with diameters of SWCNT chiralities. The dashed line in both graphs denotes a 0 nm wavelength shift.

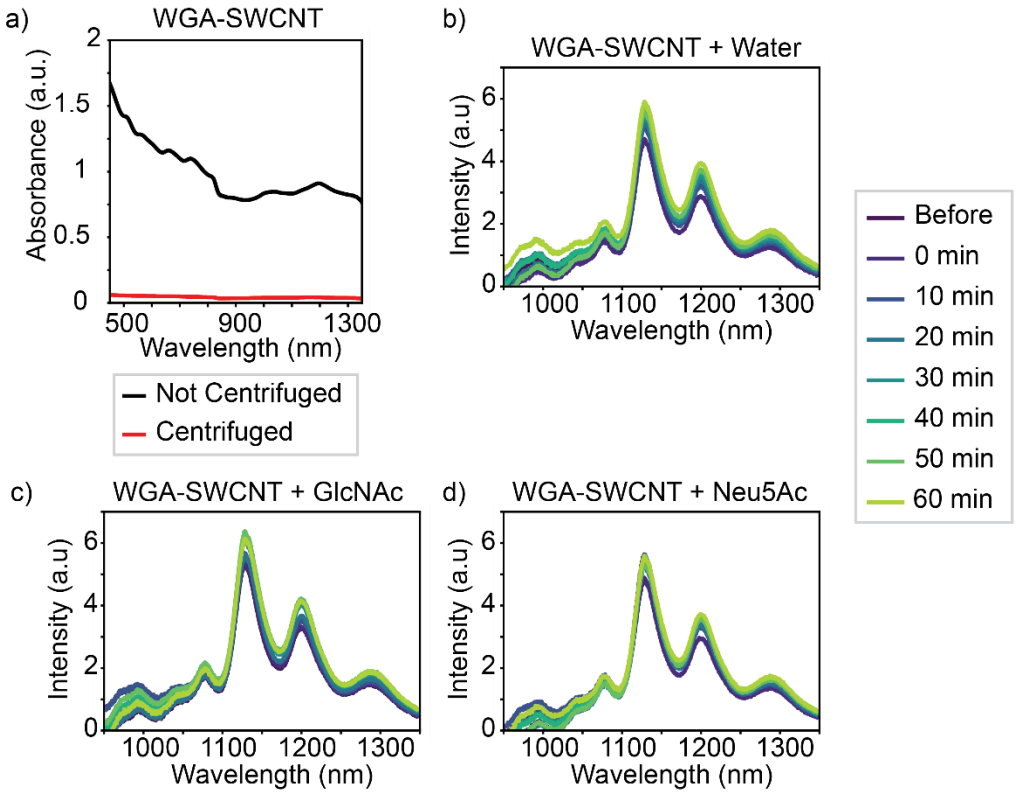

Figure 3.16: WGA Interactions with SWCNTs.

a) Absorbance spectrum of SWCNT sonicated with WGA. The WGA-SWCNT complex was only loosely associated, and centrifugation of the unstable WGA-SWCNT caused aggregation and subsequent the loss of absorbance and fluorescence. Representative fluorescence spectra of WGA-SWCNT suspensions without centrifugation shows no response to the addition of b) water as a control or WGA target sugars c) GlcNAc and d) Neu5Ac.

Peptoid-SWCNT Stability in Biological Media

We assessed whether peptoid-SWCNT nanosensors maintain their ability to detect WGA in complex biological environments. We showed that ProLoop-SWCNT nanosensors maintain their ability to respond to WGA in Dulbecco Modified Eagle's Medium (DMEM), a common medium used for mammalian cell culture. Pre-incubation of the nanosensors with DMEM for an hour maintained ProLoop-SWCNT nanosensor responsivity to 10 μM WGA (Fig. 3.17a). DMEM pre-incubated ProLoop-SWCNT nanosensors show a fluorescence decrease of -58.6 ± 8.6 % (mean ± SD) upon the addition of WGA against a baseline decrease of -29.3 ± 0.1 % (mean ± SD). Baseline decreases are caused by dilution effects and some nanosensor instability in DMEM.

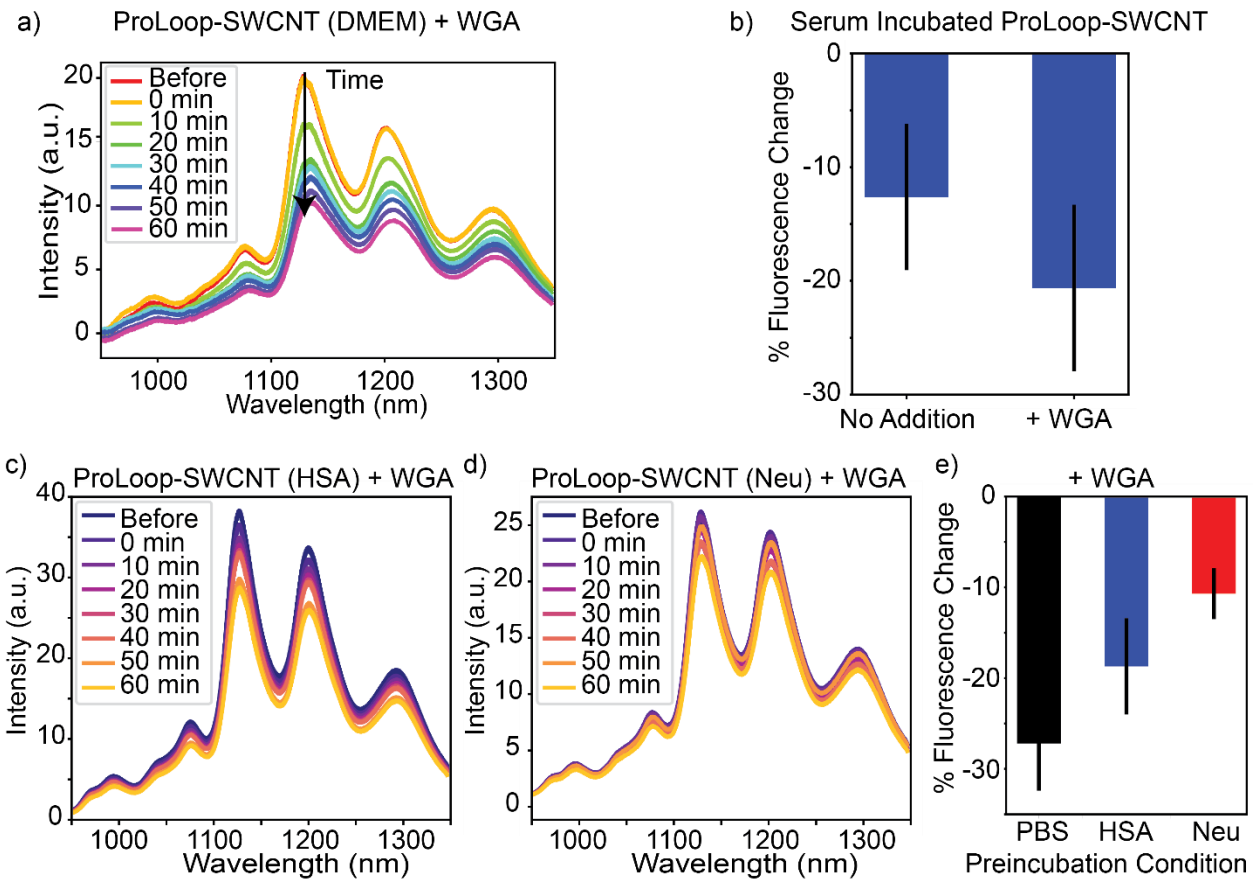

Figure 3.17: ProLoop-SWCNT Nanosensor Response in Protein-Rich Media.

The response of ProLoop-SWCNT nanosensors to WGA in protein-rich conditions; parentheses indicate the pre-incubation conditions of the ProLoop-SWCNT nanosensor an hour before the start of the imaging experiment. a) ProLoop-SWCNT responds to WGA when the nanosensor is preincubated in DMEM. b) ProLoop-SWCNT nanosensors show unstable fluorescence in serum, but still respond to WGA ($n = 9$, $p < 0.05$, error bars denote standard deviation). ProLoop-SWCNT fluorescence response to WGA can also be assessed after incubation with a single protein such as c) human serum albumin (HSA, 40 mg mL^{-1} concentration) and d) neutravidin (Neu, 5 mg mL^{-1} concentration). e) ProLoop-SWCNT response to WGA following incubation with these proteins is attenuated compared to ProLoop-SWCNT nanosensors in PBS buffer indicating some recognition interference by external proteins. Error bars denote standard deviation.

Lastly, we tested the responsivity of peptoid-SWCNT nanosensors in serum conditions. Nanosensor response was attenuated in the presence of fetal bovine serum, with peptoid-SWCNT nanosensors pre-incubated in serum for 24 hours exhibiting unstable fluorescence upon laser illumination. The fluorescence of ProLoop-SWCNT pre-incubated in serum decreased by -12.6 ± 6.4% (mean ± SD) over the course of 1 hour of spectrometry without the addition of WGA, and decreased by -20.6 ± 7.3% (mean ± SD) upon addition of WGA (Fig. 3.17b). Our results demonstrate nanosensors can recognize WGA in serum conditions, albeit with reduced sensitivity. ProLoop-SWCNT pre-incubated in neutravidin, a protein that binds bare nanotube surfaces, and recombinant human serum albumin, the most abundant protein in serum, also showed an attenuated but statistically significant fluorescence decrease response to WGA (Fig. 3.17 c-e). These results suggest that ProLoop-SWCNT nanosensors can monitor protein dynamics in *in vitro* cell cultures,

but that further optimization will be necessary to increase ProLoop-SWCNT nanosensor activity in serum and protein-rich conditions.

Single-Molecule Imaging of Peptoid-SWCNT Nanosensors

The bulk fluorescence response of ProLoop-SWCNT nanosensors to WGA can also be examined in the single-molecule regime using single ProLoop-SWCNT nanosensors immobilized on a microscope slide. This will also confirm that the fluorescence decrease of nanosensors are not the result of aggregation in bulk solutions. Negatively charged ProLoop-SWCNT nanosensors were surface-immobilized on a positively charged 3-aminopropyltriethoxysilane (APTES)-coated glass coverslip (Fig. 3.18a). When imaged using NIR microscopy, single nanosensors can be visualized as distinct regions of interest (Fig. 3.18b, c). Addition of WGA to a final protein concentration of 50 μM induces a fluorescence change in the saturated detection regime of the ProLoop-SWCNT nanosensor. Although single nanosensors exhibit variable fluorescence intensity trajectories over time, the average of the regions of interest show a significant decrease in fluorescence upon WGA addition -14.5 ± 2.0% (mean ± SD) compared to a control sample using only water -8.1 ± 3.5% (mean ± SD) (Fig. 3.18d). Single nanosensor imaging suggests that the molecular recognition of individual ProLoop-SWCNT nanosensors can be monitored optically for dynamic biological imaging.

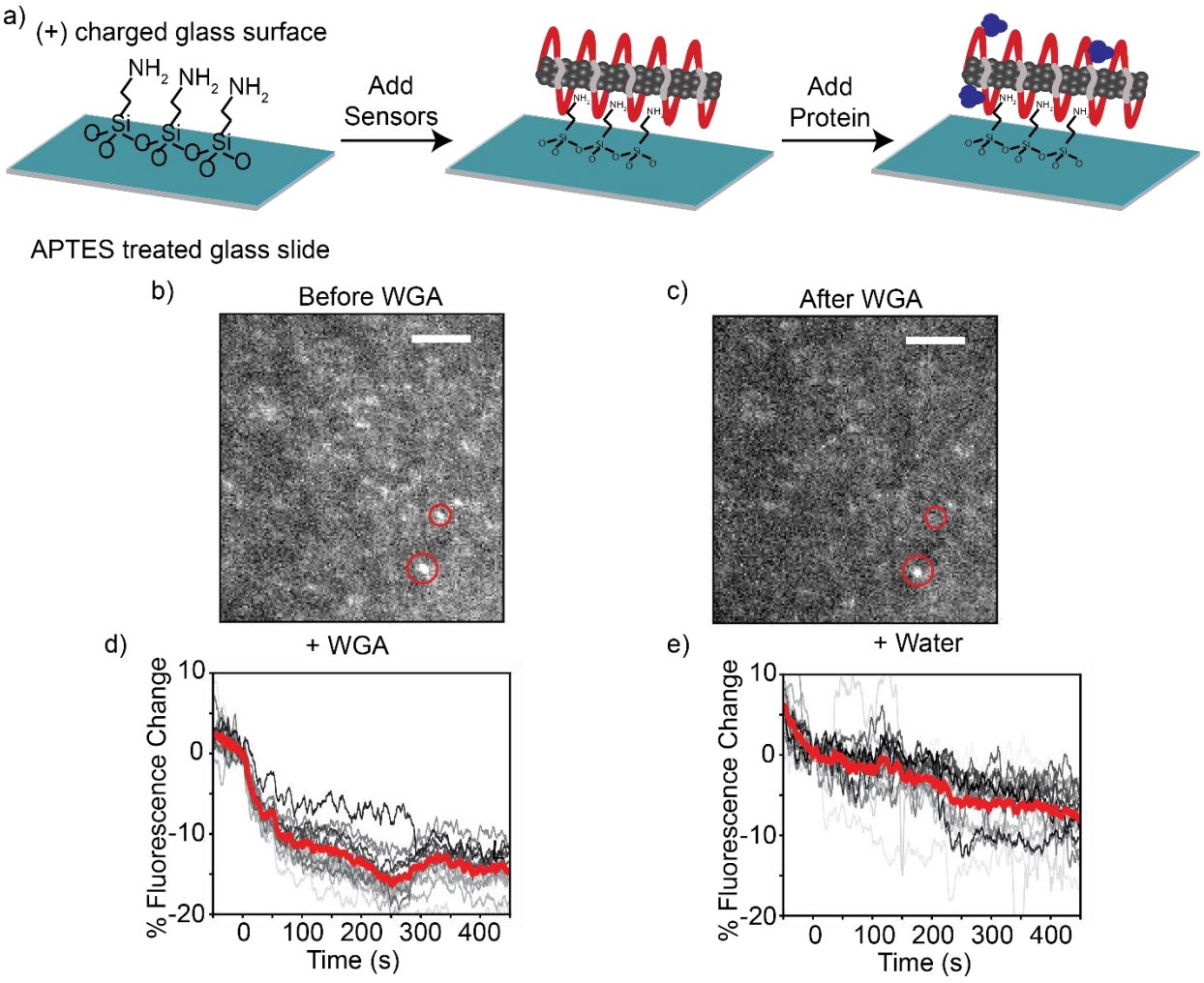

Figure 3.18: NIR Microscopy of ProLoop-SWCNT Nanosensors.

a) Schematic of single nanosensors immobilized on a (3-aminopropyl)triethoxysilane treated surface for NIR microscopy. b) Representative image of ProLoop-SWCNT nanosensors where red circles indicate regions of interest around nanosensors where fluorescence traces were recorded before and after addition of WGA. c) Same field of view after addition of WGA caused a loss of fluorescence. Scale bars: 25 μm. d) Single molecule microscopy traces of single ProLoop-SWCNT nanosensors exposed to WGA show a fluorescence response change above e) baseline drift. WGA was added at t = 0 s for single nanosensor intensities (grey) and the average of single nanosensor intensity changes (red).

WGA on Peptoid-SWCNT Enables Detection of WGA's Target Sugars

We further showed ternary nanosensor interactions of peptoid-SWCNT nanosensors, post-interaction with WGA, and a secondary analyte through lectin-sugar interactions. WGA protein is a lectin, a sugar-binding protein, with specificity to two target sugars: *N*-acetylglutaminic acid (GlcNAc) and *N*-acetylneuraminic acid (Neu5Ac).[127] Previous work has shown the recognition of glucose, fucose, and GlcNAc when enzymes and lectin proteins are grafted to the surface of SWCNTs.[128–130] These studies showed that proteins can remain active when tethered to the surface of SWCNT through a polymer intermediate, and we test to see if our synthetic peptoid system can emulate these findings.

We tested the activity of WGA when bound to the surface of ProLoop-SWCNT. We first incubated ProLoop-SWCNT in 10 μM WGA for an hour before measuring its fluorescence spectrum. A panel of sugars commonly bound by lectins were tested including fructose, galactose, glucose, mannose, and fucose and complex sugars such as sucrose and mannitol in addition to the target sugars GlcNAc and Neu5Ac. The addition of target sugars to WGA-saturated ProLoop-SWCNT yielded a significant change in nanosensor fluorescence intensity (Fig. 3.19a). This modulation of SWCNT fluorescence intensity was not observed with other sugars that other lectins are known to bind including fructose, galactose, and glucose. Interestingly, we observe an off-target response of the WGA-saturated ProLoop-SWCNT to fucose sugar, which might arise from orthogonal interactions between WGA and ProLoop-SWCNT that are not specific to the sugar-lectin interaction, but note that the sugar response selectivity for WGA adsorbed to ProLoop-SWCNT remains high with a 1 out of 9 rate for off-target sugar response.

We confirmed that WGA and ProLoop are both required and responsible for sugar-induced SWCNT fluorescence modulation. To assess whether target sugars affect the ability of ProLoop-SWCNT nanosensors to detect WGA, we pre-incubated ProLoop-SWCNT with target sugars GlcNAc and Neu5Ac an hour before measuring binding between WGA and ProLoop-SWCNT (Fig. 3.19b). Pre-incubation with sugar did not hinder ProLoop-SWCNT sensing of WGA, with the magnitude of fluorescence change upon the addition of WGA similar for each pre-incubation condition. Similarly, pre-incubation of the WGA protein with GlcNAc and Neu5Ac did not hinder ProLoop-SWCNT sensing of WGA. These control conditions yielded similar magnitudes of fluorescence response of ProLoop-SWCNT to WGA.

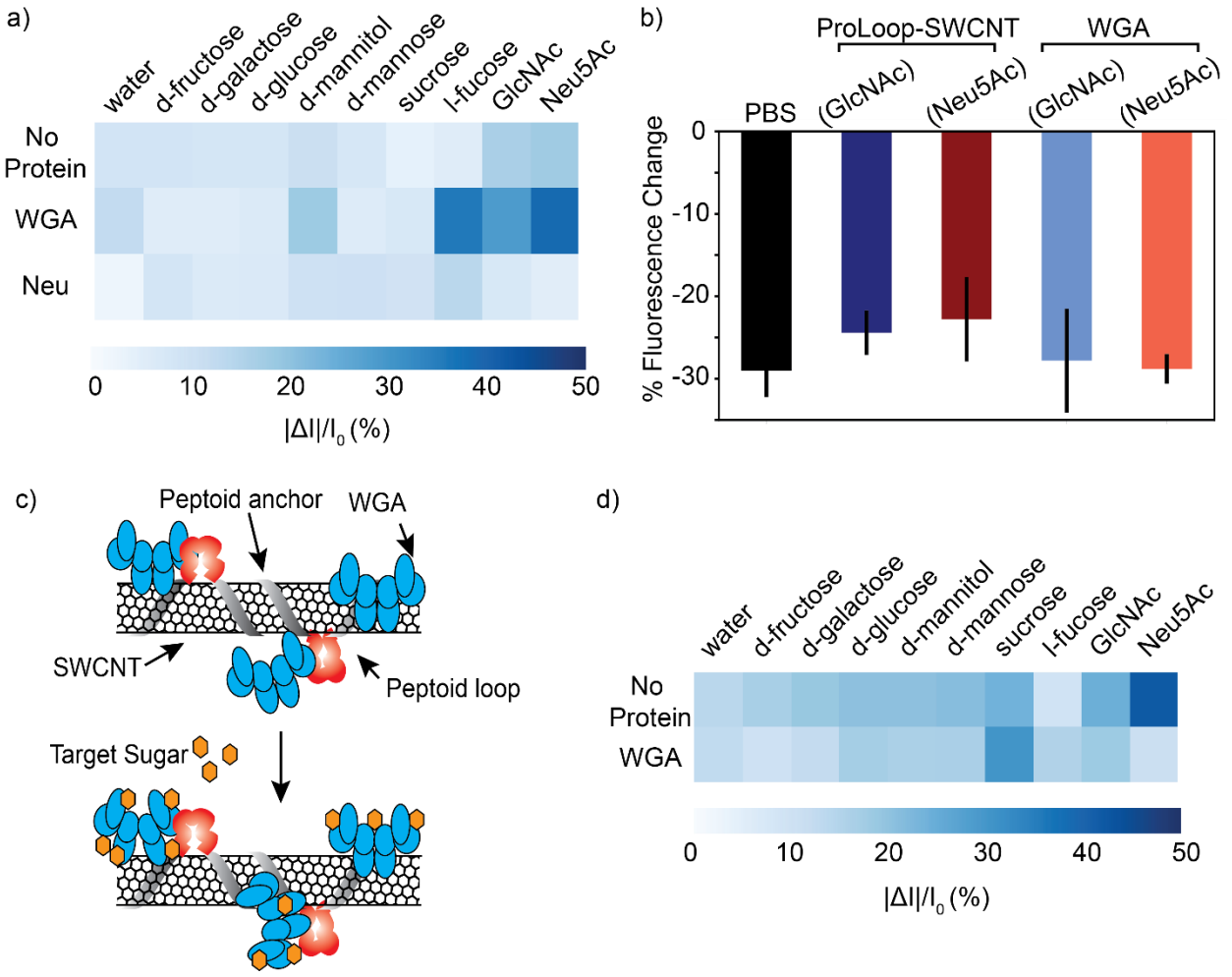

Figure 3.19: Ternary Sugar Sensing Using ProLoop-SWCNT.

a) WGA anchored to ProLoop-SWNT is selective for its target sugars GlcNAc and Neu5Ac, whereby ProLoop-SWNT nanosensors require the addition of both WGA and sugars to show this fluorescence signal modulation (n = 9). WGA-ProLoop-SWCNT nanosensor response to WGA's target sugars is absent without WGA or with NeutrAvidin (Neu) instead of WGA. b) Sugar blocking experiment, error denotes standard deviation for n = 9 (parenthesis indicate pre-incubation conditions of either ProLoop-SWCNT or WGA). Pre-incubation of ProLoop-SWCNT or WGA with WGA's target sugars (parenthesis indicate pre-incubation conditions) did not impede nanosensor response to WGA. c) A schematic of the proposed mechanism for ternary sugar interactions. Schematic not to scale. d) PC36-SWCNT response to sugars and WGA-incubated PC36-SWCNT response to sugars. No selective response to WGA conjugate sugars is observed, unlike with ProLoop-SWCNT.

We posit that sugar binding to the protein causes a protein conformational change or a perturbation to the corona phase of the ProLoop-SWCNT (Fig. 3.19c). Furthermore, we attributed this selective fluorescence response to the 6-monomer loop in the ProLoop peptoid, since WGA-incubated with PC36-SWCNT, which lacks this loop segment, does not respond to GlcNAc or Neu5Ac (Fig. 3.19d). Additionally, ProLoop-SWCNT preincubated with PNA and ConA did not yield a fluorescence response upon addition of their target sugars galactose and mannose, respectively. A common challenge in protein adsorption to nanoparticles for biosensing, enzymology, and protein delivery is a reduction in protein structure and activity.[64,131] Notably, the specificity of WGA towards its target sugars suggests WGA remains active while tethered to the SWCNT surface

through ProLoop-SWCNT. These results further suggest peptoid-SWCNT assemblies can enable detection of both proteins and also their target molecular binders. We further showed the fluorescence modulation of the ProLoop-SWCNT nanosensor towards WGA is not affected by or due to physical agitation (Fig. 3.20). Mixing of WGA-ProLoop-SWCNT complexes by pipetting did not induce WGA-ProLoop-SWCNT fluorescence modulation in the absence of target sugars.

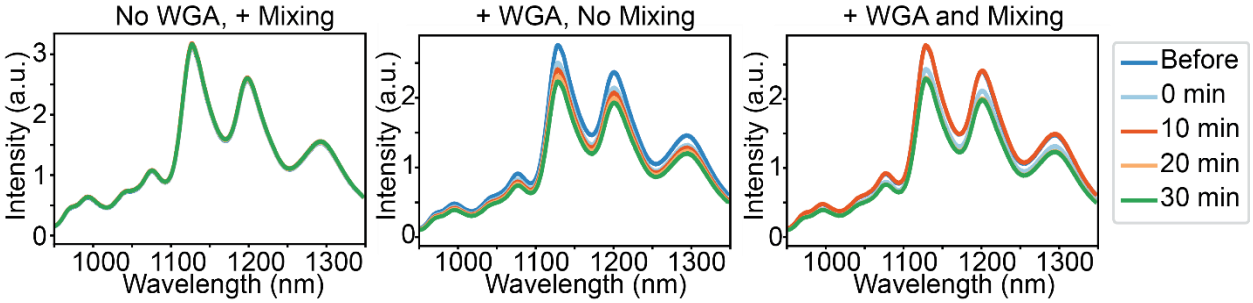

Figure 3.20: Physical Agitation of ProLoop-SWCNT Nanosensor.

Physical agitation by mixing showed that sample agitation is not the cause of nanosensor response to WGA.

3.5 Conclusions

In summary, we present design principles and validate the modular platform for assembly of protein-like *N*-substituted synthetic glycine peptoid polymers with SWCNTs. We demonstrated that certain peptoid sequences, namely ProLoop, exhibit the necessary stability to assemble on SWCNT and exhibit robust photostability under conditions necessary for real-time imaging of proteins including variable buffer conditions, continuous laser illumination, and resistance to protease degradation. We further showed that ProLoop-SWCNT can optically detect lectin protein WGA, and can also selectively detect the lectin target sugars.

An outstanding question in nanosensor development is whether molecular recognition elements can be rationally designed for analytes of interest with synthetically-tractable polymers. To this end, including peptoids in the repertoire of polymers for suspending SWCNT realizes a new space of biomimetic polymers for the development of SWCNT-based nanosensors. Peptoid polymers are resistant to protease degradation, leverage facile synthesis through automated solid phase synthesis, and exhibit a large monomer space that is unavailable for conventional biopolymers. Our results suggest peptoid polymers are promising candidates for modular design of synthetic molecular recognition elements with nanomaterial substrates to serve as signal transduction elements.[102,104,132,133] Our method of designing peptoid-SWCNT nanosensors is fundamentally general for any protein target. The primary limitation is assessing peptoid-SWCNT colloidal stability, since FRET screening of protein-binding peptoid loops can be accomplished upstream of peptoid-SWCNT assembly. By elucidating design parameters for creating peptoids that can adsorb onto SWCNT, and assessing the contributing factors to peptoid-SWCNT selectivity or sensitivity for WGA, our results set the groundwork for developing looped peptoid polymers for specific protein targets. In addition to the benefits of fluorescence detection of protein ligands, the ability to bind proteins to SWCNT with peptoid polymers could aid SWCNT-based biomolecule delivery platforms. SWCNT have been shown to internalize across a wide range of biological membranes for delivery applications[134–136], thus the ability to graft proteins selectively to SWCNT without

compromising endogenous protein function presents an enticing opportunity to deliver functional proteins to diverse biological systems. Previous work on peptoid polymers have shown success in selectively binding multivalent proteins, as well enzymes with known ligands, thus expanding the library of potential protein analytes or delivery cargoes for use in our peptoid-SWCNT platform.[107,108,137]

Lastly, our work shows that peptoid-SWCNT nanosensors can interact with proteins while preserving the protein's inherent activity. We demonstrated that ProLoop-SWCNT can bind WGA and can fluorescently respond to the two WGA target sugars GlcNAc and Neu5Ac, demonstrating that the WGA protein remains active towards its target sugars even when bound to a peptoid-SWCNT nanosensor. Despite prior reports of decreased or abolished protein activity upon protein adsorption to nanoparticles such as SWCNT, it is possible that the maintenance of protein activity is due to the ProLoop-mediated binding of WGA, in lieu of WGA binding to the SWCNT directly. Our results suggest peptoid polymers may serve a dual purpose of tethering proteins to SWCNT in a manner that enables protein detection and also preservation of the protein's endogenous activity for future applications in surface science, enzymology, and protein delivery.

Chapter 4: Covalent Surface Modification Effects on Single-Walled Carbon Nanotubes for Targeted Sensing and Optical Imaging‡

4.1 Abstract

Optical nanoscale technologies often implement covalent or noncovalent strategies for the modification of nanoparticles, whereby both functionalizations are leveraged for multimodal applications but can affect the intrinsic fluorescence of nanoparticles. Specifically, single-walled carbon nanotubes (SWCNTs) can enable real-time imaging and cellular delivery; however, the introduction of covalent SWCNT sidewall functionalizations often attenuates SWCNT fluorescence. Recent advances in SWCNT covalent functionalization chemistries preserve the SWCNT's pristine graphitic lattice and intrinsic fluorescence, and here such covalently functionalized SWCNTs maintain intrinsic fluorescence-based molecular recognition of neurotransmitter and protein analytes. Covalently modified SWCNT nanosensor preserve its fluorescence response towards its analyte for certain nanosensors, presumably dependent on the intermolecular interactions between SWCNTs or the steric hindrance introduced by the covalent functionalization that hinders noncovalent interactions with the SWCNT surface. These SWCNT nanosensors are further functionalized via their covalent handles to self-assemble on passivated microscopy slides, and these dual-functionalized SWCNT materials are explored for future use in multiplexed sensing and imaging applications.

4.2 Introduction

This chapter discusses the use of covalent strategies in the development of targeted protein SWCNT nanosensors. To orient the reader, a brief introduction is included to discuss the use of SWCNTs in covalent applications and existing fluorescent covalent techniques.

Nanomaterials are nanoscale particles that have been leveraged for biological applications such as imaging, gene or drug delivery, and therapeutics.[138,139] Nanomaterials can offer advantages over biological materials for said applications due to their tunable physicochemical properties that enable the manipulation of nanoparticles with different chemistries to create multiple modalities on a single particle. In particular, SWCNTs have been used as cellular delivery vehicles, fluorescent nanosensors, and implantable diagnostics.[38,45,134,140] Covalent and noncovalent SWCNT surface modifications enable the dispersion of hydrophobic SWCNTs in aqueous solution for their use as delivery agents and as nanosensors: covalent chemical functionalization has been used to add synthetic handles to attach cargo useful for molecular recognition and targeted delivery,[141–143] whereas noncovalent chemical functionalization is a preferred approach for sensing applications to preserve the SWCNT's intrinsic fluorescent properties. As with many other classes of nanoparticles, chemical functionalization of the SWCNT surface will often affect the nanoparticle's various optical, physical, and material properties.[72]

‡ Reprinted (adapted) with permission from Chio, L., Pinals, R. L., Murali, A., Goh, N. S., Landry, M. P., Covalent Surface Modification Effects on Single-Walled Carbon Nanotubes for Targeted Sensing and Optical Imaging. *Adv. Funct. Mater.* 2020, 1910556. https://doi.org/10.1002/adfm.201910556. Permission was obtained from supporting authors: Rebecca L. Pinals, Aishwarya Murali, Natalie S. Goh, and Markita P. Landry.

SWCNTs are an attractive class of nanomaterial for sensing applications, owing to the unique near-infrared (NIR) fluorescence of SWCNTs in the short wavelength infrared range of ~900-1500 nm. This region of NIR fluorescence is optimal for biological imaging, as the long wavelength light is minimally attenuated in biological tissues via reduced scattering and absorption of photons.[95,144] For SWCNT use as molecular nanosensors, it is necessary to preserve the intrinsic NIR fluorescence that arises from Van Hove transitions resulting from the density of states of the SWCNT lattice.[22] This fluorescence has been employed to develop a class of nanosensors that undergo fluorescence modulation upon selective binding of bioanalytes such as neurotransmitters, reactive nitrogen species, metabolites, peptides, and proteins.[33,35,36,46,48,145] The selectivity of these varied SWCNT nanosensors is created through a phenomenon termed corona phase molecular recognition (CoPhMoRe). CoPhMoRe nanosensors are capable of binding specific analytes through a constrained surface-adsorbed state formed by the noncovalent association of the SWCNT surface and a coating, such as polymer or phospholipid, not necessarily known to bind the analyte of interest. While SWCNT-based nanosensors generated with CoPhMoRe have shown recent success for imaging analytes *in vivo*[40,45,63] and for *ex vivo* imaging neuromodulation in acute brain slices,[146] their use has involved undirected biodistribution of SWCNTs in the tissue under investigation. For the purposes of tissue-specific or targeted sensing, inclusion of targeting moieties such as aptamers or proteins can be achieved via direct covalent attachment to SWCNT surfaces. Covalent chemistries offers several advantages over noncovalent chemistries for this attachment such as the formation of a strong covalent bond between the SWCNT surface and the targeting moiety and the preservation of the targeting moiety's structure through the availability of biocompatible bioconjugation attachment chemistries.[76] However, given that covalent modifications to SWCNTs often compromise intrinsic fluorescence, to date, simultaneous covalent and noncovalent functionalization of the SWCNT surface for sensing applications remains an outstanding challenge.

Obstacles for simultaneous covalent and noncovalent functionalization of fluorescent SWCNTs arise from surface defects created by covalent reactions. When the sp^2-hybridized carbon lattice of the SWCNT surface is disrupted via covalent modification, often non-radiative exciton recombination predominates, attenuating or obliterating SWCNT fluorescence which compromises the fluorescent readout of the SWCNT-based optical nanosensor.[70] Mild covalent SWCNT modifications via end-cap or defect engineering enable the creation of controlled sp^3 defects that modulate the SWCNT bandgap, resulting in a defect-based fluorescence red shift in the SWCNT fluorescence.[74,78,147,148] Additionally, recent developments in SWCNT chemistry have established a covalent functionalization reaction that re-aromatizes defect sites to re-form the original, pristine SWCNT lattice and restore intrinsic fluorescence.[79] This development could enable synergistic combination of covalent and noncovalent functionalization strategies to confer multiple functionalities to SWCNT-based technologies, such as theranostics, targeted fluorescence imaging, and towards understanding the fate of functionalized SWCNTs upon cellular delivery.

Herein, we combine covalent and noncovalent SWCNT functionalizations to study the effects of covalent modification on CoPhMoRe-based SWCNT nanosensors that rely on noncovalent functionalization for sensing. We synthesized and characterized several SWCNTs with different covalent surface modifications that are subsequently functionalized with noncovalent coatings for downstream use as fluorescent nanosensors. We show how the addition of surface groups impacts both the fluorescence and analyte responsivity of certain CoPhMoRe-based SWCNT nanosensors.

We further demonstrate how the addition of charged chemical functionalizations affects the corona formation and overall SWCNT assembly stability. Finally, we combine these findings to create dual-functional SWCNTs with targeted recognition and fluorescence sensing capabilities.

4.3 Experimental

Materials

All chemicals unless otherwise noted were purchased from Sigma-Aldrich. Raw high-pressure carbon monoxide (HiPco) synthesized single-walled carbon nanotubes (SWCNTs) were purchased from NanoIntegris. EZ-Link amine-PEG_2-biotin and neutravidin protein was purchased from ThermoFisher Scientific. Streptavidin magnetic beads were purchased from New England BioLabs.

Synthesis of Triazine-Functionalized SWCNTs (Trz-H-SWCNTs and Trz-L-SWCNTs)

Synthesis of Trz-SWCNTs was adapted from previous literature.[79] In brief, SWCNTs (1 g) were dispersed in N-methyl-2-pyrrolidone (150 mL) in a round bottom flask and bath sonicated for 1 hour. The dispersion was stirred for 1 hour at 25 °C and cooled down to 0 °C. 2,4,6-1,3,5-trichloro-triazine (10 g, 54 mmol) was dissolved in N-methyl-2-pyrrolidone (50 ml) and the obtained solution was slowly added to the SWCNT dispersion at 0 °C. Sodium azide (1.76 g, 27 mmol) was added to the mixture and stirred for 2 hours at 0 °C followed by 12 hours stirring at either 70 °C or 25 °C to yield Trz-H-SWCNTs or Trz-L-SWCNTs, respectively. The product was purified by centrifugation and washed by re-dispersion in water and organic solvents (acetone, toluene, then chloroform), and lyophilized for storage and characterization. The triazine functionalization was previously characterized by elemental analysis, XPS, thermogravimetric analysis, Raman, and IR spectroscopy.[79]

Synthesis of SH-SWCNTs or Charged SWCNTs (NH_2-SWCNTs and COOH-SWCNTs)

Trz-H-SWCNTs (10 mg) were dispersed in dimethylformamide (DMF) (5 ml) and bath sonicated for 15 minutes at room temperature. Next, 1 mg of either cysteine, ethylenediamine, or glycine (for SH-SWCNTs, NH_2-SWCNTs, and COOH-SWCNTs, respectively) and a 1.5 molar excess of triethylamine to chemical were added to the mixture that was stirred at 65 °C for 2 days. The product was purified by centrifugation and re-dispersion in washes of DMF (2 x 4 mL) followed by washes of water (2 x 4 mL). SH-SWCNTs were dialyzed against water using a Slide-A-Lyzer G2 10 kilodalton (kDa) molecular cutoff dialysis cassette (Thermo Scientific) with daily water changes for 1 week. The product was lyophilized for storage and characterization.

Synthesis of Biotin-SWCNTs

Trz-H-SWCNTs (5 mg) were dispersed in DMF (2 mL) and bath sonicated for 15 minutes at room temperature. A solution of EZ-Link amine-PEG_2-biotin in DMF (25 mg mL^{-1}) was made up. Amine-PEG_2-biotin solution (500 μL) and triethylamine (86 μL) were added to the Trz-H-SWCNT solution. The mixture was stirred at 65 °C for 2 days. The product was purified by centrifugation and re-dispersion in washes of DMF (2 x 4 mL) followed by washes of water (2 x 4 mL). The product was then dialyzed against water using a Slide-A-Lyzer G2 10 kDa molecular cutoff dialysis cassette (Thermo Scientific) with daily water changes for 1 week. The product was pelleted by centrifugation and lyophilized for storage and characterization.

Elemental Analysis
Elemental analyses (C, H, N, S) were obtained at the Microanalytical Laboratory at the University of California, Berkeley on a Perkin Elmer 2400 Series II cumbusion analyzer. Based on the classical Pregl-Dumas method, samples are combusted in a pure oxygen environment, with the resultant combustion gases measured in an automated fashion. The degree of functional groups (DFG) was calculated by determining the total mass of N or S atoms within the functional group divided by either the total N or S content of the product, respectively. This value was then divided by the remaining C content of the product. We report the geometric mean DFG assuming one functional arm or two functional arms on each triazine group.

Noncovalent Adsorption of Polymer and DPPE-PEG5k Coatings to SWCNT by Probe-Tip Sonication
$(GT)_{15}$, $(GT)_6$, and DPPE-PEG5k SWCNT nanosensors were constructed through probe-tip sonication. SWCNTs (1 mg) were added to 1x phosphate buffered saline (PBS, 500 μL, pH 7.4) and polymer (1 mg) or DPPE-PEG5k (1 mg). The solution was bath sonicated for 10 minutes, and then probe-tip sonicated using a Cole Parmer ultrasonic processor and a 3 mm stepped microtip probe with pulses of 3-7 watts every 3 seconds for 15 minutes. The solution was subsequently allowed to equilibrate on the bench at room temperature for 1 hour before centrifugation at 16.1 x 10^3 Relative Centrifugal Force (RCF) for 30 minutes to remove any unsuspended nanotube aggregates. Nanosensors formed a homogeneous dark-gray solution and concentration was characterized by UV-Vis-IR absorbance using a Shimadzu UV-3600 Plus. SWCNT concentration was calculated from absorbance at 632 nm using Beer-Lambert law with extinction coefficient, ε_{632} = 0.036 L mg^{-1} cm^{-1}.[95]

Noncovalent Adsorption of Sodium Cholate to SWCNT (SC-SWCNT)
SWCNTs (3 mg) were added to 1 wt % sodium cholate (SC, 3 mL). The solution was bath sonicated for 10 minutes, and then probe-tip sonicated using a 500 W Cole Parmer Ultrasonic Homogenizer and a 6 mm stepped microtip probe at 10% amplitude every 2 seconds for 60 minutes. The solution was subsequently allowed to equilibrate at room temperature for 1 hour before centrifugation at 23.1 x 10^3 Relative Centrifugal Force (RCF) for 50 minutes to remove any unsuspended nanotube aggregates. Assemblies formed a homogeneous dark-gray solution and concentration was characterized by UV-Vis-IR absorbance using a Shimadzu UV-3600 Plus. SWCNT concentration was calculated from absorbance at 632 nm using Beer-Lambert law with extinction coefficient, ε_{632} = 0.036 L mg^{-1} cm^{-1}.[95]

Noncovalent Adsorption of C16-PEG2k-Ceramide Coating to SWCNT through Dialysis
A solution of SC-SWCNTs (25 mg L^{-1}) and C16-PEG2k-ceramide (2 mg mL^{-1}) in 1% sodium cholate was added to a 1 kDa molecular weight cutoff dialysis cartridge (GE Healthcare). The solution was dialyzed against water with multiple water exchanges for a week, such that the C16-PEG2k-ceramide exchanged the sodium cholate coating by adsorbing onto the nanotube surface and replacing the small surfactant molecules.

Near Infrared Spectroscopy of SWCNT Nanoensors
All SWCNT nanosensor solutions were diluted to a final SWCNT concentration of 5 mg L^{-1} in 1x PBS. Spectroscopic analysis was performed by measuring the resulting SWCNT photoluminescence with a home-built near infrared fluorescence microscope. Briefly, a Zeiss

AxioVision inverted microscope was coupled to a Princeton Instruments IsoPlane 320 containing a liquid nitrogen-cooled Princeton Instruments PyLoN-IR 1D InGaAs array. SWCNT nanosensors were illuminated by a 500 mW, 721 nm laser. The spectra of SWCNT nanosensors were acquired, each in a separate well of a glass-bottom 384-well plate (Corning). Fluorescence spectra were compared between the covalently functionalized SWCNTs as previously reported for each nanosensor.[35,36,48,125] Briefly, for $(GT)_{15}$-SWCNT and $(GT)_6$-SWCNT nanosensors, we compared the change in the (7,6) chirality peak at 1122 nm. For DPPE-PEG5k nanosensors, we compared the change in intensity of the joint (9,4) and (7,6) chirality peaks at 1118 nm. C_{16}-PEG2k-ceramide nanosensor spectra were deconvoluted into separate chirality contributions and we compared the integrated intensity under the full spectra for the (10,2) chirality centered around 1053 nm.

X-ray Photoelectron Spectroscopy

Samples were drop cast onto the surface of a clean silicon wafer. XPS spectra were collected with a PHI 5600/ESCA system equipped with a monochromatic Al Kα radiation source ($h\nu$ = 1486.6 eV). High-resolution XPS spectra were deconvoluted with MultiPak software (Physical Electronics) by centering the C-C peak to 284.5 eV, constraining peak centers to ±0.1 eV the peak positions reported in previous literature[149], constraining full width at half maxima (FWHM) ≤1.5 eV, and applying Gaussian-Lorentzian curve fits with the Shirley background.

Fourier Transform Infrared Spectroscopy

Infrared spectra were measured on a Perkin-Elmer Spectrum 100 Optica FTIR spectrometer equipped with an attenuated total reflectance (ATR) accessory. Purified and vacuum-dried SWCNT samples was deposited to the surface of the ATR and scanned.

Methanol Exchange of Phospholipid to DNA Coating

Methanol-driven exchange of phospholipid to DNA coating was performed to be able to quantitively measure starting and final quantities of SWCNTs by absorbance spectroscopy. The initial suspension yields for C_{16}-PEG2k-Ceramide-coated SWCNTs were comparable for pristine-SWCNTs (214.7 mg L^{-1} ± 65.7, mean ± SD), COOH-SWCNTs (241.6 mg L^{-1} ± 50.4, mean ± SD), and NH_2-SWCNTs (220.6 mg L^{-1} ± 51.5, mean ± SD). The following protocol has been adapted from previous studies.[34,53] A solution of C16-PEG2k-Ceramide-coated SWCNTs (100 mg L^{-1} SWCNT concentration, 150 µL) in 1x PBS was mixed with a solution of DNA in 1x PBS (100 µL, 10 mg mL^{-1}). Methanol (90 µL) was added in increments followed by 5 minutes of bath sonication. 7 total additions of methanol were added to the solution for a total of 630 µL of methanol. Isopropanol (300 µL) was added immediately followed by brief centrifugation (17000 RCF for ~1 s) to immediately cause the precipitation of DNA-wrapped SWCNTs in a soft pellet. The supernatant was placed in another microcentrifuge tube and centrifuged at 17000 RCF for 15 minutes to precipitate remaining DNA. The DNA pellet was resuspended in PBS (400 µL) and subsequently used to resuspend the DNA-SWCNT pellet. The solution was bath sonicated for 10 minutes, and then probe-tip sonicated using a Cole Parmer ultrasonic processor and a 3 mm stepped microtip probe with pulses of 3-7 watts every 3 seconds for 15 minutes. The solution was subsequently allowed to equilibrate at the bench overnight before centrifugation at 16.1 x 10^3 RCF for 20 minutes to remove any unsuspended nanotube aggregates. DNA-SWCNT concentration was calculated from absorbance at 632 nm using Beer-Lambert law with extinction coefficient, ε_{632} = 0.036 L mg^{-1} cm^{-1}. From the DNA-SWCNT concentration, the percent yield was calculated

by dividing mass of DNA-SWCNT product by the initial mass of C16-PEG2k-Ceramide-coated SWCNTs.

Zeta Potential Measurements

Zeta potential measurements were taken on a Zetasizer Nano ZS (Malvern Instruments). Prior to measurements, SWCNT samples (700 μL, 10 mg L^{-1}) were purified of excess salts and DNA or phospholipids by spin-filtering and diluting in MilliQ water. Three replicates of 20 measurements were obtained for each sample after 30 seconds equilibration.

Streptavidin Bead Affinity Protocol on Biotin-SWCNTs

A solution of SWCNT (10 mg L^{-1}) nanosensors was prepared in binding buffer (300 μL, 20 mM Tris-HCl, 500 mM NaCl, 1 mM EDTA, pH 7.5). Magnetic streptavidin beads (1 mg, New England Biosciences) were aliquoted into a microcentrifuge tube, a magnet was applied to the side of the tube, and the storage buffer was removed. The beads were washed 4 times by resuspension in binding buffer (1000 μL), application of a magnet on the side of the tube, and removal of the supernatant. This wash step was repeated 3 more times. The SWCNT solution was added to the magnetic streptavidin beads and the tube was shook at a gentle speed for 2 hours. The depleted SWCNT sample was collected and the beads were washed 3 times with binding buffer (1000 μL).

Atomic Force Microscopy of SWCNT Complexes

Monodispersed SWCNT nanosensors in the presence and absence of neutravidin were analyzed with atomic force microscopy using an Asylum Research MFP-3D AFM and TAP150AL-G-10 Silicon AFM probes (Ted Pella, tip radius < 10 nm). For the addition of neutravidin, SWCNT nanosensors (20 mg L^{-1}) were incubated with neutravidin (0.025 mg mL^{-1}) for 1 hour. 20 μL of SWCNT nanosensors were deposited on freshly cleaved mica and incubated for 1 hour at room temperature. Unbound nanosensors, protein, and salts were washed from the mica three times using MilliQ water. The surface was subsequently dried under nitrogen. AFM was performed in tapping mode at a scan rate of 0.8 Hz using a sample rate of 512 lines.

4.4 Results and Discussion

Generating Covalent SWCNT Nanosensors

We generated defect-free covalently functionalized SWCNTs as previously reported[79,150] by performing a chemical re-aromatization reaction using unfunctionalized SWCNTs (pristine-SWCNTs) and cyanuric chloride to produce triazine-functionalized SWCNTs at low and high-labeling densities, denoted Trz-L-SWCNTs and Trz-H-SWCNTs, respectively. The densities of functional groups were measured for each functionalization condition using elemental analysis, and are in good agreement with previous findings (Table 4.1). Trz-H-SWCNTs were further functionalized through nucleophilic substitution of the chlorine on the triazine with a primary amine to create a library of surface-functionalized SWCNTs at positions denoted by variable R groups (Fig. 1a and 1b). In this manner, we reacted Trz-H-SWCNTs with cysteine to form thiol-functionalized SWCNTs (SH-SWCNTs). We report a higher than expected level of thiol functionalization for SH-SWCNT and amine functionalization for NH_2-SWCNT attributed to excess starting material adsorbed on the SWCNT surface.

Table 4.1: Elemental Analysis of Covalent SWCNTs.

Elemental analysis of the different covalently functionalized SWCNTs used in this study with the mass percentage of each element reported. Degree of functionalization (DFG) refers to the fraction of carbons on the surface lattice that contain the functional group of each particular SWCNT as denoted in figure 4.1b. Our results are in good agreement with previously reported for pristine-SWCNT, Trz-L-SWCNT, and Trz-H-SWCNT.[79]

Sample	% C	% H	% N	% S	DFG
Pristine- SWCNT	64.16	0.63	0.42	0.0	n/a
Trz-L-SWCNT	56.52	1.61	2.62	0.0	1/98
Trz-H-SWCNT	63.29	1.64	3.93	0.0	1/72
SH-SWCNT	55.89	3.45	5.52	11.24	1/24
NH_2-SWCNT	74.99	1.72	3.54	0.0	1/61
COOH-SWCNT	76.95	1.42	1.72	0.0	1/209
Biotin-SWCNT	69.24	2.29	4.1	1.04	1/253

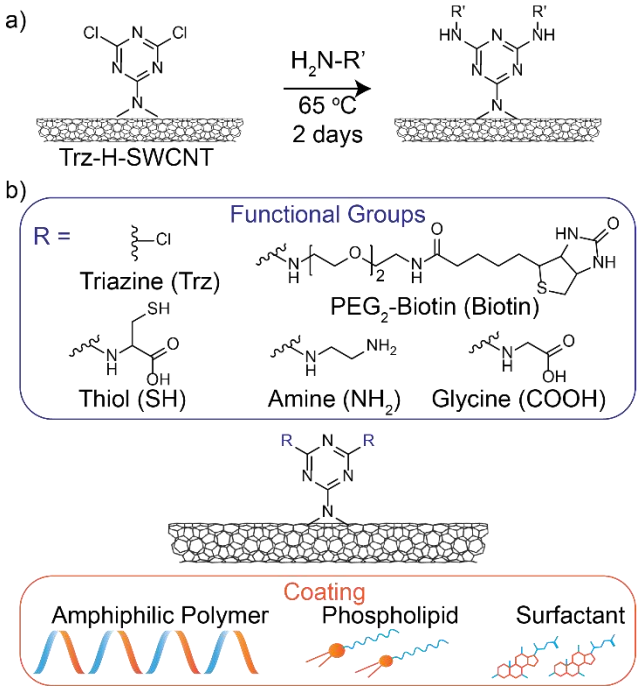

Figure 4.1: Functionalization of SWCNTs for Nanosensor Generation.

a) Functional groups are added to Trz-H-SWCNT via a nucleophilic substitution reaction whereby primary amines replace the chlorines of the triazine group. b) Overview of the different functional groups and SWCNT coatings tested to create multifunctional fluorescent nanosensors.

We next assessed the impact of the triazine and thiol covalent SWCNT surface functional groups on the performance of CoPhMoRe nanosensors generated from Trz-L-SWCNTs, Trz-H-SWCNTs and SH-SWCNTs. We tested several previously reported SWCNT-based nanosensors to image dopamine, fibrinogen, and insulin analytes. Specifically, when noncovalently adsorbed to the SWCNT surface, single-stranded DNA (ssDNA) oligomers $(GT)_{15}$ and $(GT)_6$ form known nanosensors for dopamine,[35,151] DPPE-PEG5K phospholipid for fibrinogen,[48] and C_{16}-PEG2k-ceramide phospholipid for insulin.[36] To generate each nanosensor, we induced noncovalent

association of the SWCNTs with each coating through π-π aromatic stabilization and hydrophobic packing via probe-tip sonication or dialysis as previously established (see methods for details). We prepared dopamine, fibrinogen, and insulin nanosensors with both pristine and functionalized SWCNTs. We expand upon the findings of previous literature that covalently-functionalized Trz-L-SWCNTs, Trz-H-SWCNTs, and SH-SWCNTs maintain their intrinsic optical properties and show that this remains the case when dispersed with their respective surfactant, phospholipid, or polymer coatings (Fig. 4.2), prior to assessing their use as fluorescent optical nanosensors. All nanosensors remained in solution 3 months post-synthesis, with no noticeable trends on the instability of functionalized SWCNTs relative to pristine-SWCNTs (Fig. 4.3).

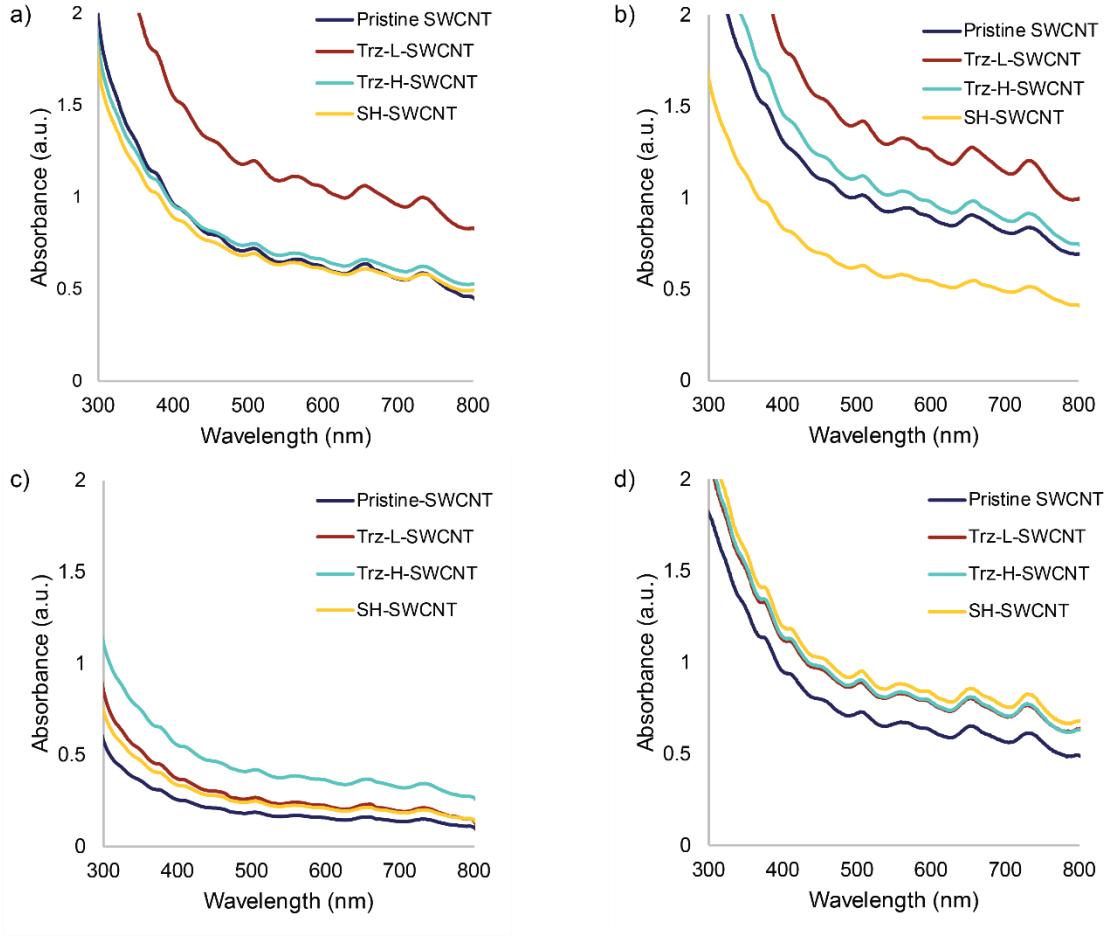

Figure 4.2: Absorbance Spectroscopy Comparing the Yields of Covalent SWCNTs After Noncovalent Functionalization.

Absorbance spectra of covalently functionalized SWCNTs suspended in: a) $(GT)_{15}$, b) $(GT)_6$, c) DPPE-PEG5k, and d) C_{16}-PEG2k-ceramide. All coatings were adsorbed through dispersion using probe-tip sonication, except C16-PEG2k-ceramide, which was suspended through dialysis. Absorbance is directly proportional to concentration, with a lower absorbance indicating lower suspension yields.

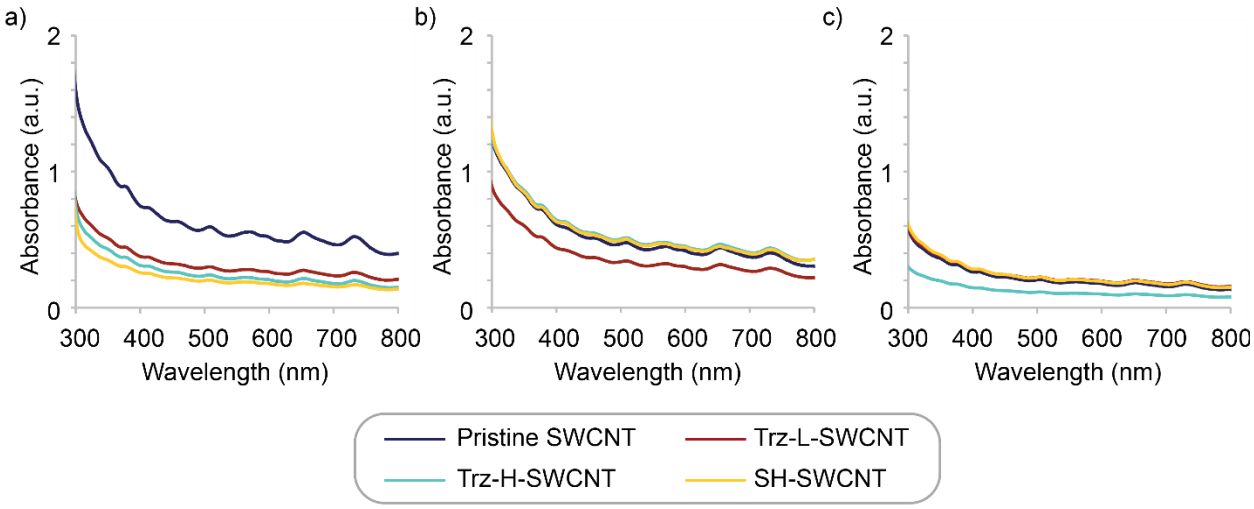

Figure 4.3: Stability of Covalent SWCNT Nanosensors Three Months Post-Synthesis.

SWCNTs were centrifuged to pellet any aggregates and normalized by initial concentration to yield absorbance spectra for a) $(GT)_{15}$-, b) $(GT)_6$-, and c) DPPE-PEG5k-coated nanosensors. There are no definitive trends observed between functional group and stability relative to pristine-SWCNT.

Comparing Performance of Covalent SWCNT Nanosensors to Pristine Nanosensors

We compared the fluorescence response to analyte for nanosensors made from pristine-SWCNTs, Trz-L-SWCNTs, Trz-H-SWCNTs, and SH-SWCNTs (Fig. 4.4a). By comparing the performance of nanosensors generated from pristine versus functionalized SWCNTs, we quantified functionalization-dependent fluorescence performance of nanosensors upon exposure to their respective analytes of dopamine, fibrinogen, and insulin (Fig. 4.4b). We measured the fluorescence change of 5 mg L^{-1} phospholipid or polymer suspended pristine-SWCNT, Trz-L-SWCNT, Trz-H-SWCNT, and SH-SWCNT nanosensors upon exposure to their respective analytes. Responses were measured before and 10 to 30 minutes after the addition of 100 µM dopamine to $(GT)_{15}$- and $(GT)_6$-SWCNT nanosensors, 1 mg mL^{-1} of fibrinogen to DPPE-PEG5k-SWCNT nanosensors, and 20 µg/mL insulin to C_{16}-PEG2k-ceramide-SWCNT nanosensors. Changes in fluorescence were calculated and normalized to the changes measured in pristine-SWCNT nanosensors to determine how surface functionalization impacts CoPhMoRe sensing (see section 4.3).

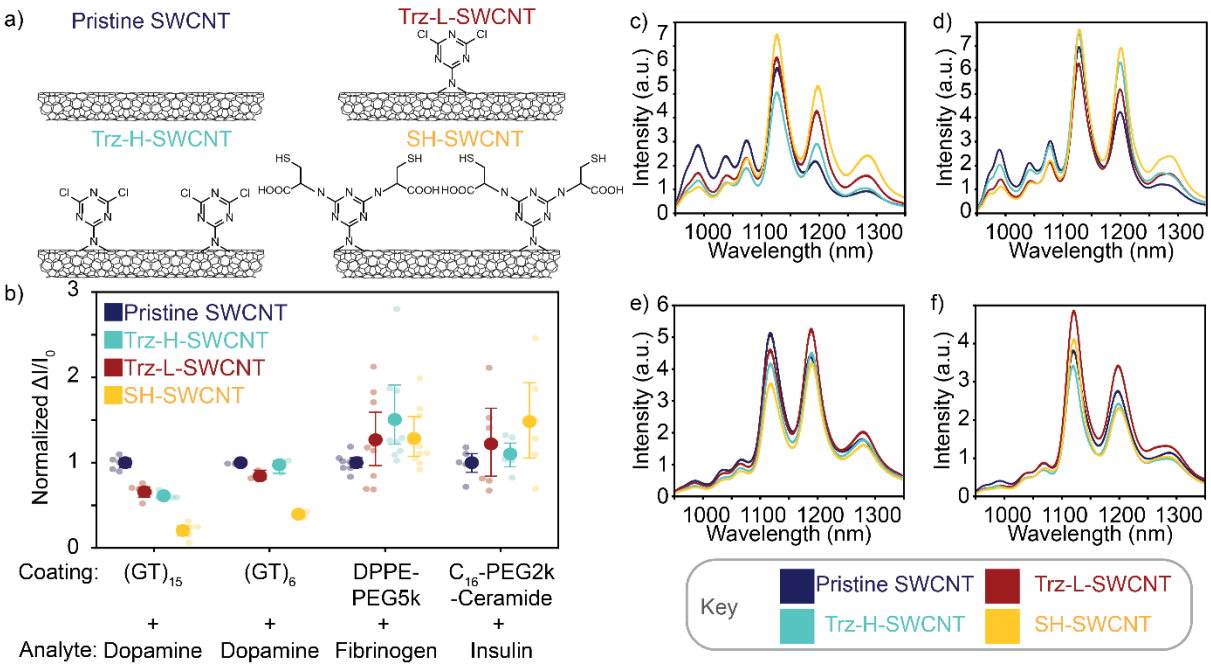

Figure 4.4: Effect of Covalent and Noncovalent Functionalization on SWCNT Nanosensor Fluorescence Response.

a) Structures of covalently functionalized SWCNTs investigated in this study. B) Normalized fluorescence change of 5 mg L^{-1} covalently modified SWCNT nanosensors upon addition of their respective dopamine (100 μM), fibrinogen (1 mg mL^{-1}), and insulin (20 μg mL^{-1}) analytes, normalized to the response of nanosensors generated from pristine-SWCNT (large dots denote mean normalized fluorescence change, each small faded dot denotes an experimental replicate, and error bars denote standard deviation for n = 3 to 9 trials). Covalently functionalized ssDNA-SWCNT nanosensors sensitive to the coating's structural conformation show an attenuated response to analyte, as compared to structure-independent phospholipid coatings. Fluorescence spectra of concentration-normalized samples of 5 mg L^{-1} c) $(GT)_{15}$-SWCNT, d) $(GT)_6$-SWCNT, e) DPPE-PEG5k-SWCNT, or f) C_{16}-PEG2k-Ceramide-SWCNT.

The performance of $(GT)_{15}$ dopamine nanosensors decreased when covalently functionalized SWCNTs were used as compared to pristine-SWCNTs. We calculated the fluorescence change ($\Delta I/I_0$) for our covalently-functionalized SWCNTs and then normalized against the $\Delta I/I_0$ of the pristine SWCNTs (to see absolute $\Delta I/I_0$ before normalization refer to Fig. 4.5). This analysis yielded normalized fluorescence response for $(GT)_{15}$-Trz-L-SWCNTs (0.661 ± 0.118, mean ± SD), $(GT)_{15}$-Trz-H-SWCNTs (0.613 ± 0.083, mean ± SD), and $(GT)_{15}$-SH-SWCNTs (0.207 ± 0.095, mean ± SD), compared to a nanosensor fluorescence response for the original dopamine nanosensor constructed from $(GT)_{15}$- pristine-SWCNTs (1.0 ± 0.121, mean ± SD). Previous molecular simulations postulate that the longer polymer $(GT)_{15}$ forms a helical conformation on the surface of the nanotube, while the shorter polymer $(GT)_6$ forms rings on the surface.[152] To assess the impact of ssDNA polymer length on adsorption to a covalently functionalized SWCNT surface, we tested the dopamine responsivity of of Trz-L-SWCNTs, Trz-H-SWCNTs, and SH-SWCNTs noncovalently functionalized with $(GT)_6$ versus $(GT)_{15}$ ssDNA. We hypothesize that the corona adopted by the ring-forming $(GT)_6$ is less sterically perturbed by the addition of chemical functional groups on the SWCNT surface. Unlike dopamine nanosensors generated from $(GT)_{15}$, we found that the normalized nanosensor fluorescence responses for $(GT)_6$ suspended Trz-L-

SWCNTs, Trz-H-SWCNTs, and SH-SWCNTs, exhibited a recovery of fluorescence response: $\Delta I/I_0$ for $(GT)_6$-Trz-L-SWCNTs (0.844 ± 0.051, mean ± SD), $(GT)_6$-Trz-H-SWCNTs (0.974 ± 0.073, mean ± SD), and $(GT)_6$-SH-SWCNTs (0.396 ± 0.031, mean ± SD), are all closer to the fluorescence response for the dopamine nanosensor constructed from $(GT)_6$-pristine-SWCNTs (1.0 ± 0.026 , mean ± SD) compared to functionalized SWCNT dopamine sensors generated with $(GT)_{15}$. The normalized $\Delta I/I_0$ performance of $(GT)_6$-based dopamine nanosensors represent a 1.27, 1.59, and 1.91-fold increase in performance over $(GT)_{15}$-based dopamine nanosensors for nanosensors generated from Trz-L-SWCNTs, Trz-H-SWCNTs, and SH-SWCNTs, respectively, suggesting that shorter ring-forming ssDNA oligomers are less sterically hindered by covalent SWCNT surface modifications than longer helix-forming ssDNA oligomers. $(GT)_6$- SH-SWCNT nanosensors still exhibit a greatly attenuated fluorescence response to dopamine, which could be due to the bulkier thiol functional groups as compared to the chlorine of the triazine SWCNTs or potential intermolecular interactions. Specifically, intermolecular interactions such as potential disulfide bridging between thiol groups could affect nanosensor performance. Attempts to study disulfide bridging in the system were inconclusive, as the addition of reducing agents to SWCNTs interferes with SWCNT fluorescence modulation (Fig. 4.6).[153] Both pristine-SWCNT and SH-SWCNT $(GT)_{15}$-coated nanosensors did not have fluorescence modulation upon the addition of dopamine. We further confirmed that differences in nanosensor performance are not due to intrinsic differences in baseline fluorescence of the concentration-normalized SWCNT samples (Fig. 4.4c-f).

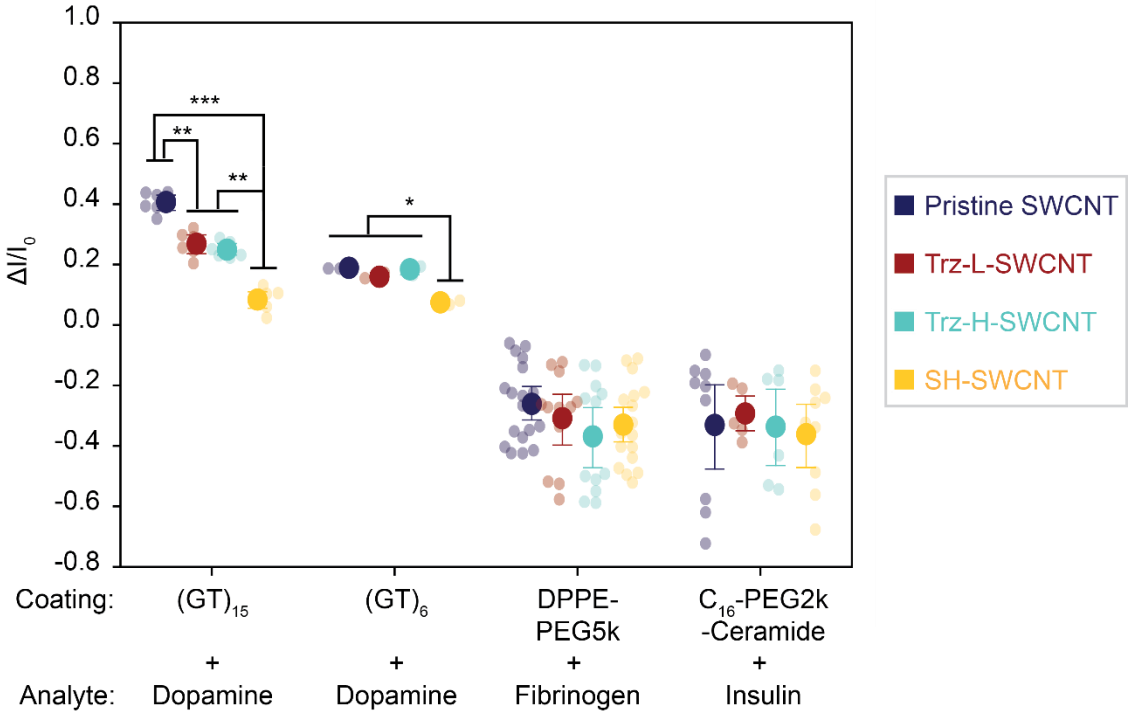

Figure 4.5: Analysis of Raw Fluorescence Modulation of Covalent SWCNT Nanosensors.

Fluorescence change of 5 mg L^{-1} covalently modified SWCNT nanosensors upon addition of their respective dopamine (100 μM), fibrinogen (1 mg mL^{-1}), and insulin (20 μg mL^{-1}) analytes (large dots denote mean, smaller faded dots denote an experimental replicate, and error bars denote standard deviation for n = 3 to 9 trials).

Significance analysis was conducted using the Student T-test with * denoting p-value < 5.0 E -3, ** denoting p-value < 5.0 E-4, and *** denoting p-value < 5.0 E-8. All other conditions are not statistically significant.

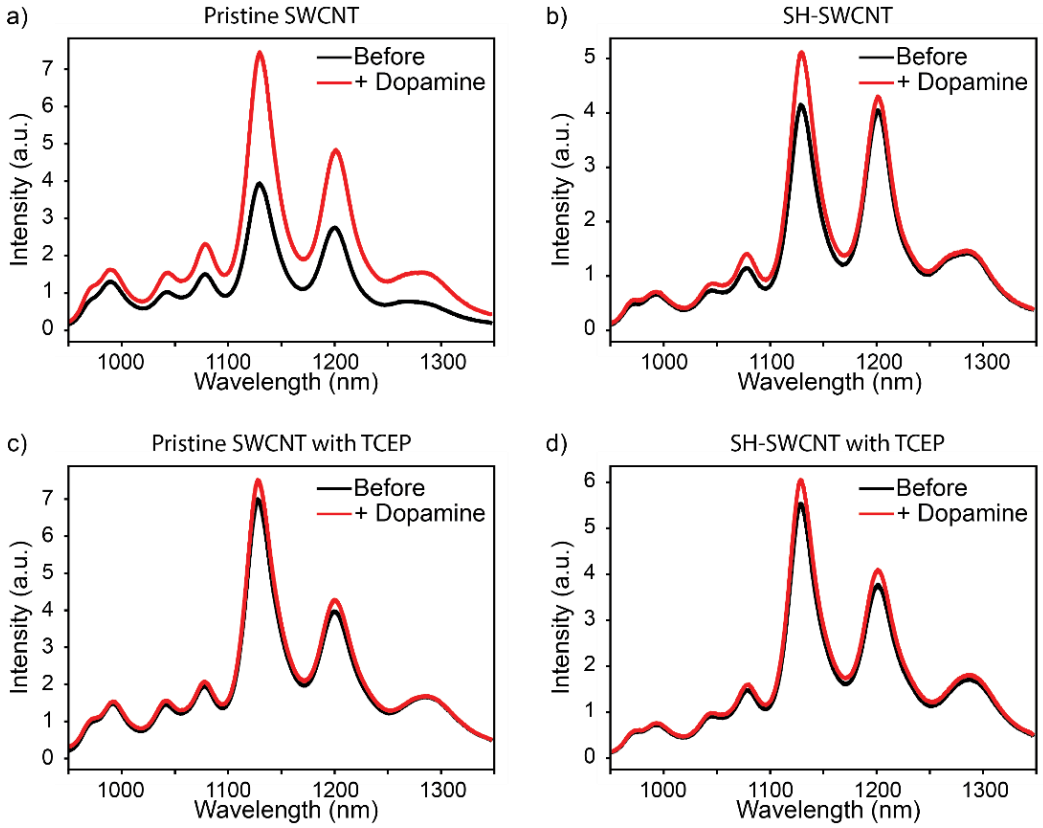

Figure 4.6: Fluorescence Modulation Following Nanosensor Reduction.

The responses for $(GT)_6$-coated SWCNTs can be compared to show the effect of reduction using tris(2-carboxyethyl)phosphine (TCEP). In the absence of TCEP both a) pristine-SWCNTs and b) SH-SWCNTs show the predicted increase in fluorescence of the (7,6) chirality peak at 1122 nm upon addition of 100 µM dopamine. In the presence of TCEP there is no longer a significant fluorescence change upon the addition of dopamine for c) pristine-SWCNTs or d) SH-SWCNTs.

To further probe the effect of steric contributions to noncovalent CoPhMoRe corona formation on the SWCNT surface, we tested the fluorescence response of phospholipid DPPE-PEG5k-SWCNT fibrinogen nanosensors. We expect that the adsorption of phospholipids, which adopt a self-assembled membrane-like structure on SWCNT surfaces, will be relatively sterically unhindered when binding to covalently-functionalized SWCNTs.[154,155] Upon addition of 1 mg mL^{-1} fibrinogen, we observed equivalent fluorescence responses of fibrinogen based on covalently-functionalized SWCNT nanosensors relative to those made from pristine-SWCNTs, corroborating that steric effects contribute to nanosensor attenuation when SWCNTs are suspended with conformationally-dependent amphiphilic polymers such as ssDNA. DPPE-PEG5k coated Trz-L-SWCNTs (1.268 ± 0.514, mean ± SD), Trz-H-SWCNTs (1.506 ± 0.575, mean ± SD), and SH-SWCNTs (1.282 ± 0.358, mean ± SD) all maintained their response to fibrinogen, compared to the original fibrinogen nanosensor constructed from DPPE-PEG5k coated pristine-SWCNTs (1.0 ± 0.097, mean ± SD). The variance observed for the phospholipid nanosensors after normalization is a result of the data processing and is not statistically significant (Figure S4). We also tested another phospholipid-based CoPhMoRe nanosensor, C_{16}-PEG2k-ceramide-SWCNT, which

responds to insulin. Similarly, C_{16}-PEG2k-ceramide coated Trz-L-SWCNTs (1.220 ± 0.561, mean ± SD), Trz-H-SWCNTs (1.101 ± 0.186, mean ± SD), and SH-SWCNTs (1.482 ± 0.617, mean ± SD) all maintained their response to insulin, compared to a nanosensor fluorescence response for the native insulin nanosensor constructed from pristine-SWCNTs (1.0 ± 0.157, mean ± SD). We hypothesize that phospholipid-based nanosensor responses are maintained with covalently functionalized SWCNTs because phospholipids are smaller molecules than amphiphilic polymers and may pack more unhindered on the surface of the SWCNT, maintaining a corona similar to that formed on pristine-SWCNTs.

Tuning the Intrinsic Properties of Covalently Functionalized SWCNTs

We next investigated how the intrinsic properties of the covalent functionalization, such as charge, affect the formation of noncovalent coatings on the SWCNT surface. We generated SWCNTs with a positive charge through covalent addition of ethylenediamine (NH_2-SWCNTs) and, separately, SWCNTs with a negative charge through covalent addition of glycine (COOH-SWCNTs) to the triazine handles of Trz-H-SWCNTs (Fig. 4.7a). We confirmed the generation of these charged SWCNT constructs through elemental analysis, X-ray photoelectron spectroscopy, and Fourier-transform infrared spectroscopy (Table 4.1, Fig. 4.8 and 4.9).

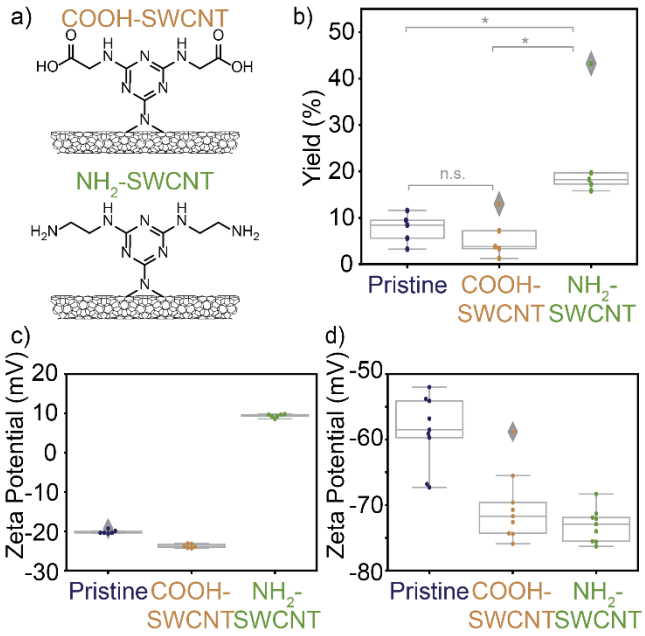

Figure 4.7: Charged SWCNT Experiments.

SWCNT surface charge is imparted by covalent functionalization and impacts subsequent noncovalent functionalization. a) Structures of negatively-charged COOH-SWCNT and positively-charged NH_2-SWCNT. b) Box-and-whisker plot showing percent yields of negatively-charged $(GT)_{15}$-coated SWCNTs upon methanol exchange. (n = 5 trials and * denotes $p < 0.05$ (uncorrelated independent student T-test), data points surrounded by gray diamonds denote outliers). Box-whisker-plots of zeta potential measurements (n = 6) of SWCNTs with c) a neutral C_{16}-PEG2k-ceramide phospholipid coating or d) negatively-charged $(GT)_{15}$ ssDNA polymer coating (data points surrounded by gray diamonds denote outliers).

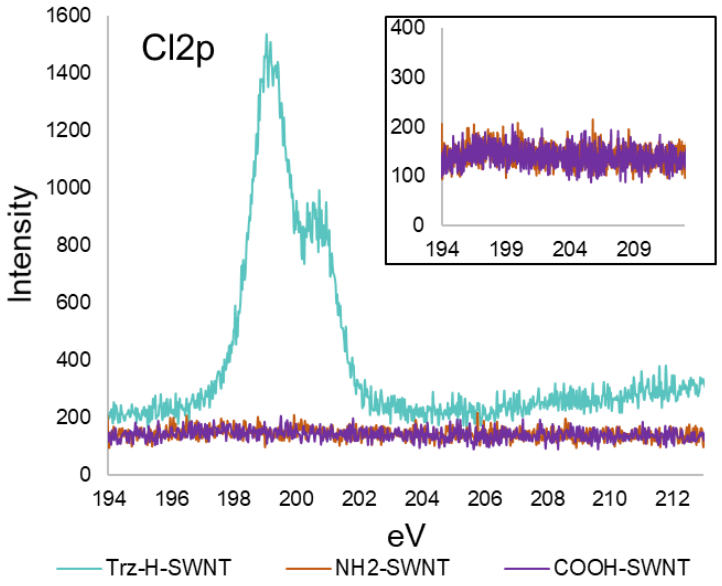

Figure 4.8: X-ray Photoelectron Spectroscopy of Charged SWCNTs.

High-resolution XPS analysis of the functionalized SWCNTs at the chlorine peak shows a disappearance of chlorine upon reaction to form NH_2-SWCNTs and COOH-SWCNTs (see inset), indicating successful nucleophilic substitution of primary amine functional groups with chloride on the triazine of Trz-H-SWCNTs.

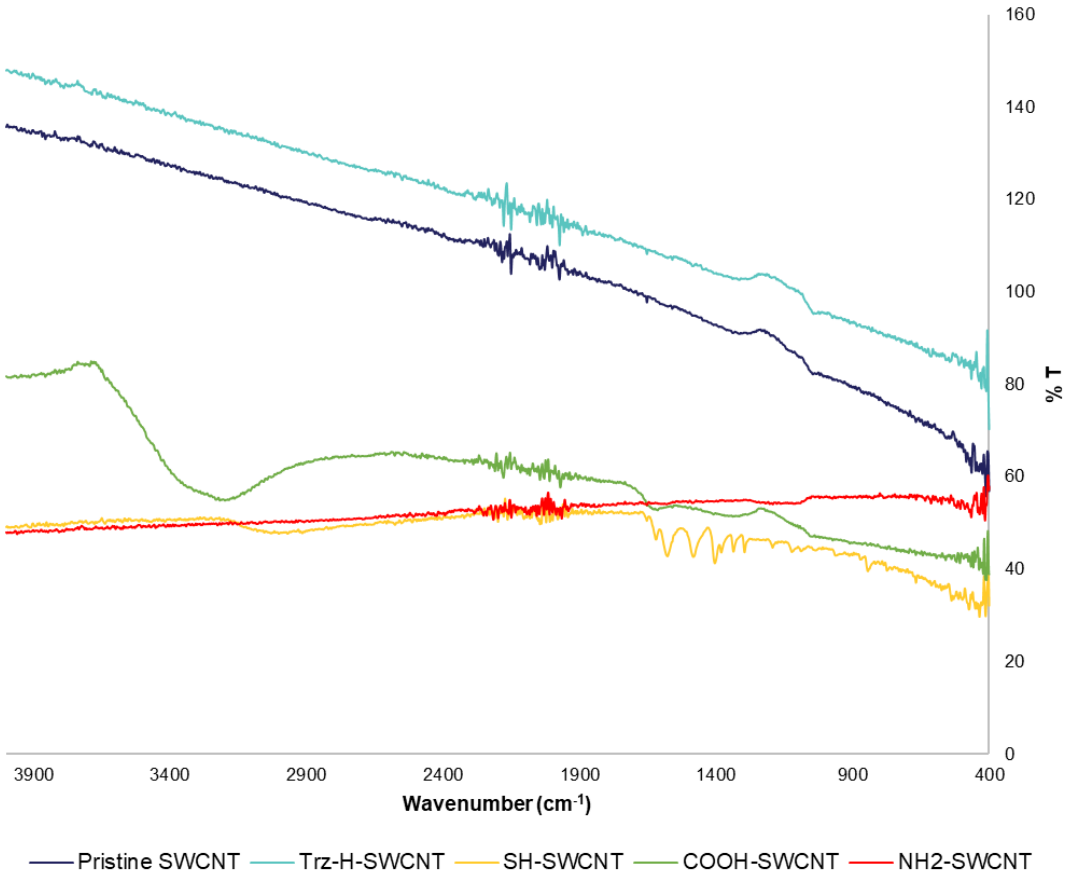

Figure 4.9: Fourier-Transform Infrared Spectroscopy of Covalent SWCNTs.

FTIR measurements of covalent SWCNTs show the introduction of new chemical bonds, including OH stretching for COOH-SWCNTs (broad envelope from 3500 - 2500 cm^{-1}) and thiol peaks for SH-SWCNTs (broad peak around 3000 cm^{-1}).

We sought to assess whether the $(GT)_{15}$–SWCNT dopamine nanosensor yields, as a proxy for coating stability, would be affected by the surface charges using a methanol-driven coating exchange method (Fig. 4.10).[34,53] We measured yield as the mass percentage of SWCNT recovered following the exchange protocol. We show that the yield of $(GT)_{15}$ coated SWCNTs is highest for the positively charged NH_2-SWCNTs (Fig. 4.7b), as expected given the negative charge of $(GT)_{15}$. The positive charge of the amine group on the surface of NH_2-SWCNTs presumably favors the association with negatively charged $(GT)_{15}$, and displays a 22.9% nanosensor yield that is significantly higher than those of pristine-SWCNTs and COOH-SWCNTs ($p < 0.05$, uncorrelated independent student T-test). The yields for $(GT)_{15}$ coated pristine-SWCNTs and COOH-SWCNTs were less than 10% and not significantly different (p-value = 0.47 > 0.05, uncorrelated independent student T-test), suggesting $(GT)_{15}$ is more stably adsorbed to NH_2-SWCNTs than to COOH- or pristine-SWCNTs. We attribute the lower ssDNA-COOH-SWCNT yield to the negatively charged COOH-SWCNT, which electrostatically repels the negative $(GT)_{15}$ polymer. These results indicate that coating formation could be driven or hindered by the intrinsic charge properties of the covalent functional group.

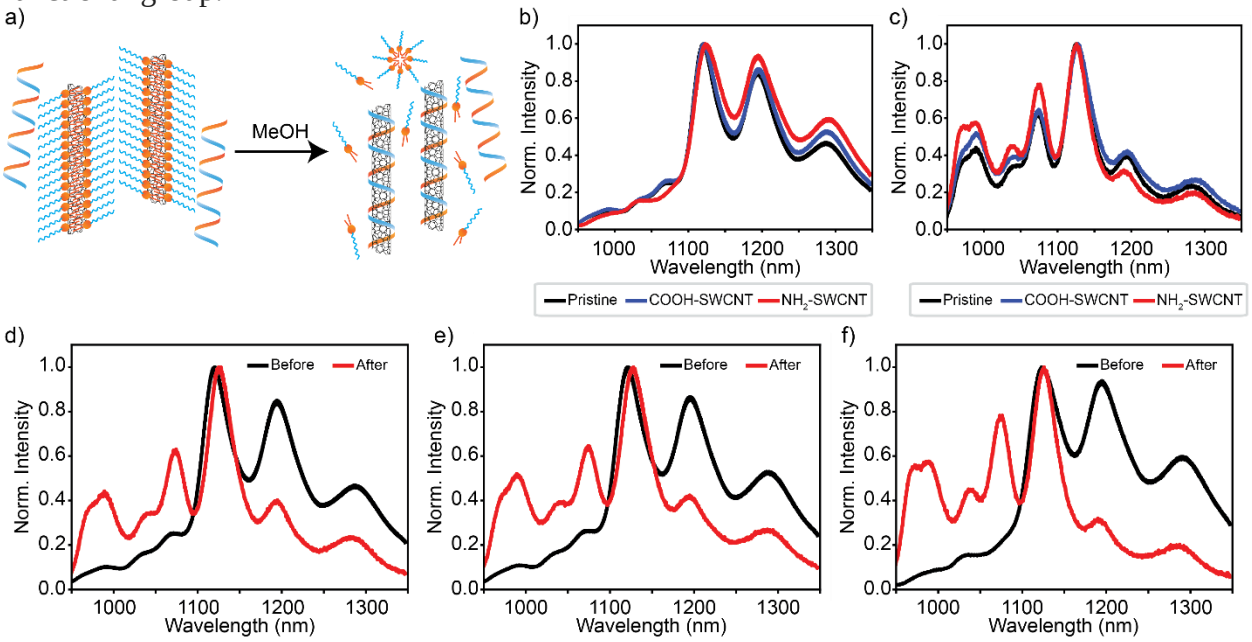

Figure 4.10: Methanol Exchange Protocol and Resultant NIR Spectra.

a) Schematic of the methanol exchange protocol. b) Overlaid spectra of all C_{16}-PEG2k-ceramide-SWCNTs before exchange. c) Overlaid spectra of all $(GT)_{15}$-SWCNTs after exchange. Successful exchange of the coatings results in a fluorescence wavelength shift as seen for d) pristine-SWCNTs, e) COOH-SWCNTs, and f) NH_2-SWCNTs.

To demonstrate that the charge properties of NH_2 and COOH covalently functionalized SWCNTs can be maintained, we suspended COOH-SWCNTs, NH_2-SWCNTs, and pristine-SWCNTs with a neutral (uncharged) phospholipid, C_{16}-PEG2k-ceramide. The zeta potentials, which characterize the electrokinetic potential at the slipping plane and provide a proxy for particle surface charge, were measured for these three SWCNT constructs with C_{16}-PEG2k-ceramide coatings. C_{16}-PEG2k-ceramide coated COOH-SWCNTs (-23.8 mV ± 0.501, mean ± SD) displayed the most negative zeta potential and C_{16}-PEG2k-ceramide coated NH_2-SWCNTs (9.38 mV ± 0.446, mean ± SD) displayed the most positive zeta potential, as compared to C_{16}-PEG2k-ceramide coated

pristine-SWCNTs (-20.1 mV ± 0.468, mean ± SD) (Fig. 4.7c and Fig. 4.11a). We repeated this experiment with a negatively charged $(GT)_{15}$ polymer coating instead, and measured the zeta potentials for pristine-SWCNTs (-55.0 mV ± 3.69, mean ± SD), COOH-SWCNTs (-70.39 mV ± 5.33, mean ± SD), and NH_2-SWCNTs (-73.1 mV ± 2.54, mean ± SD). As expected, all complexes showed a more negative surface charge than the complexes formed with the C_{16}-PEG2k-ceramide coating (Fig. 4.7d and 4.11b). Tuning of intrinsic properties of SWCNT surfaces in this manner could aid SWCNT design for cellular delivery applications, where charge is a driving factor for nanoparticle internalization and subsequent cytotoxicity.[156]

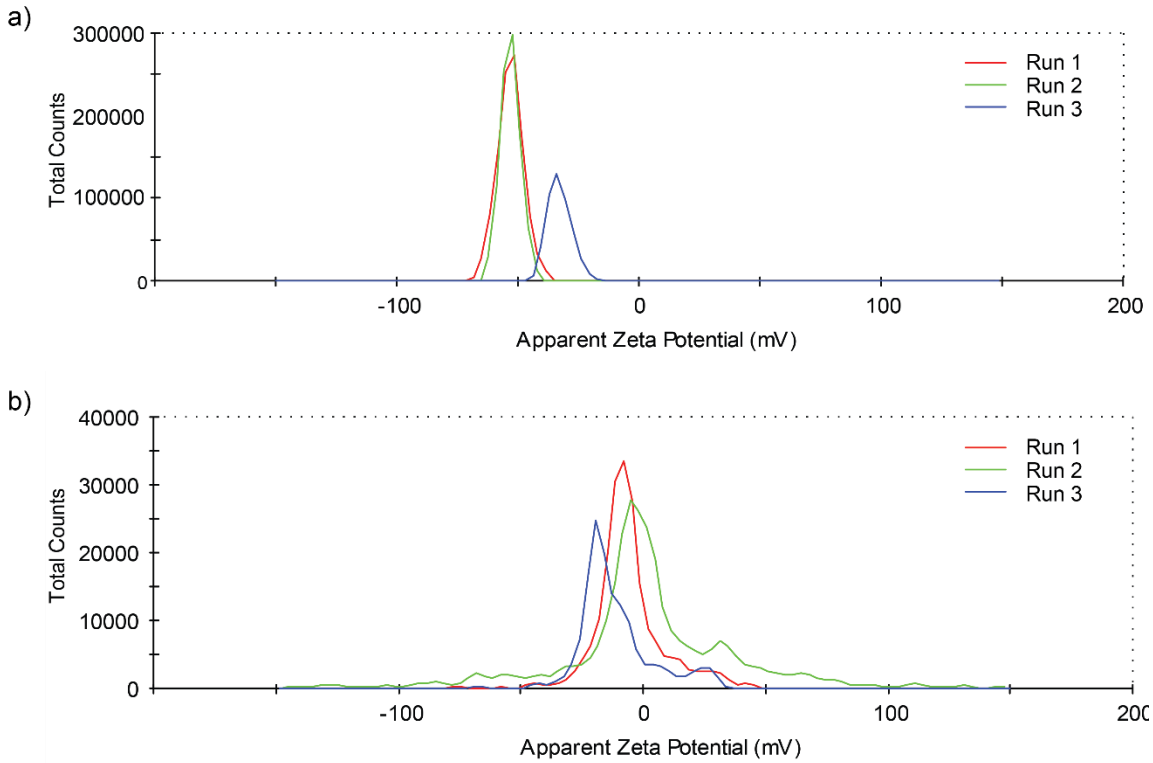

Figure 4.11: Zeta Potential of $(GT)_{15}$ ssDNA and C_{16}-PEG2k-Ceramide.

Triplicate zeta potential measurements of the coatings in the absence of SWCNTs for a) $(GT)_{15}$ ssDNA and b) C_{16}-PEG2k-ceramide.

Dual Functional SWCNT Nanosensors with Molecular Targeting

Finally, we tested the use of covalent modifications to provide additional function to optical SWCNT nanosensors. Covalent attachment offers a method for the addition of molecular recognition elements such as antibodies and nanobodies, targeting modalities, and therapeutics.[45,157] We explored this dual functionality of SWCNTs through the attachment of biotin as an affinity pair with avidin protein as a model system (Fig. 4.12a). Biotin is known to form a high affinity noncovalent association with the avidin protein and its analogues such as neutravidin and streptavidin.[158] We generated biotin-SWCNTs by covalently attaching amine-PEG2k-biotin to SWCNTs through the triazine handles of Trz-H-SWCNTs. Biotin-SWCNTs were then coated with $(GT)_{15}$ ssDNA polymers to test the use of multifunctional SWCNTs.

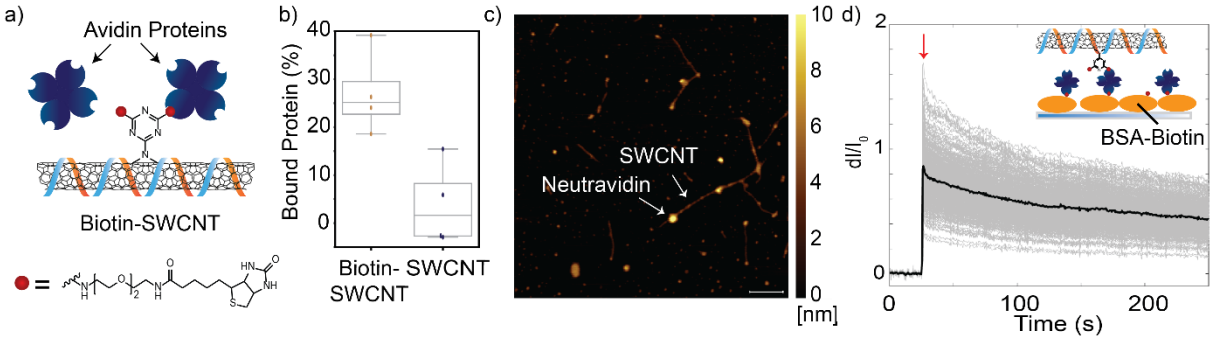

Figure 4.12: Covalent Modification of SWCNTs with Amine-PEG2-Biotin Adds Functional Handles for Avidin Protein Attachment.

a) $(GT)_{15}$-biotin-SWCNTs bind tetrameric avidin proteins such as neutravidin and streptavidin. b) A mass balance shows a higher percentage of bound $(GT)_{15}$-biotin-SWCNTs on streptavidin beads compared to $(GT)_{15}$-pristine-SWCNTs alone. c) AFM images show neutravidin protein bound to $(GT)_{15}$-biotin-SWCNTs. d) $(GT)_{15}$-biotin-SWCNTs immobilized on a neutravidin-coated microscopy surface (inset) and imaged with a near-infrared epifluorescence microscope with 721 nm excitation shows fluorescence response following exposure to 25 μM dopamine (addition denoted by the red arrow). The black line denotes the average fluorescence trace with individual microscopic regions of interest denoted by the gray lines.

We performed an affinity assay with streptavidin-coated magnetic beads to verify the attachment of biotin to the SWCNT surface. A significantly higher amount of $(GT)_{15}$-biotin-SWCNTs remained bound to magnetic beads (23.0% ± 4.0, mean ± SD) than pristine-SWCNTs (0.1 % ± 5.0, mean ± SD) (Fig. 4.12b). The attachment of biotin to SWCNTs was further validated through atomic force microscopy (AFM). AFM was used to visualize the presence of neutravidin protein along the length of individual $(GT)_{15}$-biotin-SWCNTs (Fig. 4.12c). SWCNT heights were measured as 0.5 nm to 1 nm and the neutravidin protein heights were measured as ~4 – 6 nm similar to previous reports.[145,159] We found that 58.9% of $(GT)_{15}$-biotin-SWCNTs (66 out of 112 SWCNTs total from multiple fields of view) as compared to 38.8% $(GT)_{15}$-pristine-SWCNTs (19 out of 49 SWCNTs total from multiple fields of view) appear to bind neutravidin protein (Fig. 4.12d). Discrepancies in the magnitude of protein bound between the affinity assay and AFM measurements are due to the physical state of the experiments. The magnetic bead affinity assay is conducted in solution with constant mixing, while AFM is performed on a dehydrated surface susceptible to nonspecific protein deposition and salt artifacts. Lastly, we tested the ability to use $(GT)_{15}$-biotin-SWCNTs for dopamine imaging. $(GT)_{15}$-biotin-SWCNTs were deposited onto a microscope slide surface-functionalized with a neutravidin monolayer, then the surface-bound nanosensors were exposed to 25 μM dopamine (Fig. 4.13). As shown in Figure 4.12d, exposure to dopamine generated an integrated fluorescence response $\Delta I/I_0$ = 0.8658 ± 0.1986 (mean ± SD), suggesting that SWCNTs that are dual-functionalized with both covalent handles and noncovalent polymeric ligands can be used for analyte-specific imaging applications. Taken together, these results suggest the potential of using covalent functional groups on SWCNTs for multifunctional applications.

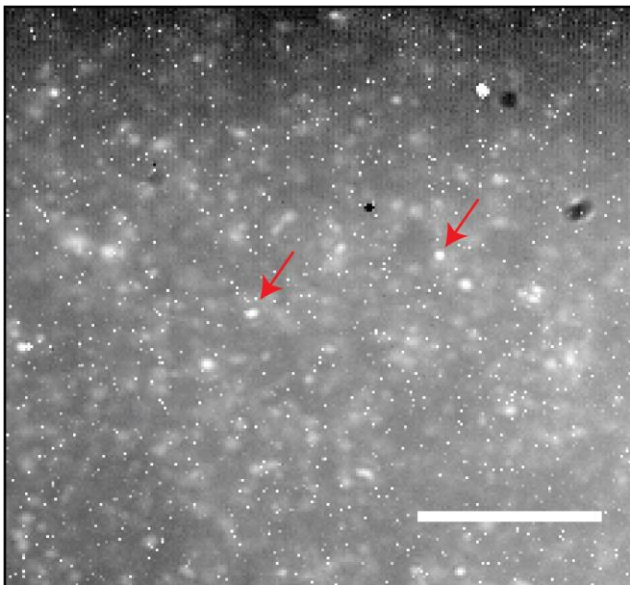

Figure 4.13: NIR Microscopy of Biotin-SWCNTs.

NIR microscopy image of Biotin-SWCNTs immobilized on a neutravidin passivated surface shows a homogenous surface with individual nanosensors (representative nanosensors denoted by red arrows). Scale bar denotes 10 μm.

4.5 Conclusions

We generated and characterized the properties of optically-active, covalently functionalized SWCNTs for use as fluorescent nanosensors. Comparisons of covalently functionalized SWCNT to pristine-SWCNT showed that the introduction of chemical handles could impact a SWCNT-based nanosensor response to its analyte, depending on the structural perturbation of the noncovalent coating adsorption upon corona formation. Nanosensors generated with long amphiphilic polymers showed the greatest analyte-specific fluorescence response attenuation following covalent addition of chemical handles on the SWCNT surface, whereas nanosensors generated from phospholipid-based coronas did not exhibit analyte-specific fluorescence response attenuation. Notably, following covalent functionalization of the SWCNT, all SWCNT complexes successfully formed through the noncovalent association of amphiphilic polymers or phospholipids, and were still capable of acting as optical nanosensors. These results validate the use of covalently functionalized SWCNTs as CoPhMoRe fluorescent nanosensors with unique analyte specificity, corona stability, and spatiotemporal readout appropriate for *in vivo* and *ex vivo* imaging.

This study further suggests the promise of utilizing dual covalent and noncovalent SWCNT functionalizations to create multifunctional nanoscale tools. The surface charge of SWCNT complexes can be altered via addition of covalent handles without perturbation of the SWCNT fluorescence, enabling CoPhMoRe-based sensing together with chemical handles for charge-based functionalizations and addition of ligands based on electrostatics. Furthermore, we show successful covalent attachment of the targeting moiety biotin to $(GT)_{15}$-SWCNT dopamine nanosensors and show the biotin group can be used for surface-immobilized dopamine imaging with near-infrared microscopy. These results demonstrate the possibility of dual covalent and noncovalent SWCNT functionalization for multiplexed purposes with future applications in

targeted delivery, theranostics, targeted fluorescence imaging, and towards understanding the fate of functionalized SWCNTs upon cellular delivery.

Chapter 5: Conclusions and Future Outlook

Armed with several strategies for the development of novel molecular recognition elements, we can enable the discovery of nanosensors for our desired protein analytes. Peptoids provide a modular noncovalent functionalization platform for the design of variable binding loops on SWCNT nanosensor. Dual covalent and noncovalent functionalization using 1,2-cycloaddition of cyanuric chloride provides a method to create multifunctional SWCNT nanosensors. Each technique provides a robust framework for nanosensor creation, with further optimization possible such as through the tuning of concentration of starting reagents or reaction conditions. Future work exciting to explore include improving library construction for peptoid noncovalent design, the covalent attachment of proteins to SWCNTs, and applications of nanoparticle modification beyond protein detection. Additionally, to utilize SWCNTs for biological applications certain limitations of nanoparticles *in vivo* must also be addressed, including biocompatibility and *in vivo* activity. With the further development of this SWCNT nanosensor platform, it will be possible to study signaling proteins in their native environment and understand their role in the mechanism of disease.

5.1 Library and Rational Design for the Development of SWCNT Protein Nanosensors

Although peptoids provide chemical diversity to the discovery of molecular recognition elements, the process of validating peptoid-SWCNT protein nanosensors still require extensive library screening. Library creation of peptoids for the development of SWCNT protein nanosensors could be improved through the rational design of binding loops to expedite screening. Rational design entails the discovery of peptoid binding loops by using natural analogues and design parameters as a starting blueprint for polymer synthesis.

Preliminary work of using rational design in aiding the discovery of novel protein binding loops has revealed a peptoid nanoloop capable of binding anthrax protective antigen (PA). PA is a non-immunogenic subunit of the anthrax toxin, and a nanosensor for this protein can aid in the detection of bioweapons. The Zuckermann group created a 6-mer peptoid loop capable of selective and sensitive binding of PA peptoid by using a naturally-occurring peptide binding loop as a template.[160] A combinatorial library was assembled by matching each amino acid on the peptide sequence with a monomer of similar size and hydrophobicity on the peptoid sequence. By having a starting template, fewer loops needed to be screened before finding a peptoid loop that was sensitive and selective against PA.

This peptoid nanoloop has been installed through noncovalent functionalization on SWCNTs using the same anchor peptoid design as the previous ProLoop peptoid to create PA-Loop-SWCNTs, and preliminary screening reveals its success as a nanosensor for PA. PA-Loop-SWCNT is shown to be stable to heat induced destabilization as compared to the anchor peptoid sequence (Fig. 5.1 a, b). Upon PA addition, the fluorescence intensity of the nanosensor decreases, and the limit of detection was determined to be 76.6 nM (Fig. 5.1c). Since this limit of detection is lower than ProLoop-SWCNT, the sensitivity of peptoid-nanosensors appears to depend on the protein-loop pair with further optimization of sensitivity possible for future targets. Selectivity of PA was shown to be dependent on the loop, as there is a fluorescence response only in the presence of the PA peptoid loop and not for anchor-only peptoid-coated SWCNT (Fig. 5.1d). It remains to be tested

if PA-Loop-SWCNT is selective for only PA, as opposed to other relevant targets like biotoxins and structural analogues of PA. However, these findings show that peptoid-loop noncovalent functionalization of SWCNTs is generalizable to yield novel nanosensors to new proteins, and can be accelerated through rational design using known molecular recognition elements.

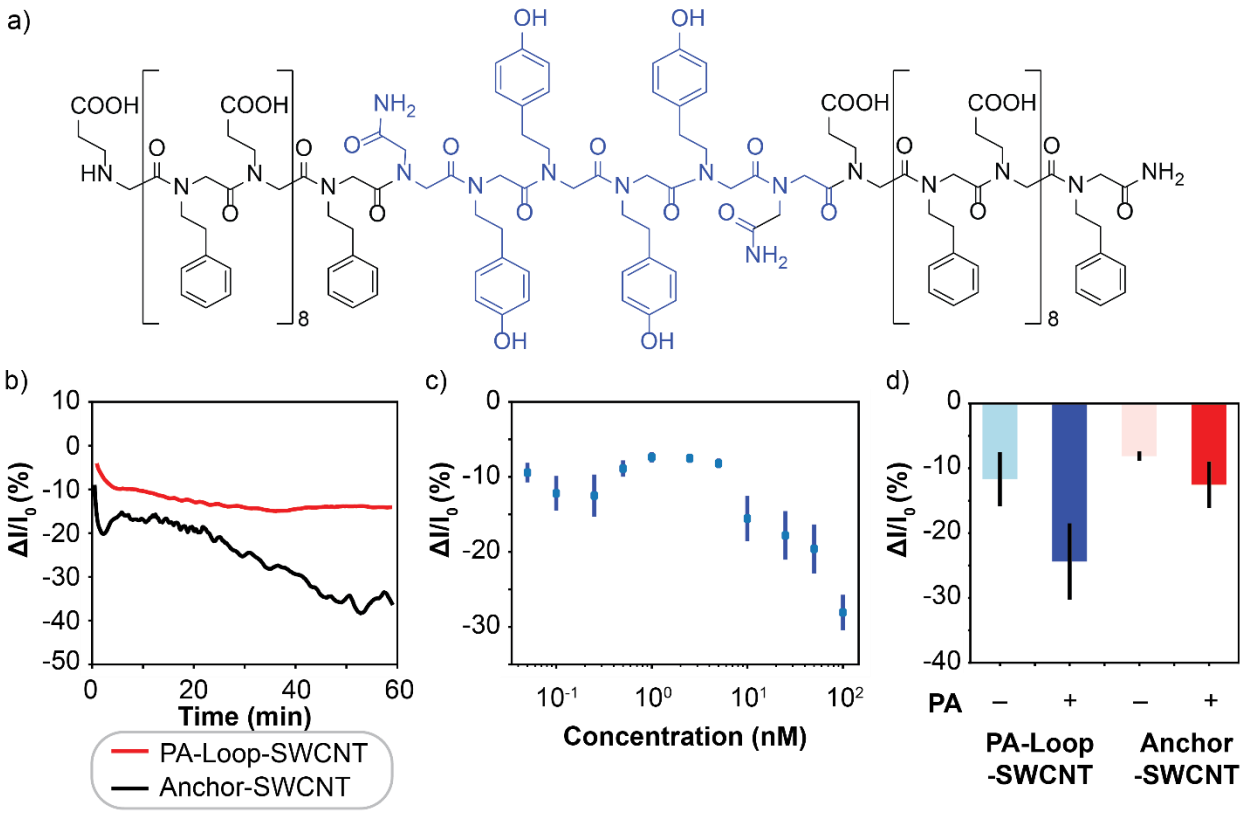

Figure 5.1: PA-Loop-SWCNT Experiments.

a) The peptoid-loop method of creation of protein SWCNT nanosensors has been shown to be general with the creation of a peptoid loop (denoted on blue) that binds anthrax protective antigen (PA). b) This nanosensor is shown to be stable to continuous laser illumination. c) The sensitivity of the PA-Loop-SWCNT nanosensor was determined to be 76.6 nM. The error represents the standard error for n = 6 trials. d) The selectivity of the PA-Loop-SWCNT nanosensor is shown to be the result of the PA-Loop binding sequence. In this preliminary study, sample size was n = 3.

5.2 Building Protein-Conjugated SWCNT Nanosensors

The covalent functionalization of SWCNT provides a template for the modular attachment of molecular recognition elements, especially for the attachment of larger biomolecules such as proteins. Proteins are dependent on their structure for their function, and covalent techniques allow for more controlled conjugation of proteins to SWCNT surfaces. There are two classes of proteins that show particular promise for the development of nanosensors: enzymes and antibodies.

Enzymes are proteins that can catalyze a highly specific reaction on a particular substrate or a class of substrates. Previously, enzymes have been noncovalently attached to SWCNTs through dialysis

methods for SWCNT solubilization and sensing.[50,51] For example, Barone and colleagues demonstrated the noncovalent attachment of glucose oxidase (GOx) to the SWCNT surface through dialysis for the sensing of glucose.[50] Upon exposure to glucose, GOx generates protons that modulate the charge transfer environment of the SWCNT leading to a detectable fluorescence change. However, for the long-term stability of enzymes on SWCNT surfaces and the attachment of enzymes that are less capable of noncovalent interactions with SWCNTs, it will be advantageous to covalently attach enzymes to SWCNTs. Several enzymes interact with important metabolites and ligands in the body. We identified horseradish peroxidase (HRP) as a model enzyme for covalent attachment to SWCNTs. HRP catalyzes the conversion of hydrogen peroxide (H_2O_2) to water in the presence of a proton-donor.[161] Currently, it is difficult to spatially and temporally track the presence and breakdown of H_2O_2 in the body, which is important since H_2O_2 is responsible for the generation and trafficking of free radicals in oxidative stress.[162] HRP-conjugated SWCNTs could enable the specific binding and fluorescence sensing of H_2O_2.

Similarly, antibodies are a class of proteins with high specificity for analytes and antigens that infect the body, and antibody-antigen binding have dissociation constants (K_d) in the range of picomolars.[163] Antibodies have found several applications in the binding of circulating analytes such as cytokines and in immunohistochemistry. Coupled with the tissue penetrative NIR fluorescence of SWCNT, antibodies can enable the staining of tissues *in vivo* to differentiate tissue types and label extracellular biomarkers. For example, the anti-ERB2 antibody is a known binder of HER2 receptors that are overexpressed in 20-30% of all breast cancers and are known to be a marker of an aggressive subtype of breast cancer.[164,165] This could serve as a model system for the use of antibody-SWCNTs for the staining of biological systems for noninvasive imaging.

5.3 Beyond SWCNT Protein Nanosensors

Noncovalently and covalently functionalization of SWCNT can be applied for the development of new nanomaterial tools. These methods provide chemical diversity and modular chemical functionalization on the SWCNT surface, and provide opportunities to use functionalized SWCNTs in gene delivery and nanomedicine.

The delivery of biomolecules into plant cells for genetic engineering has been enabled by SWCNTs.[134] Unlike mammalian cells, plant cells have an additional barrier to entry called the cell wall with a size exclusion limit of ~10 nm. SWCNTs are one of few particles with a dimension small enough to penetrate this molecular sieve and have enough surface area to load functional cargo. SWCNT have been shown to penetrate the plant cell wall and successfully deliver functional plasmid DNA and siRNA for the alteration of gene expression in plant cells. At the moment, the delivery is limited to nucleic acid cargos, but efficient and specific gene editing can be promoted through the use of gene editing tools such as CRISPR-Cas9. In this system, Cas9 endonuclease protein is required for the site-specific alteration of genomic DNA. SWCNTs can be designed for the delivery of Cas9 using either noncovalent and covalent functionalization. Peptoids have shown promise in the stable tethering of an active protein on SWCNT surface, as seen with the use of wheat germ agglutinin as a sugar recognition element. A binding loop could be generated for the attachment of Cas9 to SWCNT surfaces, and peptoids provide the chemical diversity to tune the interaction of protein on SWCNTs. Similarly, covalent strategies can form a stable bond between

Cas9 and SWCNTs, and site-specific attachment chemistries can be used to preserve the function of the protein.

Similarly, nanomaterials like SWCNTs could be useful in nanomedicine through the creation of theranostic tools. Theranostics combines therapeutics and diagnostics on the same particle. With the dual noncovalent and covalent functionalization of SWCNTs, it is conceivable to attach a therapeutic cargo and track the effect of this therapy using optical imaging using the same SWCNT. Previously, SWCNTs have been used as theranostics agents through the combination of photoacoustic or Raman imaging with photothermal therapy.[166,167] However, few examples use SWCNTs for optical imaging and with the attachment of active therapeutic compounds and this could be a future area of exploration.

5.4 Mitigating Existing Challenges

As the role of SWCNT nanosensors expands for the use of *in vivo* imaging, gene delivery, and theranostics, several questions must be addressed about SWCNT activity and biocompatibility when administered *in vivo*. To date, these remain active areas of research for biological nanomaterials of which SWCNTs are a subset. However, recent studies have provided a promising outlook and strategies on the creation of SWCNTs suitable for *in vivo* administration.

Nanomaterial functionality, including retention in the body and the availability of targeting nanoparticle surface ligands, is often attenuated when administered *in vivo* due to the adsorption of proteins to form what is known as the protein corona. This protein corona can lead to the activation of the immune system, clearance by mononuclear phagocytes, accumulation in the liver or spleen, and the disruption of ligands on SWCNT surface.[168] Several techniques can be utilized to mitigate the complications caused by the protein corona, through both noncovalent and covalent strategies. Certain polymer coatings are known to mitigate the formation of an unfavorable protein corona. Polyethylene glycol (PEG), the most well-studied option, is a hydrophilic polymer known to form dense brushes on the surface that can sterically and electrostatically exclude the adsorption of proteins on SWCNT surfaces.[169] Zwitterionic polymers, composed of both positively and negatively charge monomers, are also shown to mitigate corona formation.[170] Polymer coatings that prevent corona formation can be created through noncovalent functionalization using commercially available polymers or peptoid anchor design, as well as covalent functionalization through the grafting of beneficial polymer groups. Additionally, the formation of the protein corona could be advantageously applied through the preincubation of nanoparticles in certain plasma proteins, called dysopsonins, shown to improve overall fate of the nanoparticle.[171] A pre-formed beneficial protein corona prevents biofouling by unfavorable proteins upon administration.[172] These strategies can enable the creation of biocompatible SWCNT assemblies that have suitable retention times necessary for their application. In order to understand the full fate of SWCNT nanosensors in the body, downstream testing should be performed *in vivo* or in environments that directly mimic the environment of the biological question under investigation.

In order to safely administer SWCNTs *in vivo*, it is also important to track nanoparticle fate and biocompatibility. Typically, SWCNTs are not readily excreted through renal passage, and often accumulate in the organ to which they were administered or within phagocytic organs such as the liver and spleen after administration.[173] However, one recent study shows evidence of renal

clearance in nonhuman primates of 99.8% of injected material after 3 days for ammonium functionalized SWCNTs.[174] Though not optimal, the bioaccumulation of SWCNT does not necessarily lead to greater toxicity or adverse side effects, as a study of the bioaccumulation of SWCNTs in mice was not shown to lead to severe toxic responses.[175] It is also important to note that bioaccumulation is currently an issue for most nanoparticle systems, but SWCNT research enables strategies for clearance. For example, recent reports have demonstrated that the plant and animal peroxidases, such as myeloperoxidase and eosinophil catalyze the biodegradation of carbon nanomaterial.[176] This degradation occurs following SWCNT encapsulation by immune cells and have been observed in both eosinophils and macrophages.[177] However, in these literature examples, SWCNTs are often functionalized with carboxylic acid functional groups that are more prone to oxidation and attack through defect sites. The biodegradation of pristine SWCNTs still requires further investigation.

Moreover, it is important to test the effect of SWCNTs *in vivo*, which depends greatly on their surface functionalization by covalent or noncovalent surface passivation. Signs of toxicity, such as higher levels of inflammatory cytokines, such as IL-6 and TNF-α, are seen to be mitigated by surface functionalized SWCNTs.[178] Additionally, recent investigations have shown that SWCNT at low doses are tolerated *in vivo*. The system by which SWCNTs are administered and tested is also crucial for understanding biocompatibility.[179] For example, SWCNT-caused inflammation is seen more acutely in 2D-tissue cultures as opposed to 3D tissue cultures, and calls into question the best way to test SWCNT toxicity.[180] Each SWCNT nanosensor must be studied for each unique construct *in vivo*, as the coatings and functional groups on SWCNT surfaces are shown to impact biocompatibility findings.

SWCNTs provide a robust platform for creating nanomaterial tools that can probe and manipulate biological systems. Their fluorescence properties are well suited for the creation of optical nanosensors capable of *in vivo* imaging to help us understand the mechanism of signaling molecules in disease. The platforms discussed in this dissertation have laid the groundwork for noncovalent and covalent functionalization for the development of multimodal tools and the chemical diversity necessary to probe proteins in their native environments.

References

(1) Dodson, G. G.; Dodson, E. J.; Hodgkin, D. C.; Isaacs, N. W.; Vijayan, M. The Structure of 2ZN Pig Insulin Crystals at 1.5 Angstroms Resolution. **1990**.

(2) Yoon, C.; Johnston, S. C.; Tang, J.; Stahl, M.; Tobin, J. F.; Somers, W. S. Charged Residues Dominate a Unique Interlocking Topography in the Heterodimeric Cytokine Interleukin-12. *EMBO J.* **2000**, *19* (14), 3530–3541.

(3) Lotharius, J.; Brundin, P. Pathogenesis of Parkinson's Disease: Dopamine, Vesicles and α-Synuclein. *Nat. Rev. Neurosci.* **2002**, *3* (12), 932–942.

(4) Zoli, M.; Torri, C.; Ferrari, R.; Jansson, A.; Zini, I.; Fuxe, K.; Agnati, L. F. The Emergence of the Volume Transmission Concept. *Brain Res. Rev.* **1998**, *26* (2–3), 136–147.

(5) Rice, M. E.; Cragg, S. J. Dopamine Spillover after Quantal Release: Rethinking Dopamine Transmission in the Nigrostriatal Pathway. *Brain Res. Rev.* **2008**, *58* (2), 303–313.

(6) Atkinson, M. A.; Eisenbarth, G. S.; Michels, A. W. Type 1 Diabetes. *Lancet* **2014**, *383* (9911), 69–82.

(7) Leroith, D. B-Cell Dysfunction and Insulin Resistance in Type 2 Diabetes.Pdf. **2002**.

(8) Pesic, M.; Greten, F. R. Inflammation and Cancer: Tissue Regeneration Gone Awry. *Curr. Opin. Cell Biol.* **2016**, *43* (Figure 1), 55–61.

(9) Park, J. Il; Lee, M. G.; Cho, K.; Park, B. J.; Chae, K. S.; Byun, D. S.; Ryu, B. K.; Park, Y. K.; Chi, S. G. Transforming Growth Factor-B1 Activates Interleukin-6 Expression in Prostate Cancer Cells through the Synergistic Collaboration of the Smad2, P38-NF-KB, JNK, and Ras Signaling Pathways. *Oncogene* **2003**, *22* (28), 4314–4332.

(10) Jiang, Y. N.; Yan, H. Q.; Huang, X. B.; Wang, Y. N.; Li, Q.; Gao, F. G. Interleukin 6 Trigged Ataxia-Telangiectasia Mutated Activation Facilitates Lung Cancer Metastasis via MMP-3/MMP-13 up-Regulation. *Oncotarget* **2015**, *6* (38), 40719–40733.

(11) Li, J.; Mo, H. Y.; Xiong, G.; Zhang, L.; He, J.; Huang, Z. F.; Liu, Z. W.; Chen, Q. Y.; Du, Z. M.; Zheng, L. M.; et al. Tumor Microenvironment Macrophage Inhibitory Factor Directs the Accumulation of Interleukin-17-Producing Tumor-Infiltrating Lymphocytes and Predicts Favorable Survival in Nasopharyngeal Carcinoma Patients. *J. Biol. Chem.* **2012**, *287* (42), 35484–35495.

(12) Kingsmore, S. F. Multiplexed Protein Measurement : Technologies and Applications of Protein and Antibody Arrays. *Nat. Rev. Drug Discov.* **2006**, *5*, 310–321.

(13) Chikkaveeraiah, B. V; Bhirde, A. A.; Morgan, N. Y.; Eden, H. S.; Chen, X. Electrochemical Immunosensors for Detection of Cancer Protein Biomarkers. *ACS Nano* **2012**, *6* (8), 6546–6561.

(14) Freeman, R.; Girsh, J.; Jou, A. F.; Ho, J. A.; Hug, T.; Dernedde, J.; Willner, I. Optical Aptasensors for the Analysis of the Vascular Endothelial Growth Factor (VEGF). *Anal. Chem.* **2012**, *84*, 6192–6198.

(15) Mita, C.; Abe, K.; Fukaya, T.; Ikebukuro, K. Vascular Endothelial Growth Factor (VEGF) Detection Using an Aptamer and PNA-Based Bound/Free Separation System. *Materials (Basel).* **2014**, *7*, 1046–1054.

(16) Strunk, J. J.; Gregor, I.; Becker, Y.; Lamken, P.; Lata, S.; Reichel, A.; Enderlein, J.; Piehler, J. Probing Protein Conformations by in Situ Non-Covalent Fluorescence Labeling. *Bioconjug. Chem.* **2009**, *20* (1), 41–46.

(17) Zakeri, B.; Fierer, J. O.; Celik, E.; Chittock, E. C.; Schwarz-Linek, U.; Moy, V. T.; Howarth, M. Peptide Tag Forming a Rapid Covalent Bond to a Protein, through Engineering a Bacterial Adhesin. *Proc. Natl. Acad. Sci. U. S. A.* **2012**, *109* (12).

(18) Snapp, E. Design and Use of Fluorescent Fusion Proteins in Cell Biology. *Curr. Protoc. Cell Biol.* **2005**, *27* (1), 21.4.1-21.4.13.

(19) Iijima, S.; Ichihashi, T. Single-Shell Carbon Nanotubes of 1-Nm Diameter. *Nature* **1993**, *363* (3), 603–605.

(20) Saito, R.; Fujita, M.; Dresselhaus, G.; Dresselhaus, M. S. Electronic Structure of Chiral Graphene Tubules. *Appl. Phys. Lett.* **1992**, *60* (18), 494–500.

(21) Jorio, A.; Saito, R.; Hertel, T.; Weisman, R. B.; Dresselhaus, G.; Dresselhaus, M. S. Carbon Nanotube Photophysics. *MRS Bull.* **2004**, *29* (4), 276–280.

(22) Bachilo, S. M.; Strano, M. S.; Kittrell, C.; Hauge, R. H.; Smalley, R. E.; Weisman, R. B. Structure-Assigned Optical Spectra of Single-Walled Carbon Nanotubes. *Science (80-.).* **2002**, *298* (5602), 2361–2366.

(23) Ahmari, S. E.; Smith, S. J. Knowing a Nascent Synapse When You See It. *Neuron* **2002**, *34* (3), 333–336.

(24) WIEDEMAN, M. P. Dimensions of Blood Vessels from Distributing Artery to Collecting Vein. *Circ. Res.* **1963**, *12*, 375–378.

(25) Hong, G.; Antaris, A. L.; Dai, H. Near-Infrared Fluorophores for Biomedical Imaging. *Nat. Biomed. Eng.* **2017**, *1*.

(26) Wray, S.; Cope, M.; Delpy, D. T.; Wyatt, J. S.; Reynolds, E. O. R. Characterization of the near Infrared Absorption Spectra of Cytochrome Aa3 and Haemoglobin for the Non-Invasive Monitoring of Cerebral Oxygenation. *Biochim. Biophys. Acta* **1988**, *933*, 184–192.

(27) Boghossian, A. A.; Zhang, J.; Barone, P. W.; Reuel, N. F.; Kim, J.; Heller, D. A.; Ahn, J.; Hilmer, A. J.; Rwei, A.; Arkalgud, J. R.; et al. Near-Infrared Fluorescent Sensors Based on Single-Walled Carbon Nanotubes for Life Sciences Applications. *ChemSusChem* **2011**, *4*, 848–863.

(28) Efros, A. L.; Nesbitt, D. J. Origin and Control of Blinking in Quantum Dots. *Nat. Nanotechnol.* **2016**, *11* (8), 661–671.

(29) Bronikowski, M. J.; Willis, P. a.; Colbert, D. T.; Smith, K. a.; Smalley, R. E. Gas-Phase Production of Carbon Single-Walled Nanotubes from Carbon Monoxide via the HiPco

Process: A Parametric Study. *J. Vac. Sci. Technol. A Vacuum, Surfaces, Film.* **2001**, *19* (4), 1800.

(30) Weidenkaff, A.; Ebbinghaus, S. G.; Mauron, P.; Reller, A.; Zhang, Y.; Züttel, A. Metal Nanoparticles for the Production of Carbon Nanotube Composite Materials by Decomposition of Different Carbon Sources. *Mater. Sci. Eng. C* **2002**, *19* (1–2), 119–123.

(31) Gomez-Gualdro, D. A.; Burgos, J. C.; Yu, J.; Balbuena, P. B. Carbon Nanotubes : Engineering Biomedical Applications I . Introduction. In *Progress in Molecular Biology and Translational Science*; 2011; Vol. 104, pp 175–245.

(32) Tabakman, S. M.; Welsher, K.; Hong, G.; Dai, H. Optical Properties of Single-Walled Carbon Nanotubes Separated in a Density Gradient: Length, Bundling, and Aromatic Stacking Effects. *J. Phys. Chem. C* **2010**, *114* (46), 19569–19575.

(33) Zhang, J.; Landry, M. P.; Barone, P. W.; Kim, J.-H.; Lin, S.; Ulissi, Z. W.; Lin, D.; Mu, B.; Boghossian, A. A.; Hilmer, A. J.; et al. Molecular Recognition Using Corona Phase Complexes Made of Synthetic Polymers Adsorbed on Carbon Nanotubes. *Nat. Nanotechnol.* **2013**, *8* (12), 959–968.

(34) Giraldo, J. P.; Landry, M. P.; Kwak, S.-Y.; Jain, R. M.; Wong, M. H.; Iverson, N. M.; Ben-Naim, M.; Strano, M. S. A Ratiometric Sensor Using Single Chirality Near-Infrared Fluorescent Carbon Nanotubes: Application to in Vivo Monitoring. *Small* **2015**, *11* (32), 3973–3984.

(35) Kruss, S.; Landry, M. P.; Vander Ende, E.; Lima, B.; Reuel, N. F.; Zhang, J.; Nelson, J. T.; Mu, B.; Hilmer, A. J.; Strano, M. S. Neurotransmitter Detection Using Corona Phase Molecular Recognition on Fluorescent Single-Walled Carbon Nanotube Sensors. *J. Am. Chem. Soc.* **2014**, *136* (2), 713–724.

(36) Bisker, G.; Bakh, N. A.; Lee, M. A.; Ahn, J.; Park, M.; O'Connell, E. B.; Iverson, N. M.; Strano, M. S. Insulin Detection Using a Corona Phase Molecular Recognition Site on Single-Walled Carbon Nanotubes. *ACS Sensors* **2018**, *3* (2), 367–377.

(37) Liu, Z.; Cai, W.; He, L.; Nakayama, N.; Chen, K.; Sun, X.; Chen, X.; Dai, H. In Vivo Biodistribution and Highly Efficient Tumour Targeting of Carbon Nanotubes in Mice. *Nat. Nanotechnol.* **2007**, *2* (1), 47–52.

(38) Del Bonis-O'Donnell, J. T.; Chio, L.; Dorlhiac, G. F.; McFarlane, I. R.; Landry, M. P. Advances in Nanomaterials for Brain Microscopy. *Nano Res.* **2018**, *11* (10), 5144–5172.

(39) Leeuw, T. K.; Michelle Reith, R.; Simonette, R. A.; Harden, M. E.; Cherukuri, P.; Tsyboulski, D. A.; Beckingham, K. M.; Weisman, R. B. Single-Walled Carbon Nanotubes in the Intact Organism: Near-IR Imaging and Biocompatibility Studies in Drosophila. *Nano Lett.* **2007**, *7* (9), 2650–2654.

(40) Hong, G.; Diao, S.; Chang, J.; Antaris, A. L.; Chen, C.; Zhang, B.; Zhao, S.; Atochin, D. N.; Huang, P. L.; Andreasson, K. I.; et al. Through-Skull Fluorescence Imaging of the Brain in a New near-Infrared Window. *Nat. Photonics* **2014**, *8* (9), 723–730.

(41) Del Bonis-O'Donnell, J. T.; Page, R. H.; Beyene, A. G.; Tindall, E. G.; McFarlane, I. R.; Landry, M. P. Dual Near-Infrared Two-Photon Microscopy for Deep-Tissue Dopamine

Nanosensor Imaging. *Adv. Funct. Mater.* **2017**, *27* (39), 1702112.

(42) Budhathoki-Uprety, J.; Langenbacher, R. E.; Jena, P. V.; Roxbury, D.; Heller, D. A. A Carbon Nanotube Optical Sensor Reports Nuclear Entry via a Noncanonical Pathway. *ACS Nano* **2017**, *11* (4), 3875–3882.

(43) Liu, Z.; Yang, K.; Lee, S. T. Single-Walled Carbon Nanotubes in Biomedical Imaging. *J. Mater. Chem.* **2011**, *21* (3), 586–598.

(44) Williams, R. M.; Lee, C.; Heller, D. A. A Fluorescent Carbon Nanotube Sensor Detects the Metastatic Prostate Cancer Biomarker UPA. *ACS Sensors* **2018**.

(45) Williams, R. M.; Lee, C.; Galassi, T. V.; Harvey, J. D.; Leicher, R.; Sirenko, M.; Dorso, M. A.; Shah, J.; Olvera, N.; Dao, F.; et al. Noninvasive Ovarian Cancer Biomarker Detection via an Optical Nanosensor Implant. *Sci. Adv.* **2018**, *4* (4), eaaq1090.

(46) Landry, M. P.; Ando, H.; Chen, A. Y.; Cao, J.; Kottadiel, V. I.; Chio, L.; Yang, D.; Dong, J.; Lu, T. K.; Strano, M. S. Single-Molecule Detection of Protein Efflux from Microorganisms Using Fluorescent Single-Walled Carbon Nanotube Sensor Arrays. *Nat. Nanotechnol.* **2017**, *12*, 368–377.

(47) Lee, K.; Lee, J.; Ahn, B. Design of Refolding DNA Aptamer on Single-Walled Carbon Nanotubes for Enhanced Optical Detection of Target Proteins. *Anal. Chem.* **2019**.

(48) Bisker, G.; Dong, J.; Park, H. D.; Iverson, N. M.; Ahn, J.; Nelson, J. T.; Landry, M. P.; Kruss, S.; Strano, M. S. Protein-Targeted Corona Phase Molecular Recognition. *Nat. Commun.* **2016**, *7*, 10241.

(49) Basedow, A. M.; Ebert, K. H. Ultrasonic Degradation of Polymers in Solution. In *Physical Chemistry. Advances in Polymer Science*; 1977; Vol. 22, pp 84–148.

(50) Barone, P. W.; Strano, M. S. Reversible Control of Carbon Nanotube Aggregation for a Glucose Affinity Sensor. *Angew. Chemie - Int. Ed.* **2006**, *118*, 8318–8321.

(51) Karajanagi, S. S.; Yang, H.; Asuri, P.; Sellitto, E.; Dordick, J. S.; Kane, R. S. Protein-Assisted Solubilization of Single-Walled Carbon Nanotubes. *Langmuir* **2006**, *22* (4), 1392–1395.

(52) Karajanagi, S. S.; Vertegel, A. A.; Kane, R. S.; Dordick, J. S. Structure and Function of Enzymes Adsorbed onto Single-Walled Carbon Nanotubes. *Langmuir* **2004**, *20* (26), 11594–11599.

(53) Streit, J. K.; Fagan, J. A.; Zheng, M. A Low Energy Route to DNA-Wrapped Carbon Nanotubes via Replacement of Bile Salt Surfactants. *Anal. Chem.* **2017**, *89* (19), 10496–10503.

(54) Del Bonis-O'Donnell, J. T.; Pinals, R. L.; Jeong, S.; Thakrar, A.; Wolfinger, R. D.; Landry, M. P. Chemometric Approaches for Developing Infrared Nanosensors to Image Anthracyclines. *Biochemistry* **2019**, *58* (1), 54–64.

(55) Stoltenburg, R.; Reinemann, C.; Strehlitz, B. SELEX-A (r)Evolutionary Method to Generate High-Affinity Nucleic Acid Ligands. *Biomol. Eng.* **2007**, *24* (4), 381–403.

(56) Arnold, F. H. Directed Evolution: Bringing New Chemistry to Life. *Angew. Chemie - Int. Ed.* **2018**, *57* (16), 4143–4148.

(57) Jeong, S.; Yang, D.; Beyene, A. G.; Del Bonis-O'Donnell, J. T.; Gest, A. M. M.; Navarro, N.; Sun, X.; Landry, M. P. High-Throughput Evolution of near-Infrared Serotonin Nanosensors. *Sci. Adv.* **2019**, *5* (12), 1–13.

(58) Lambert, B.; Gillen, A. J.; Schuergers, N.; Wu, S. J.; Boghossian, A. A. Directed Evolution of the Optoelectronic Properties of Synthetic Nanomaterials. *Chem. Commun.* **2019**, *55* (22), 3239–3242.

(59) Yang, Y.; Zheng, M.; Jagota, A. Learning to Predict Single-Wall Carbon Nanotube-Recognition DNA Sequences. *npj Comput. Mater.* **2019**, *5* (1), 1–7.

(60) Landry, M. P.; Vukovic, L.; Kruss, S.; Bisker, G.; Landry, A. M.; Islam, S.; Jain, R. M.; Schulten, K.; Strano, M. S. Comparative Dynamics and Sequence Dependence of DNA and RNA Binding to Single Walled Carbon Nanotubes. *J. Phys. Chem. C* **2015**, *119* (18), 10048–10058.

(61) Pinals, R. L.; Yang, D.; Lui, A.; Cao, W.; Landry, M. P. Corona Exchange Dynamics on Carbon Nanotubes by Multiplexed Fluorescence Monitoring. *J. Am. Chem. Soc.* **2020**, *142* (3), 1254–1264.

(62) Harvey, J. D.; Baker, H. A.; Ortiz, M. V.; Kentsis, A.; Heller, D. A. HIV Detection via a Carbon Nanotube RNA Sensor. *ACS Sensors* **2019**, *4* (5), 1236–1244.

(63) Harvey, J. D.; Jena, P. V.; Baker, H. A.; Zerze, G. H.; Williams, R. M.; Galassi, T. V.; Roxbury, D.; Mittal, J.; Heller, D. A. A Carbon Nanotube Reporter of MicroRNA Hybridization Events in Vivo. *Nat. Biomed. Eng.* **2017**, *1* (March), 0041.

(64) Antonucci, A.; Kupis-Rozmyslowicz, J.; Boghossian, A. A. Non-Covalent Protein and Peptide Functionalization of Single-Walled Carbon Nanotubes for Bio-Delivery and Optical Sensing Applications. *ACS Appl. Mater. Interfaces* **2017**, acsami.7b00810.

(65) Reuel, N. F.; Grassbaugh, B.; Kruss, S.; Mundy, J. Z.; Opel, C.; Ogunniyi, A. O.; Egodage, K.; Wahl, R.; Helk, B.; Zhang, J.; et al. Emergent Properties of Nanosensor Arrays: Applications for Monitoring IgG Affinity Distributions, Weakly Affined Hypermannosylation, and Colony Selection for Biomanufacturing. *ACS Nano* **2013**, *7* (9), 7472–7482.

(66) Nelson, J. T.; Kim, S.; Reuel, N. F.; Salem, D. P.; Bisker, G.; Landry, M. P.; Kruss, S.; Barone, P. W.; Kwak, S.; Strano, M. S. Mechanism of Immobilized Protein A Binding to Immunoglobulin G on Nanosensor Array Surfaces. *Anal. Chem.* **2015**, *87* (16), 8186–8193.

(67) Dong, J.; Salem, D. P.; Sun, J. H.; Strano, M. S. Analysis of Multiplexed Nanosensor Arrays Based on Near-Infrared Fluorescent Single-Walled Carbon Nanotubes. *ACS Nano* **2018**, *12* (4), 3769–3779.

(68) Salem, D. P.; Gong, X.; Liu, A. T.; Koman, V. B.; Dong, J.; Strano, M. S. Ionic Strength-Mediated Phase Transitions of Surface-Adsorbed DNA on Single-Walled Carbon Nanotubes. *J. Am. Chem. Soc.* **2017**, *139* (46), 16791–16802.

(69) Gillen, A. J.; Kupis-Rozmyslowicz, J.; Gigli, C.; Schürgers, N.; Boghossian, A. A. Xeno Nucleic Acid Nanosensors for Enhanced Stability Against Ion-Induced Perturbations. *J. Phys. Chem. Lett.* **2018**, acs.jpclett.8b01879.

(70) Banerjee, S.; Hemraj-Benny, T.; Wong, S. S. Covalent Surface Chemistry of Single-Walled Carbon Nanotubes. *Adv. Mater.* **2005**, *17* (1), 17–29.

(71) Li, F.; Cheng, H. M.; Bai, S.; Su, G.; Dresselhaus, M. S. Tensile Strength of Single-Walled Carbon Nanotubes Directly Measured from Their Macroscopic Ropes. *Appl. Phys. Lett.* **2000**, *77* (20), 3161–3163.

(72) Peng, X.; Wong, S. S. Functional Covalent Chemistry of Carbon Nanotube Surfaces. *Adv. Mater.* **2009**, *21* (6), 625–642.

(73) Cognet, L.; Tsyboulski, D. A.; Rocha, J.-D. R.; Doyle, C. D.; Tour, J. M.; Weisman, R. B. Stepwise Quenching of Exciton. *Science (80-.).* **2007**, *316* (8), 1465–1469.

(74) Palma, M.; Wang, W.; Penzo, E.; Brathwaite, J.; Zheng, M.; Hone, J.; Nuckolls, C.; Wind, S. J. Controlled Formation of Carbon Nanotube Junctions via Linker-Induced Assembly in Aqueous Solution. *J. Am. Chem. Soc.* **2013**, *135* (23), 8440–8443.

(75) Bruot, C.; Xiang, L.; Palma, J. L.; Li, Y.; Tao, N. Tuning the Electromechanical Properties of Single DNA Molecular Junctions. **2015**.

(76) Freeley, M.; Worthy, H. L.; Ahmed, R.; Bowen, B.; Watkins, D.; Macdonald, J. E.; Zheng, M.; Jones, D. D.; Palma, M. Site-Specific One-to-One Click Coupling of Single Proteins to Individual Carbon Nanotubes: A Single-Molecule Approach. *J. Am. Chem. Soc.* **2017**, *139* (49), 17834–17840.

(77) Piao, Y.; Meany, B.; Powell, L. R.; Valley, N.; Kwon, H.; Schatz, G. C.; Wang, Y. Brightening of Carbon Nanotube Photoluminescence through the Incorporation of Sp 3 Defects. *Nat. Chem.* **2013**, *5* (10), 840–845.

(78) Kwon, H.; Furmanchuk, A.; Kim, M.; Meany, B.; Guo, Y.; Schatz, G. C.; Wang, Y. Molecularly Tunable Fluorescent Quantum Defects. *J. Am. Chem. Soc.* **2016**, *138* (21), 6878–6885.

(79) Setaro, A.; Adeli, M.; Glaeske, M.; Przyrembel, D.; Bisswanger, T.; Gordeev, G.; Maschietto, F.; Faghani, A.; Paulus, B.; Weinelt, M.; et al. Preserving π-Conjugation in Covalently Functionalized Carbon Nanotubes for Optoelectronic Applications. *Nat. Commun.* **2017**, *8*, 1–7.

(80) Stephanopoulos, N.; Francis, M. B. Choosing an Effective Protein Bioconjugation Strategy. *Nat. Chem. Biol.* **2011**, *7* (12), 876–884.

(81) Wang, J.; Han, J.; Chen, X.; Wang, X. Design Strategies for Two-dimensional Material Photodetectors to Enhance Device Performance. *InfoMat* **2019**, *1* (1), 33–53.

(82) Heller, D. A.; Pratt, G. W.; Zhang, J.; Nair, N.; Hansborough, A. J.; Boghossian, A. A.; Reuel, N. F.; Barone, P. W.; Strano, M. S. Peptide Secondary Structure Modulates Single-Walled Carbon Nanotube Fluorescence as a Chaperone Sensor for Nitroaromatics. *Proc. Natl. Acad. Sci.* **2011**, *108* (21), 8544–8549.

(83) Kruss, S.; Salem, D. P.; Vukovic, L.; Lima, B.; Vander Ende, E.; Boyden, E. S.; Strano, M. S. High-Resolution Imaging of Cellular Dopamine Efflux Using a Fluorescent Nanosensor Array. **2017**, *3*.

(84) Naidu, P. S. R.; Denham, E.; Bartlett, C. A.; McGonigle, T.; Taylor, N. L.; Norret, M.; Smith, N. M.; Dunlop, S. A.; Iyer, K. S.; Fitzgerald, M. Protein Corona Formation Moderates the Release Kinetics of Ion Channel Antagonists from Transferrin-Functionalized Polymeric Nanoparticles. *RSC Adv.* **2020**, *10* (5), 2856–2869.

(85) Battig, M. R.; Wang, Y. *Nucleic Acid Aptamers for Biomaterials Development*; Elsevier Inc., 2014.

(86) Berg, J. M.; Tymoczko, J. L.; Gatto Jr., G. J.; Stryer, L. *Biochemistry*, 8th ed.; W.H. Freeman: New York, 2015.

(87) Xie, L.; Chou, S. G.; Pande, A.; Pande, J.; Zhang, J.; Dresselhaus, M. S.; Kong, J.; Liu, Z. Single-Walled Carbon Nanotubes Probing the Denaturation of Lysozyme. *J. Phys. Chem. C* **2010**, *114* (17), 7717–7720.

(88) Lee, K.; Nojoomi, A.; Jeon, J.; Lee, C. Y.; Yum, K. Near-Infrared Fluorescence Modulation of Refolded DNA Aptamer-Functionalized Single-Walled Carbon Nanotubes for Optical Sensing. *ACS Appl. Nano Mater.* **2018**, acsanm.8b01377.

(89) Kishimoto, S.; Nakashimada, Y.; Yokota, R.; Hatanaka, T.; Adachi, M.; Ito, Y. Site-Specific Chemical Conjugation of Antibodies by Using Affinity Peptide for the Development of Therapeutic Antibody Format. *Bioconjug. Chem.* **2019**, *30* (3), 698–702.

(90) Stürzl, N.; Hennrich, F.; Lebedkin, S.; Kappes, M. M. Near Monochiral Single-Walled Carbon Nanotube Dispersions in Organic Solvents. *J. Phys. Chem. C* **2009**, *113* (33), 14628–14632.

(91) Liu, H.; Nishide, D.; Tanaka, T.; Kataura, H. Large-Scale Single-Chirality Separation of Single-Wall Carbon Nanotubes by Simple Gel Chromatography. *Nat Commun* **2011**, *2*, 309.

(92) Ao, G.; Khripin, C. Y.; Zheng, M. DNA-Controlled Partition of Carbon Nanotubes in Polymer Aqueous Two-Phase Systems. *J. Am. Chem. Soc.* **2014**, *136* (29), 10383–10392.

(93) Fagan, J. A.; Khripin, C. Y.; Batista, C. A. S.; Simpson, J. R.; Hároz, E. H.; Walker, A. R. H.; Zheng, M. Isolation of Specifi c Small-Diameter Single-Wall Carbon Nanotube Species via Aqueous Two-Phase Extraction. **2014**, 2800–2804.

(94) Barone, P. W.; Baik, S.; Heller, D. A.; Strano, M. S. Near-Infrared Optical Sensors Based on Single-Walled Carbon Nanotubes. *Nat. Mater.* **2005**, *4*, 86–92.

(95) Del Bonis-O'Donnell, J. T. D.; Page, R. H.; Beyene, A. G.; Tindall, E. G.; McFarlane, I. R.; Landry, M. P. Dual Near-Infrared Two-Photon Microscopy for Deep-Tissue Dopamine Nanosensor Imaging. *Adv. Funct. Mater.* **2017**, *27*, 1702112.

(96) Bruns, O. T.; Bischof, T. S.; Harris, D. K.; Franke, D.; Shi, Y.; Riedemann, L.; Bartelt, A.; Jaworski, F. B.; Carr, J. A.; Rowlands, C. J.; et al. Next-Generation in Vivo Optical Imaging with Short-Wave Infrared Quantum Dots. *Nat. Biomed. Eng.* **2017**, *1* (4).

(97) Salem, D. P.; Landry, M. P.; Bisker, G.; Ahn, J.; Kruss, S.; Strano, M. S. Chirality Dependent Corona Phase Molecular Recognition of DNA-Wrapped Carbon Nanotubes. *Carbon N. Y.* **2016**, *97*, 147–153.

(98) Roxbury, D.; Jena, P. V.; Shamay, Y.; Horoszko, C. P.; Heller, D. A. Cell Membrane Proteins Modulate the Carbon Nanotube Optical Bandgap via Surface Charge Accumulation. *ACS Nano* **2016**, *10* (1), 499–506.

(99) Arnold, M. S.; Guler, M. O.; Hersam, M. C.; Stupp, S. I. Encapsulation of Carbon Nanotubes by Self-Assembling Peptide Amphiphiles. *Langmuir* **2005**, *21* (10), 4705–4709.

(100) Budhathoki-Uprety, J.; Jena, P. V; Roxbury, D.; Heller, D. A. Helical Polycarbodiimide Cloaking of Carbon Nanotubes Enables Inter-Nanotube Exciton Energy Transfer Modulation. *J. Am. Chem. Soc.* **2014**, *136*, 15545–15550.

(101) Ahn, J.; Kim, J.; Reuel, N. F.; Barone, P. W.; Boghossian, A. A.; Zhang, J.; Yoon, H.; Chang, A. C.; Hilmer, A. J.; Strano, M. S. Label-Free, Single Protein Detection on a Near-Infrared Fluorescent Single-Walled Carbon Nanotube/Protein Microarray Fabricated by Cell-Free Synthesis. **2011**, 2743–2752.

(102) Sun, J.; Zuckermann, R. N. Peptoid Polymers: A Highly Designable Bioinspired Material. *ACS Nano* **2013**, *7* (6), 4715–4732.

(103) Jang, H.; Fafarman, A.; Holub, J. M.; Kirshenbaum, K. Click to Fit: Versatile Polyvalent Display on a Peptidomimetic Scaffold. *Org. Lett.* **2005**, *7* (10), 1951–1954.

(104) Knight, A. S.; Kulkarni, R. U.; Zhou, E. Y.; Franke, J. M.; Miller, E. W.; Francis, M. B. A Modular Platform to Develop Peptoid-Based Selective Fluorescent Metal Sensors. *Chem. Commun.* **2017**, *53*, 3477–3480.

(105) Fuller, A. A.; Seidl, F. J.; Bruno, P. A.; Plescia, M. A.; Palla, K. S. Use of the Environmentally Sensitive Fluorophore 4-N,N-Dimethylamino-1,8-Naphthalimide to Study Peptoid Helix Structures. *Biopolymers* **2011**, *96* (5), 627–638.

(106) Miller, S. M.; Simon, R. J.; Ng, S.; Zuckermann, R. N.; Kerr, J. M.; Moos, W. H. Proteolytic Studies of Homologous Peptide and N-Substituted Glycine Peptoid Oligomers. *Bioorganic Med. Chem. Lett.* **1994**, *4* (22), 2657–2662.

(107) Olivier, G. K.; Cho, A.; Sanii, B.; Connolly, M. D.; Tran, H.; Zuckermann, R. N. Antibody-Mimetic Peptoid Nanosheets for Molecular Recognition. *ACS Nano* **2013**, *7* (10), 9276–9286.

(108) Battigelli, A.; Kim, J. H.; Dehigaspitiya, D. C.; Proulx, C.; Robertson, E. J.; Murray, D. J.; Rad, B.; Kirshenbaum, K.; Zuckermann, R. N. Glycosylated Peptoid Nanosheets as a Multivalent Scaffold for Protein Recognition. *ACS Nano* **2018**, *12* (3), 2455–2465.

(109) Knight, A. S.; Zhou, E. Y.; Francis, M. B.; Zuckermann, R. N. Sequence Programmable Peptoid Polymers for Diverse Materials Applications. *Adv. Mater.* **2015**, *27* (38), 5665–5691.

(110) Chio, L.; Yang, D.; Landry, M. P. Surface Engineering of Nanoparticles to Create

Synthetic Antibodies. *Methods Mol. Biol.* **2017**, *1575*, 363–380.

(111) Zuckermann, R. N.; Kerr, J. M.; Moosf, W. H.; Kent, S. B. H. Efficient Method for the Preparation of Peptoids [Oligo(N-Substituted Glycines)] by Submonomer Solid-Phase Synthesis. *J. Am. Chem. Soc.* **1992**, *114* (26), 10646–10647.

(112) Nam, K. T.; Shelby, S. A.; Choi, P. H.; Marciel, A. B.; Chen, R.; Tan, L.; Chu, T. K.; Mesch, R. a; Lee, B.-C.; Connolly, M. D.; et al. Free-Floating Ultrathin Two-Dimensional Crystals from Sequence-Specific Peptoid Polymers. *Nat. Mater.* **2010**, *9* (5), 454–460.

(113) Pizarro-Cerdá, J.; Cossart, P. Bacterial Adhesion and Entry into Host Cells. *Cell* **2006**, *124* (4), 715–727.

(114) Grove, J.; Marsh, M. The Cell Biology of Receptor-Mediated Virus Entry. *J. Cell Biol.* **2011**, *195* (7), 1071–1082.

(115) Pinho, S. S.; Reis, C. A. Glycosylation in Cancer : Mechanisms and Clinical Implications. *Nat. Rev.* **2015**, *15* (9), 540–555.

(116) Blagbrough, I. S.; Metwally, A. A.; Geall, A. J. Measurement of Polyamine PKa Values. In *Polyamines: Methods and Protocols*; Pegg, A. E., Casero Jr., R. A., Eds.; Humana Press: Totowa, NJ, 2011; pp 493–503.

(117) Pramanik, C.; Gissinger, J. R.; Kumar, S.; Heinz, H. Carbon Nanotube Dispersion in Solvents and Polymer Solutions: Mechanisms, Assembly, and Preferences. *ACS Nano* **2017**, *11* (12), 12805–12816.

(118) Kallmyer, N. E.; Musielewicz, J.; Sutter, J.; Reuel, N. F. Substrate-Wrapped, Single-Walled Carbon Nanotube Probes for Hydrolytic Enzyme Characterization. *Anal. Chem.* **2018**, *90* (8), 5209–5216.

(119) Zhao, R.; So, M.; Maat, H.; Ray, N. J.; Arisaka, F.; Goto, Y.; Carver, J. A.; Hall, D. Measurement of Amyloid Formation by Turbidity Assay—seeing through the Cloud. *Biophys. Rev.* **2016**, *8* (4), 445–471.

(120) Wu, A. M.; Wu, J. H.; Song, S. C.; Tsai, M. S.; Herp, A. Studies on the Binding of Wheat Germ Agglutinin (Triticum Vulgaris) to O-Glycans. *FEBS Lett.* **1998**, *440* (3), 315–319.

(121) Hertel, T.; Himmelein, S.; Ackermann, T.; Stich, D.; Ḱ, J. C. Diffusion Limited Photoluminescence Quantum Yields in 1-D Semiconductors : *ACS Nano* **2010**, *4* (12), 7161–7168.

(122) Portillo-Tellez, M. D. C.; Bello, M.; Salcedo, G.; Gutierrez, G.; Gomez-Vidales, V.; García-Hernández, E. Folding and Homodimerization of Wheat Germ Agglutinin. *Biophys. J.* **2011**, *101* (6), 1423–1431.

(123) Andrade, J. D.; Hlady, V.; Wei, A. P. Adsorption of Complex Proteins at Interfaces. *Pure Appl. Chem.* **1992**, *64* (11), 1777–1781.

(124) Holt, B. D.; Dahl, K. N.; Islam, M. F. Quantification of Uptake and Localization of Bovine Serum Albumin-Stabilized Single-Wall Carbon Nanotubes in Different Human Cell Types. *Small* **2011**, *7* (16), 2348–2355.

(125) Beyene, A. G.; Alizadehmojarad, A. A.; Dorlhiac, G.; Streets, A. M.; Král, P.; Vuković, L.; Landry, M. P. Ultralarge Modulation of Single Wall Carbon Nanotube Fluorescence Mediated by Neuromodulators Adsorbed on Arrays of Oligonucleotide Rings. *Nano Lett.* **2018**, DOI: 10.1101/351627.

(126) Ham, H. O.; Park, S. H.; Kurutz, J. W.; Szleifer, I. G.; Messersmith, P. B. Antifouling Glycocalyx-Mimetic Peptoids. *J. Am. Chem. Soc.* **2013**, *135* (35), 13015–13022.

(127) Monsigny, M.; Roche, A.-C.; Sene, C.; Maget-Dana, R.; Delmotte, F. Sugar-Lectin Interactions: How Does Wheat-Germ Agglutinin Bind Sialoglycoconjugates. *Eur. J. Biochem.* **1980**, *104* (1), 147–153.

(128) Reuel, N. F.; Ahn, J. H.; Kim, J. H.; Zhang, J.; Boghossian, A. A.; Mahal, L. K.; Strano, M. S. Transduction of Glycan-Lectin Binding Using near-Infrared Fluorescent Single-Walled Carbon Nanotubes for Glycan Profiling. *J. Am. Chem. Soc.* **2011**, *133* (44), 17923–17933.

(129) Zubkovs, V.; Schuergers, N.; Lambert, B.; Ahunbay, E.; Boghossian, A. A. Mediatorless, Reversible Optical Nanosensor Enabled through Enzymatic Pocket Doping. *Small* **2017**, *13* (42), 1–10.

(130) Barone, P. W.; Yoon, H.; Ortiz-García, R.; Zhang, J.; Ahn, J. H.; Kim, J. H.; Strano, M. S. Modulation of Single-Walled Carbon Nanotube Photoluminescence by Hydrogel Swelling. *ACS Nano* **2009**, *3* (12), 3869–3877.

(131) Vaitheeswaran, S.; Garcia, A. E. Protein Stability at a Carbon Nanotube Interface. *J. Chem. Phys.* **2011**, *134* (12), 1–10.

(132) Parker, B. F.; Knight, A. S.; Vukovic, S.; Arnold, J.; Francis, M. B. A Peptoid-Based Combinatorial and Computational Approach to Developing Ligands for Uranyl Sequestration from Seawater. *Ind. Eng. Chem. Res.* **2016**, *55*, 4187–4194.

(133) Turner, J. P.; Lutz-Rechtin, T.; Moore, K. A.; Rogers, L.; Bhave, O.; Moss, M. A.; Servoss, S. L. Rationally Designed Peptoids Modulate Aggregation of Amyloid-Beta 40. *ACS Chem. Neurosci.* **2014**, *5* (7), 552–558.

(134) Demirer, G. S.; Zhang, H.; Matos, J. L.; Goh, N.; Cunningham, F.; Sung, Y.; Chang, R.; Aditham, A. J.; Chio, L.; Cho, M.; et al. High Aspect Ratio Nanomaterials Enable Delivery of Functional Genetic Material Without DNA Integration in Mature Plants. *Nat. Nanotechnol.* **2019**, No. 14, 456–464.

(135) Cui, X.; Wan, B.; Yang, Y.; Ren, X.; Guo, L. H. Length Effects on the Dynamic Process of Cellular Uptake and Exocytosis of Single-Walled Carbon Nanotubes in Murine Macrophage Cells. *Sci. Rep.* **2017**, *7* (1), 1–13.

(136) Kafa, H.; Wang, J. T. W.; Al-Jamal, K. T. Current Perspective of Carbon Nanotubes Application in Neurology. In *International Review of Neurobiology*; Academic Press, 2016; Vol. 130, pp 229–263.

(137) Alluri, P. G.; Reddy, M. M.; Bachhawat-Sikder, K.; Olivos, H. J.; Kodadek, T. Isolation of Protein Ligands from Large Peptoid Libraries. *J. Am. Chem. Soc.* **2003**, *125* (46), 13995–14004.

(138) Doane, T. L.; Burda, C. The Unique Role of Nanoparticles in Nanomedicine: Imaging, Drug Delivery and Therapy. *Chem. Soc. Rev.* **2012**, *41* (7), 2885–2911.

(139) Scheinberg, D. A.; Grimm, J.; Heller, D. A.; Stater, E. P.; Bradbury, M.; McDevitt, M. R. Advances in the Clinical Translation of Nanotechnology. *Curr. Opin. Biotechnol.* **2017**, *46*, 66–73.

(140) Iverson, N. M.; Barone, P. W.; Shandell, M. A.; Trudel, L. J.; Sen, S.; Sen, F.; Ivanov, V.; Atolia, E.; Farias, E.; Mcnicholas, T. P.; et al. In Vivo Biosensing via Tissue-Localizable near-Infrared-Fluorescent Single-Walled Carbon Nanotubes. *Nat. Nanotechnol.* **2013**, *8* (11), 873–880.

(141) Kwon, O. S.; Park, S. J.; Jang, J. A High-Performance VEGF Aptamer Functionalized Polypyrrole Nanotube Biosensor. *Biomaterials* **2010**, *31* (17), 4740–4747.

(142) Meng, L.; Zhang, X.; Lu, Q.; Fei, Z.; Dyson, P. J. Single Walled Carbon Nanotubes as Drug Delivery Vehicles: Targeting Doxorubicin to Tumors. *Biomaterials* **2012**, *33* (6), 1689–1698.

(143) Chen, J.; Chen, S.; Zhao, X.; Kuznetsova, L. V.; Wong, S. S.; Ojima, I. Functionalized Single-Walled Carbon Nanotubes as Rationally Designed Vehicles for Tumor-Targeted Drug Delivery. *J. Am. Chem. Soc.* **2008**, *130* (49), 16778–16785.

(144) Hilderbrand, S. A.; Weissleder, R. Near-Infrared Fluorescence: Application to in Vivo Molecular Imaging. *Curr. Opin. Chem. Biol.* **2010**, *14* (1), 71–79.

(145) Chio, L.; Del Bonis-O'Donnell, J. T.; Kline, M. A.; Kim, J. H.; McFarlane, I. R.; Zuckermann, R. N.; Landry, M. P. Electrostatic Assemblies of Single-Walled Carbon Nanotubes and Sequence-Tunable Peptoid Polymers Detect a Lectin Protein and Its Target Sugars. *Nano Lett.* **2019**, *19* (11), 7563–7572.

(146) Beyene, A. G.; Delevich, K.; Del Bonis-O'Donnell, J. T.; Piekarski, D. J.; Lin, W. C.; Wren Thomas, A.; Yang, S. J.; Kosillo, P.; Yang, D.; Prounis, G. S.; et al. Imaging Striatal Dopamine Release Using a Nongenetically Encoded near Infrared Fluorescent Catecholamine Nanosensor. *Sci. Adv.* **2019**, *5* (7), eaaw3108.

(147) Onitsuka, H.; Fujigaya, T.; Nakashima, N.; Shiraki, T. Control of the Near Infrared Photoluminescence of Locally Functionalized Single-Walled Carbon Nanotubes via Doping by Azacrown-Ether Modification. *Chem. - A Eur. J.* **2018**, *24* (37), 9393–9398.

(148) Luo, H. Bin; Wang, P.; Wu, X.; Qu, H.; Ren, X.; Wang, Y. One-Pot, Large-Scale Synthesis of Organic Color Center-Tailored Semiconducting Carbon Nanotubes. *ACS Nano* **2019**, *13* (7), 8417–8424.

(149) Kundu, S.; Wang, Y.; Xia, W.; Muhler, M. Thermal Stability and Reducibility of Oxygen-Containing Functional Groups on Multiwalled Carbon Nanotube Surfaces : A Quantitative High-Resolution XPS and TPD / TPR Study. **2008**, 16869–16878.

(150) Godin, A. G.; Setaro, A.; Gandil, M.; Haag, R.; Adeli, M.; Reich, S.; Cognet, L. Photoswitchable Single-Walled Carbon Nanotubes for Super-Resolution Microscopy in the near-Infrared. *Sci. Adv.* **2019**, *5* (9), eaax1166.

(151) Beyene, A. G.; Alizadehmojarad, A. A.; Dorlhiac, G.; Goh, N.; Streets, A. M.; Král, P.; Vuković, L.; Landry, M. P. Ultralarge Modulation of Fluorescence by Neuromodulators in Carbon Nanotubes Functionalized with Self-Assembled Oligonucleotide Rings. *Nano Lett.* **2018**, *18* (11), 6995–7003.

(152) Carr, J. A.; Franke, D.; Caram, J. R.; Perkinson, C. F.; Saif, M.; Askoxylakis, V.; Datta, M.; Fukumura, D.; Jain, R. K.; Bawendi, M. G.; et al. Shortwave Infrared Fluorescence Imaging with the Clinically Approved Near-Infrared Dye Indocyanine Green. *Proc. Natl. Acad. Sci.* **2018**, 201718917.

(153) Polo, E.; Kruss, S. Impact of Redox-Active Molecules on the Fluorescence of Polymer-Wrapped Carbon Nanotubes. *J. Phys. Chem. C* **2016**, *120* (5), 3061–3070.

(154) Wang, H.; Michielssens, S.; Moors, S. L. C.; Ceulemans, A. Molecular Dynamics Study of Dipalmitoylphosphatidylcholine Lipid Layer Self-Assembly onto a Single-Walled Carbon Nanotube. *Nano Res.* **2009**, *2* (12), 945–954.

(155) Lee, H.; Kim, H. Self-Assembly of Lipids and Single-Walled Carbon Nanotubes: Effects of Lipid Structure and PEGylation. *J. Phys. Chem. C* **2012**, *116* (16), 9327–9333.

(156) Fröhlich, E. The Role of Surface Charge in Cellular Uptake and Cytotoxicity of Medical Nanoparticles. *Int. J. Nanomedicine* **2012**, *7*, 5577–5591.

(157) Mann, F. A.; Lv, Z.; Grosshans, J.; Opazo, F.; Kruss, S. Nanobody Conjugated Nanotubes for Targeted Near-Infrared in Vivo Imaging and Sensing. *Angew. Chemie Int. Ed.* **2019**.

(158) Marttila, A. T.; Laitinen, O. H.; Airenne, K. J.; Kulik, T.; Bayer, E. A.; Wilchek, M.; Kulomaa, M. S. Recombinant NeutraLite Avidin: A Non-Glycosylated, Acidic Mutant of Chicken Avidin That Exhibits High Affinity for Biotin and Low Non-Specific Binding Properties. *FEBS Lett.* **2000**, *467* (1), 31–36.

(159) Neish, C. S.; Martin, I. L.; Henderson, R. M.; Edwardson, J. M. Direct Visualization of Ligand-Protein Interactions Using Atomic Force Microscopy. *Br. J. Pharmacol.* **2002**, *135* (8), 1943–1950.

(160) Kim, J. H.; Kim, S. C.; Kline, M. A.; Grzincic, E. M.; Tresca, B. W.; Cardiel, J.; Karbaschi, M.; Dehigaspitiya, D. C.; Chen, Y.; Udumula, V.; et al. Discovery of Stable and Selective Antibody Mimetics from Combinatorial Libraries of Polyvalent, Loop-Functionalized Peptoid Nanosheets. **2019**.

(161) Rodríguez-López, J. N.; Lowe, D. J.; Hernández-Ruiz, J.; Hiner, A. N. P.; García-Cánovas, F.; Thorneley, R. N. F. Mechanism of Reaction of Hydrogen Peroxide with Horseradish Peroxidase: Identification of Intermediates in the Catalytic Cycle. *J. Am. Chem. Soc.* **2001**, *123* (48), 11838–11847.

(162) Sies, H. Hydrogen Peroxide as a Central Redox Signaling Molecule in Physiological Oxidative Stress: Oxidative Eustress. *Redox Biol.* **2017**, *11* (December 2016), 613–619.

(163) Landry, J. P.; Ke, Y.; Yu, G. L.; Zhu, X. D. Measuring Affinity Constants of 1450 Monoclonal Antibodies to Peptide Targets with a Microarray-Based Label-Free Assay Platform. *J. Immunol. Methods* **2015**, *417*, 86–96.

(164) Shukla, R.; Thomas, T. P.; Peters, J. L.; Desai, A. M.; Kukowska-Latallo, J.; Patri, A. K.; Kotlyar, A.; Baker, J. R. HER2 Specific Tumor Targeting with Dendrimer Conjugated Anti-HER2 MAb. *Bioconjug. Chem.* **2006**, *17* (5), 1109–1115.

(165) Mitri, Z.; Constantine, T.; O'Regan, R. The HER2 Receptor in Breast Cancer: Pathophysiology, Clinical Use, and New Advances in Therapy. *Chemother. Res. Pract.* **2012**, *2012*, 1–7.

(166) Song, J.; Wang, F.; Yang, X.; Ning, B.; Harp, M. G.; Culp, S. H.; Hu, S.; Huang, P.; Nie, L.; Chen, J.; et al. Gold Nanoparticle Coated Carbon Nanotube Ring with Enhanced Raman Scattering and Photothermal Conversion Property for Theranostic Applications. *J. Am. Chem. Soc.* **2016**, *138* (22), 7005–7015.

(167) Chen, D.; Wang, C.; Nie, X.; Li, S.; Li, R.; Guan, M.; Liu, Z.; Chen, C.; Wang, C.; Shu, C.; et al. Photoacoustic Imaging Guided Near-Infrared Photothermal Therapy Using Highly Water-Dispersible Single-Walled Carbon Nanohorns as Theranostic Agents. *Adv. Funct. Mater.* **2014**, *24* (42), 6621–6628.

(168) Cai, R.; Chen, C. The Crown and the Scepter: Roles of the Protein Corona in Nanomedicine. *Adv. Mater.* **2019**, *31* (45), 1–13.

(169) Sanchez-Cano, C.; Carril, M. Recent Developments in the Design of Non-Biofouling Coatings for Nanoparticles and Surfaces. *Int. J. Mol. Sci.* **2020**, *21* (3), 1–24.

(170) García, K. P.; Zarschler, K.; Barbaro, L.; Barreto, J. A.; O'Malley, W.; Spiccia, L.; Stephan, H.; Graham, B. Zwitterionic-Coated "Stealth" Nanoparticles for Biomedical Applications: Recent Advances in Countering Biomolecular Corona Formation and Uptake by the Mononuclear Phagocyte System. *Small* **2014**, *10* (13), 2516–2529.

(171) Ritz, S.; Schöttler, S.; Kotman, N.; Baier, G.; Musyanovych, A.; Kuharev, J.; Landfester, K.; Schild, H.; Jahn, O.; Tenzer, S.; et al. Protein Corona of Nanoparticles: Distinct Proteins Regulate the Cellular Uptake. *Biomacromolecules* **2015**, *16* (4), 1311–1321.

(172) Lu, X.; Xu, P.; Ding, H. M.; Yu, Y. S.; Huo, D.; Ma, Y. Q. Tailoring the Component of Protein Corona via Simple Chemistry. *Nat. Commun.* **2019**, *10* (1).

(173) Kang, B.; Yu, D.; Dai, Y.; Chang, S.; Chen, D.; Ding, Y. Biodistribution and Accumulation of Intravenously Administered Carbon Nanotubes in Mice Probed by Raman Spectroscopy and Fluorescent Labeling. *Carbon N. Y.* **2009**, *47* (4), 1189–1192.

(174) Alidori, S.; Thorek, D. L. J.; Beattie, B. J.; Ulmert, D.; Almeida, A.; Monette, S.; Scheinberg, D. A.; Mcdevitt, M. R. Carbon Nanotubes Exhibit Fibrillar Pharmacology in Primates. **2017**, 1–25.

(175) Yang, S. T.; Wang, X.; Jia, G.; Gu, Y.; Wang, T.; Nie, H.; Ge, C.; Wang, H.; Liu, Y. Long-Term Accumulation and Low Toxicity of Single-Walled Carbon Nanotubes in Intravenously Exposed Mice. *Toxicol. Lett.* **2008**, *181* (3), 182–189.

(176) Kotchey, G. P.; Zhao, Y.; Kagan, V. E.; Star, A. Peroxidase-Mediated Biodegradation of Carbon Nanotubes in Vitro and in Vivo. *Adv. Drug Deliv. Rev.* **2013**, *65* (15), 1921–1932.

(177) Ding, Y.; Tian, R.; Yang, Z.; Chen, J.; Lu, N. NADPH Oxidase-Dependent Degradation

of Single-Walled Carbon Nanotubes in Macrophages. *J. Mater. Sci. Mater. Med.* **2017**, *28* (1), 1–8.

(178) Ali-Boucetta, H.; Nunes, A.; Sainz, R.; Herrero, M. A.; Tian, B.; Prato, M.; Bianco, A.; Kostarelos, K. Asbestos-like Pathogenicity of Long Carbon Nanotubes Alleviated by Chemical Functionalization. *Angew. Chemie - Int. Ed.* **2013**, *52* (8), 2274–2278.

(179) Ema, M.; Gamo, M.; Honda, K. A Review of Toxicity Studies of Single-Walled Carbon Nanotubes in Laboratory Animals. *Regul. Toxicol. Pharmacol.* **2016**, *74*, 42–63.

(180) Movia, D.; Prina-Mello, A.; Bazou, D.; Volkov, Y.; Giordani, S. Screening the Cytotoxicity of Single-Walled Carbon Nanotubes Using Novel 3D Tissue-Mimetic Models. *ACS Nano* **2011**, *5* (11), 9278–9290.

(181) Armbruster, D. A.; Pry, T. Limit of Blank, Limit of Detection and Limit of Quantitation. *Clin. Biochem. Rev.* **2008**, *29 Suppl 1* (August), S49-52.

Appendix I - The Spectral Data for Individual SWCNTs Chiralities[§]

Each SWCNT chirality has unique electronic properties that gives rise to distinct excitation and emission wavelengths. This table will help guide decisions on proper imaging equipment and downstream applications including ratiometric sensing or hyperspectral imaging. The excitation wavelength is denoted as λ_{22} and emission wavelength is denoted λ_{11}. Similarly, the bandgap energy for absorption is given as E_{22} and the bandgap energy for fluorescence is given as E_{11}.

λ_{11} (nm)	λ_{22} (nm)	E_{11} (eV)	E_{22} (eV)	Chirality
833	483	1.488	2.567	(5, 4)
873	581	1.420	2.134	(6, 4)
912	693	1.359	1.789	(9, 1)
952	633	1.302	1.870	(8, 3)
975	567	1.272	2.187	(6, 5)
1023	644	1.212	1.925	(7, 5)
1053	734	1.177	1.689	(10, 2)
1101	720	1.126	1.722	(9, 4)
1113	587	1.114	2.112	(8, 4)
1122	647	1.105	1.916	(7, 6)
1139	551	1.088	2.250	(9, 2)
1171	797	1.059	1.556	(12, 1)
1172	716	1.058	1.732	(8, 6)
1197	792	1.036	1.565	(11, 3)
1244	671	0.997	1.848	(9, 5)
1250	633	0.992	1.959	(10, 3)
1250	786	0.992	1.577	(10, 5)
1263	611	0.982	2.029	(11, 1)
1267	728	0.979	1.703	(8, 7)
1307	859	0.949	1.443	(13, 2)
1323	790	0.937	1.569	(9, 7)
1342	857	0.924	1.447	(12, 4)
1372	714	0.904	1.736	(11, 4)
1376	685	0.901	1.810	(12, 2)
1380	756	0.898	1.640	(10, 6)
1397	858	0.887	1.445	(11, 6)
1414	809	0.877	1.533	(9, 8)
1425	927	0.870	1.337	(15, 1)
1474	868	0.841	1.428	(10, 8)
1485	928	0.835	1.336	(13, 5)
1496	795	0.829	1.559	(12, 5)
1497	760	0.828	1.631	(13, 3)
1555	892	0.797	1.390	(10, 9)

[§] This table is adapted with permission from Bachilo, S. M.; Strano, M. S.; Kittrell, C.; Hauge, R. H.; Smalley, R. E.; Weisman, R. B. Structure-Assigned Optical Spectra of Single-Walled Carbon Nanotubes. *Science (80-.).* **2002**, *298* (5602), 2361–2366. Reprinted with permission from AAAS

Appendix II – **Curve Fitting for Concentration Titration and SWCNT Response**

In order to understand the thermodynamics involved in analyte binding to SWCNTs, NIR fluorescence can be used to develop a relationship between equilibrium change in fluorescence as it relates to concentration. For a kinetics approach to SWCNT binding of analyte, new studies have developed real-time fluorescence assays capable of capturing information in both the SWCNT, coating, and analyte interactions, and will not be discussed further here.

For the discussion of binding models, we discuss the system that was developed for WGA binding to ProLoop-SWCNT nanosensors. However, we postulate that this analysis can be done generally on different nanosensor and analyte pairs.

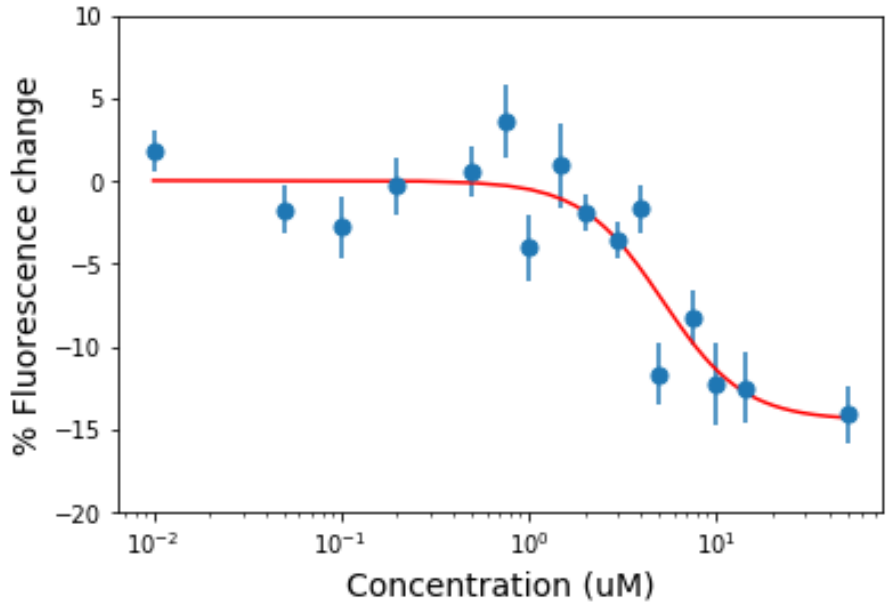

Figure S1. Curve Fitting to Determine Goodness of Fit of Equilibrium Binding Model
To determine the WGA limit of detection of ProLoop-SWCNT, we model the change in nanosensor fluorescence with respect to WGA concentration and calculate the limit of detection (LOD) at equilibrium. The red line denotes our model ($R^2 = 0.83$).

For our system, fluorescence modulation is governed by interactions between WGA, the peptoid loop, and the SWCNT surface exciton recombination. CoPhMoRe systems can be modeled with two main approaches: 1) understanding fluorescence as a result of analyte binding to the corona with a receptor-ligand model following Langmuirian adsorption equilibrium 2) understanding fluorescence in the context of SWCNT exciton recombination in the presence of quenching sites. Both models are considered below:

Approach 1: Assuming each fluorescent site binds one WGA protein, the fluorescence of the nanosensor can be treated as directly proportional to the number of protein-bound sites on the nanosensor.

The protein binding sites are assumed to form a monolayer, with each nanosensor site binding one protein site, thus WGA binding is described by:

$$WGA + \theta \leftrightarrow [WGA\text{-}\ \theta]$$

At equilibrium the equilibrium constant is given as:

$$K = \frac{[WGA-\theta]}{[WGA][\theta]}$$

The total concentration of available binding sites is a constant value $[\theta]_{tot}$ given by the sum of the free [θ] and protein-bound states [WGA- θ]:

$$[\theta]tot = [\theta] + [WGA\text{-}\ \theta]$$

$$= \frac{[WGA-\theta]}{K[WGA]} + [WGA\text{-}\ \theta]$$

$$= [WGA - \theta]\left(1 + \frac{1}{[\mathrm{WGA}]K}\right)$$

$$= [WGA - \theta]\left(\frac{[\mathrm{WGA}]K+1}{[\mathrm{WGA}]K}\right)$$

Assuming the nanosensor intensity change is proportional to the number of bound sites out of the total available nanosensor sites:

$$\frac{I - I_0}{I_0} = a\frac{[WGA - \theta]}{[\theta]_{tot}} = a\frac{(K[WGA])^n}{(K[WGA])^n + 1} + b$$

Where n accounts for WGA binding cooperativity. Since WGA is functional as a dimer, we restrict n to be a maximum of 2 for the fit to converge with WGA binding data.

Plotting the data with the model we obtain:

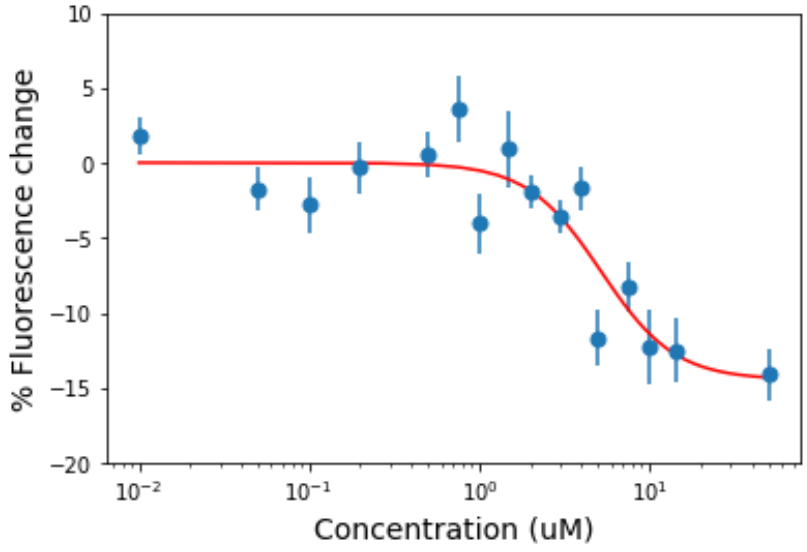

We plotted residual values for the goodness of fit of the above model, for which we obtained a scattered distribution of residual values (uncorrelated residuals), suggesting the model is not inherently biased by the data.

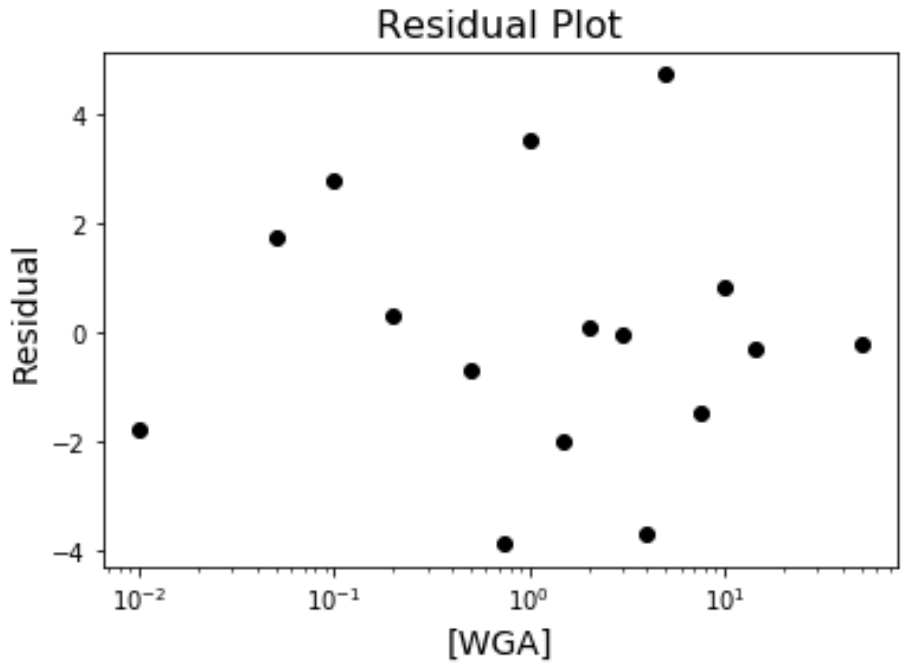

The sum of residuals given by an n = 2 fit is Σ_{res} = -0.0061, and R^2 = 0.83

Approach 2: We also investigated a fit to our data using an exciton diffusion model previously postulated by Hertel et al.[121]

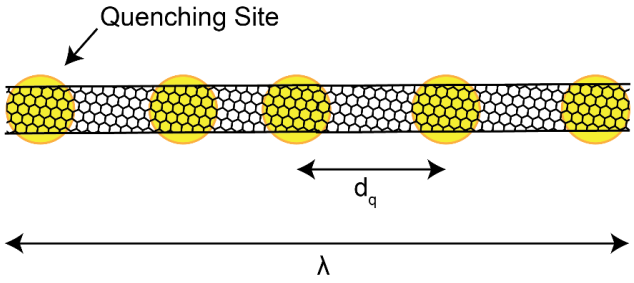

The length of the nanotube is denoted as λ and characteristic distance between quenching sites as d_q. Changes in fluorescence intensity can be calculated as a function of the addition of n additional quenched sites, to give us the following model:

$$\frac{\Delta I}{I_0} = -\frac{n^2 + 2n(\frac{\lambda}{d_q} + 1)}{(\frac{\lambda}{d_q} + n)^2}$$

Since the number of additional quenched sites as compared to concentration of protein is not known, we fit our data using a fitting parameter n_{conc}, where:

$$n = n_{conc} * [WGA]$$

So our equation becomes

$$\frac{\Delta I}{I_0} = -\frac{(n_{conc} * [WGA])^2 + 2(n_{conc} * [WGA])(\frac{\lambda}{d_q} + 1)}{(\frac{\lambda}{d_q} + n_{conc} * [WGA])^2}$$

Setting $\lambda/d_q = 10$, the characteristic density of quenching sites along the nanotube as shown in reference 43, we find $n_{conc} = 0.055\ \mu M^{-1}$ wtih the following fit to our data ($R^2 = 0.52$).

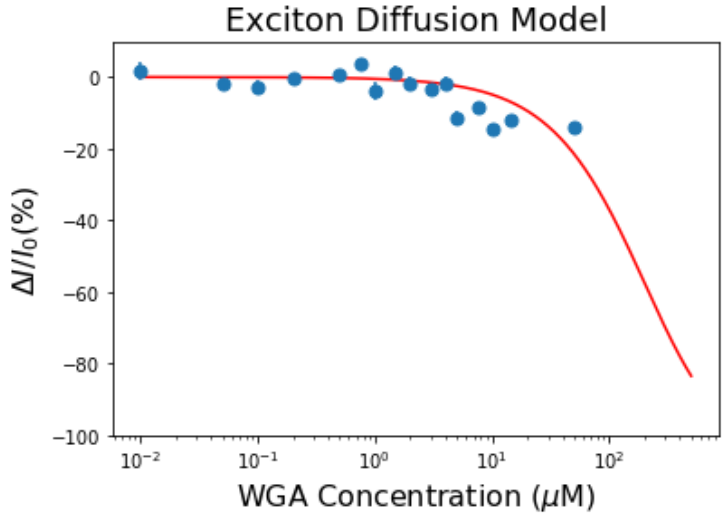

We find that the Langmuirian model fits better to our data.

Calculating the Limit of Detection

To calculate the limit of detection (LoD) of the ProLoop-SWCNT nanosensor, we defined the LoD as the lowest analyte concentration likely to be reliably distinguished from the limit of blank (LoB).[181] The limit of blank is the highest apparent analyte concentration expected to be found when replicates of a blank sample containing no analyte are tested.

$LoB = mean_{blank} + 1.645\ (SE_{blank})$

$LoD = LoB + 1.645\ (SE_{low\ concentration\ sample})$
For our system, LoB = 0 + 1.645 (-1.3904)

LOD = LoB + 1.645 (-1.2107) = -4.2788 (fluorescence change value) which corresponds to a WGA concentration of 3.4 μM.